PROCESS SIMULATION OF THE CARBOTHERMAL REDUCTION OF ILMENITE IN ROTARY KILN REACTORS

Thesis submitted to the

University of Kerala

for the award of the Degree of

DOCTOR OF PHILOSOPHY

in Chemical Engineering under the Faculty of Engineering

By

MANJU M.S.

Under the Supervision of

Dr. S. Savithri

Process Engineering and Environmental Technology Division

National Institute for Interdisciplinary Science and Technology (CSIR)

Thiruvananthapuram -695 019

India

November 2010

I dedicate this thesis to the fond and inspiring memory of my father

DECLARATION

I hereby declare that the Ph.D. thesis entitled "**PROCESS SIMULATION OF THE CARBOTHERMAL REDUCTION OF ILMENITE IN ROTARY KILN REACTORS"** is an independent work carried out by me and it has not been submitted anywhere else for any other degree, diploma or title.

Manju M.S.

National Institute for Interdisciplinary Science & Technology
(Formerly Regional Research Laboratory)
(Council of Scientific & Industrial Research) India
Industrial Estate P.O., Pappanamcode, Trivandrum – 695 019

Dr. S. Savithri
Scientist

Tel: +91 471 2515264; Fax: +91 471 2490186
E-mail: sivakumarsavi@gmail.com

CERTIFICATE

This is to certify that the work embodied in the thesis entitled "**PROCESS SIMULATION OF THE CARBOTHERMAL REDUCTION OF ILMENITE IN ROTARY KILN REACTORS"** has been carried out by **Ms. Manju M. S.** under my supervision and guidance at the Process Engineering and Environmental Technology Division of National Institute for Interdisciplinary Science and Technology (CSIR), Thiruvananthapuram and this work has not been submitted anywhere else for any other degree, diploma or title.

Dr. S. Savithri
(Thesis Supervisor)

ACKNOWLEDGEMENT

वागर्थाविव सम्पृक्तौ वागर्थप्रतिपत्तये ।
जगतःपितरौ वन्दे पार्वतीपरमेश्वरौ ॥

A source of effervescent energy and a meticulous mentor, my PhD supervisor Dr. S. Savithri, Scientist, National Institute for Interdisciplinary Science and Technology (NIIST), is the guiding star for me during this journey. Without her constant encouragement, support and in time corrections this thesis would have never been a reality. I wholeheartedly thank her for supervising my PhD work with all her dedication, knowledge, passion and sincerity. I shall cherish forever the affection, care and emotional support that she always holds for me.

The foundation stone of my PhD work was laid by late Dr. G. D. Surender, Director Grade Scientist (Rtd.), NIIST to whom I owe the enthusiasm of entering into such a challenging field of study. I thank him for all his encouragement and guidance.

I thank the Director, NIIST for permitting me to carry out my PhD work in the Computational Modeling and Simulation Section (CMS) of NIIST. I thank Dr. Raghavan (Head, PEET), Dr. Roschen Sasikumar (Head, CMS), Dr. Elizabeth Jacob, Dr. C.H. Suresh and Dr. P. Vijayalekshmi of CMS Section for their support and encouragement. I thank Dr. J.D. Sudha of Chemical Sciences Division for her affection and encouragement.

I take this opportunity to extend my sincere thanks to Dr. T. R. Sivakumar for sparing his valuable time for correcting the thesis and also for his support and encouragement all through the tenure of my work. Thanks are also due to Priyadarsini and Jayalekshmi for their affection and cooperation.

Friends have always been a great source of inspiration throughout my life. Though the list is never complete and the feeling of gratitude is beyond words, I explicitly thank Adersh, Ajitha, Alex, Ani, Basha, Bejoy, Binu, Hareesh, Fathima, Gigi, Gopika, Jijoy, Jomon, Lakshmi, Neetha, Manoj, Panneer, Radhika, Rejitha, Santhosh, Sajith, Sandhya, Shaija, Shyja and Sudeep of CMS section and

Chameshwary, Reena, Reshmi and Sasikala of NIIST and Dr. Viola B. Morris of SCIMST for their care, companionship, affection and timely help.

Above all, I am deeply indebted to my husband Pradeep. It is his unconditional love and unbounded support that helped me strive through the most difficult and extremely busy situations during the tenure of this work. I acknowledge with thanks, the profound support, patience and affection of my kids, my parents and parents-in-law throughout my work.

The assistance and support from the Library, IT department, Administration and other supporting sections of NIIST are gratefully acknowledged.

I acknowledge the research fellowship from the Kerala State Council for Science Technology and Environment (KSCSTE) for this PhD work.

Once again, I thank each and every one who has directly or indirectly been associated with me and assisted me during the tenure of my Ph.D. work.

Manju M. S.

CONTENTS

		Page Number
DECLARATION		i
CERTIFICATE		ii
ACKNOWLEDGEMENT		iii
CONTENTS		v
LIST OF TABLES		viii
LIST OF FIGURES		ix
LIST OF SYMBOLS		xiii
PREFACE		xviii
CHAPTER 1: INTRODUCTION		
1.1	Introduction	1
1.2	Titanium – Metal & Alloys	1
1.3	History of Titanium	3
1.4	Raw Materials	5
1.5	Ilmenite Reserves	6
1.6	Synthetic Rutile manufacturing Process	10
1.7	NIIST Process for Synthetic Rutile Production	13
1.8	Background of the Thesis	14
1.8.1	Objective of the Thesis	14
1.8.2	Thesis Framework	17
CHAPTER 2: KINETICS OF CARBOTHERMAL REDUCTION OF ILMENITE		
2.1	Introduction	18
2.2	Literature Survey	20
2.3	Model Development	28
2.3.1	Identification of Control Mechanism for Kinetics	28
2.3.2	Mathematical Model for the Carbothermal reduction of Ilmenite	37
2.3.2.1	Experimental Work	38
2.3.2.2	Combined Reaction Model	40
2.3.2.3	The Semi Empirical Model	45
2.4	Conclusions	51

CHAPTER 3: CFD SIMULATION OF PNEUMATIC COAL INJECTION PROCESS

3.1	Introduction	52
3.2	Description of the process and mathematical model	55
3.2.1	Assumptions/Simplifications	56
3.2.2	Governing Equations	57
3.2.2.1	Gas phase	58
3.2.2.2	Standard k-ε Model for Turbulence	60
3.2.2.3	Particle Phase	61
3.2.2.4	Heat Transfer Equations	63
3.2.2.5	Coal Devolatilisation and Combustion	64
3.2.3	Geometry and Simulation Conditions	68
3.3	Results and discussion	76
3.3.1	Validation Result	76
3.3.1.1	Cold Model Validation	76
3.3.1.2	Hot Model Validation	79
3.3.2	Pneumatic Coal Injection Simulation Results	80
3.3.2.1	Grid Resolution Study	80
3.3.2.2	Effect of Particle Size Distribution	82
3.3.2.3	Effect of Particle Size	87
3.3.2.4	Effect of Initial Particle Velocity	89
3.3.2.5	Effect of kiln wall temperature	91
3.4	Integrating to the overall one-dimensional simulator	92
3.4.1	Axially Averaged Species Concentration	92
3.4.2	Carbon Load to the Solid Bed	92
3.5	Conclusions	93

CHAPTER 4: STEADY STATE SIMULATION OF ROTARY KILN

4.1	Introduction	94
4.2	Literature Survey	94
4.2.1	Literature survey for solid-hold up and residence time distribution	95
4.2.2	Literature Survey on Heat Transfer	98
4.2.3	Literature Survey on Steady State Models for Rotary Kilns	100

4.3	Process Description	103
4.4	Challenges involved in Modeling	106
4.5	Mathematical Model	109
4.5.1	Modeling of the Holdup Profile of the Solid Bed	109
4.5.2	Steady State Heat and Mass Balance	111
4.5.3	Assumptions/Simplifications	112
4.6	Governing Equations	113
4.6.1	Mass Balances	113
4.6.2	Heat Balances	117
4.6.3	Rate Equations	120
4.7	Solution Methodology	123
4.8	Results and Discussion	125
4.8.1	Validation for Ilmenite Reduction (Ramakrishnan and Sai (1999)	125
4.8.2	Effect of Pneumatic Coal Injection	129
4.8.3	Effect of Air Distribution	132
4.9	Conclusions	136

CHAPTER 5: CONCLUSIONS AND FUTURE SCOPE

5.1	Conclusions	137
5.2	Scope for Future Work	139

REFERENCES 140

LIST OF PUBLICATIONS 148

LIST OF TABLES

Table No.	Caption	Page No.
1.1	Installed Capacity of Ilmenite Plants in India	8
1.2	Quality Aspects of Indian Ilmenite	9
1.3	Global Synthetic Rutile Production as in 2004	12
2.1	Fitting Parameters for Mixed Control Mechanism	35
3.1	Physical Dimensions and Process Parameters	74
3.2	Proximate and Ultimate Analysis of Coal with Size Distribution and Reaction Parameters	75
3.3	Dimensions and Process Parameters for Cold Model Validation (Biswas (1993))	77
3.4	Comparison of Simulated Particle Trajectory Data with the Data of Biswas (1993)	78
3.5	Carbon Load Provided to the Solid Bed by Pneumatic Coal Injection Process	93
4.1	Values Used for Kinetics of Devolatilisation	121
4.2	Input Parameters (Ramakrishnan and Sai (1999)	125
4.3	Different Air Distribution Profiles	132

LIST OF FIGURES

Figure No.	Caption	Page No.
1.1	Beneficiation Technologies for Synthetic Rutile	10
2.1	Kinetic Plot Corresponding to Equation (2.9)	31
2.2	Kinetic Plot Corresponding to Equation (2.10	32
2.3	Conversion Data of Sucre (1979) Fitted to Equation (2.14)	34
2.4	Conversion Data of Nicholson (1995) Fitted to Equation (2.14)	35
2.5	Variation of reduction rate constant k_{ore} with coal/Ilmenite ratio β	37
2.6	Comparison of Combined Reaction Model with Conversion Data of Nicholson (1995) (a) at 1050 ^{0}C (b) at 1100 ^{0}C (c) at 1150 ^{0}C	43
2.7	Comparison of Combined Reaction Model with Conversion Data of Sucre (1979) (a) at $\beta = 0.21$ (b) at $\beta = 0.24$ (c) at $\beta = 0.30$	44
2.8	Experimental Reduction Data (Present Work) at 1000 ^{0}C for varying Coal/Ilmenite ratio (β)	48
2.9	Comparison of Experimental and Simulated Reduction Data (Sucre (1979))	49
2.10	Comparison of Experimental and Simulated Reduction Data (Wouterlood (1979))	49
2.11	Variation of Carbon Activity with respect toCoal/Ilmenite ratio (β)	50
3.1	Schematic Diagram of Pneumatic Coal injection Unit in a Direct Reduction Rotary Kiln (Biswas (2003))	55
3.2	Schematic View of the Rotary Kiln along with Coal Injector Tube	69
3.3	Computational Mesh Created for Coal Injection Simulation	69
3.4	Main Dimensions (in mm) of the Geometry used for Validation	72

	(a) Coal Combustor (Guo et al. (2005)) and (b) Injection Lance (Shen(2008))	
3.5	Computational Mesh for Validation	73
3.6	Temperature and species mass fraction isopleths in Y-Z plane for (a) results reported by Guo *et al.,(*2005) (b) present CFD simulation	80
3.7	Variation of (a) Particle velocity and (b) Gas velocity along the Axial Distance for Three Different Meshes	81
3.8	Distribution of (a) Particle Temperature and (b) Mean Particle Diameter along the Particle Trajectories for Particle Size Distribution I.	82
3.9	Distribution of (a) Particle Temperature and (b) Mean Particle Diameter along the Particle Trajectories for Particle Size Distribution II.	83
3.10	Distribution of (a) Gas temperature (b) CO_2 mass fraction (c) O_2 mass fraction and (d) Volatile mass fraction in plain perpendicular to the solid bed surface, along kiln axis for particle size distribution I.	84
3.11	Distribution of (a) Gas temperature (b) CO_2 mass fraction (c) O_2 mass fraction and (d) Volatile mass fraction in plain perpendicular to the solid bed surface, along kiln axis for particle size distribution I.	86
3.12	Variation of (a) CO_2 Mass Fraction (b) H_2O Mass Fraction (c) Volatile Mass Fraction and (d) O_2 Mass Fraction for different Particle Sizes	87
3.13	Influence of Particle Size on (a) Particle Temperature (b) Char Burnout	89
3.14	Effect of Particle Velocity on the Particle Dynamics for (a) Particle size 0.5 mm (b) Particle size 3 mm	90

3.15	Variation of Particle Temperature with Wall Temperature for (a) Particle size 0.5 mm (b) Particle size 3 mm	91
3.16	Axial Profile of Free Board Gases Resulting from Pneumatic Coal Injection Process	92
4.1	Granular Flow Patterns of the Solid Bed in a Rotary Kiln	96
4.2	Various Heat Transfer Paths in a Rotary Kiln (Boateng (1996))	99
4.3	Schematic View of the Ilmenite Reduction Kiln	105
4.4	Schematic View of the Granular Material Motion in a Rotating Cylinder (Spurling (2000))	110
4.5	Material and Energy Flows in a Control Volume	112
4.6	Flow Chart of the Algorithm	124
4.7	Air Profile used for Ilmenite Reduction (Ramakrishnan and Sai (1999))	126
4.8	Temperature Distribution for Ilmenite Reduction (Ramakrishnan and Sai (1999))	126
4.9	Variation of Fractional Reduction along the Axial Length (Ramakrishnan and Sai (1999))	127
4.10	Partial Pressure Profile for Various Gas Components (Present Simulation)	128
4.11	Partial Pressure Profile for Various Gas Components (Ramakrishnan and Sai (1999))	128
4.12	Comparison of Partial Pressure Profile for H_2O	129
4.13	Variation of Gas Temperature along the Axial Length of the Kiln	130
4.14	Variation of Solid Temperature along the Axial Length of the Kiln	131
4.15	Variation of Fractional Reduction along the Axial Length of the Kiln	131
4.16	Effect of Air Distribution on Gas Temperature	133

4.17	Effect of Air Distribution on Solid Temperature	133
4.18	Effect of Air Distribution on Fractional Reduction	134
4.19	Effect of Air Distribution on Partial Pressure of CO_2	135
4.20	Effect of Air Distribution on Partial Pressure of O_2	135

LIST OF SYMBOLS

A	*pre-exponential factor of devolatilization reactions, s^{-1}(Chapter 3)* *surface area of the pellet, m^2 (Chapter 2)*
A_c	*pre-exponential factors in Gibb model, m s^{-1} K^{-1}*
A_{cw}	*area of contact between the covered bed and the covered wall, m^2*
$_F$	*effective particle cross sectional area, m^2*
A_{g-eb}	*heat transfer area of the exposed bed*
A_{g-ew}	*heat transfer area of the exposed wall*
A_s	*constant in Gibb model (Chapter 3)* *cross sectional area, m^2 (Chapter 4)*
a_c	*carbon activity*
C_D	*drag coefficient*
Cp	*specific heat, J kg^{-1} K^{-1}*
D	*external diffusion coefficient of oxygen in Gibb model, m^2s^{-1}*
D_I	*kinematic diffusivity of component I, m^2 s^{-1}*
D_e	*effective diffusivity of the reactant through the product layer, m^2 s^{-1} (Chapter 2)* *hydraulic diameter of the kiln, m (Chapter 4)*
$Dref$	*reference dynamic diffusivity in Gibb model, kg m^{-1} s^{-1}*
d_p	*particle diameter, mm*
E	*activation energy of devolatilization reactions, K*
E_Y	*activation energy of volatile component Y, J mol-1*
F_{all}	*sum of all forces acting on the particle*
f_D	*drag force from a particle, N*
F_p	*shape factor (1,2 or 3 for a slab, a long cylinder or a sphere)*
$F(X)$	*conversion function which forms part of the rate equation*
G_{gj}	*mass flux of gas species j, , kg m-2s-1*

G_{si}	*mass flux of solids, kg m-2s-1*
H	*mean enthalpy, J kg^{-1}*
h	*height of the solid bed (equation 4.5)* *heat transfer coefficient (other equations)*
I	*radiation intensity on particle surface, W m^{-2}*
k	*reaction rate constant (Chapter 2)*
k_B	*rate constant of Boudouard reaction, g g-1 s-1 atm-1*
k_b	*thermal conductivity of solid bed*
k_c	*interface reaction rate constant (Chapter 2)* *carbon oxidation rate in Gibb model, m s^{-1} (Chapter 3)*
k_g	*thermal conductivity, J/m K*
k_{obs}	*overall rate constant*
k_{ore}	*reaction rate constant, g g-1 s-1 atm-1*
k_R	*rate constants for reduction of Ilmenite by CO*
k_Y	*pre-exponential factor of volatile component Y, s-1*
k_1	*inhibition rate constant which represents the inhibiting effects of CO on the Boudouard reaction (Chapter 2)* *rate of external diffusion in Gibb model, s^{-} (Chapter 3)^{1}*
k_2	*rate of surface reaction rate in Gibb model, s^{-1}*
k_3	*rate of internal diffusion and surface reaction in Gibb model, s^{-1}*
M	*kiln solid hold-up*
M_c	*molecular weight of carbon*
M_O	*atomic weight of oxygen*
M_{ore}	*molecular weight of ore*
MRT	*mean residence time of the solids in the bed, s*
$\dot{m}$	*mass transfer rate from a particle, kg s^{-1} (Chapter 3)*
	mass feed rate of solids, , kg m^{-2}s^{-1} (Chapter 4)

m_c	*amount of unreacted carbon, g (Chapter 2)* *mass of char, kg (Chapter 3)*
m_{ore}	*amount of unreacted ore, g*
n	*refractive index of the continuous phase (Chapter 3)* *kiln rotational speed (Chapter 4)*
p	*pressure, Pa*
p_{CO}	*local partial pressure of CO, atm*
p_{CO_2}	*local partial pressure of CO2, atm*
$p_{CO_2}^{c}$	*equilibrium partial pressure of CO2 for boudouard reaction, atm*
p_{CO}^{ore}	*equilibrium partial pressure of CO for the reduction reaction, atm*
Q	*heat transfer, W*
Q_c	*convective heat transfer term, W*
Q_M	*heat transfer term associated with mass transfer, W*
Q_R	*heat transfer term associated with radiative heat transfer, W*
R	*kiln radius*
Re_D	*axial Reynolds number*
Re_ω	*angular Reynolds number*
R_Y	*rate of evolution of volatile component Y*
r_c	*rate of consumption per unit volume of individual components due to chemical reactions*
r_g	*rate of generation per unit volume of individual components due to chemical reactions*
r_p	*particle radius, m*
T	*temperature, K*
T_c	*activation energy in Gibb model, K*
T_g	*average axial gas temperature, K*

T_{ref}	*reference temperature in Gibb model, K*
T_s	*constant in Gibb model (Chapter 3)*
	average axial solid temperature, K (Chapter 4)
T_w	*temperature of the wall, K*
t^*	*dimensionless time*
U	*mean velocity of gas, m s^{-1}*
V	*volume of the pellet, m3*
V_s	*velocity of the solid bed, ms-1*
u, v, w	*gas velocity components, m s^{-1}*
X	*fractional reduction (conversion)*
X_a	*ash mass fraction*
$X_{a,0}$	*original ash mass fraction*
Y_{si}	*mass fraction of species* i
y_I	*mass fraction of component I*

Greek Symbols

α	*oxygen removal rate to carbon removal rate ratio (Chapter 2)* *volume/internal surface area ratio in Gibb model (Chapter 3)* *thermal diffusivity, m2/s (equation 4.19)*
β	*coal/Ilmenite ratio (Chapter 2)* *kiln inclination with respect to horizontal (Chapter 4)*
γ	*angle of repose of solids (equation 4.4)* *production rates for various species involved in either chemical reactions (equations 4.15, 4.16)*
ε	*Emissivity* *turbulent dissipation rate, m2 s-3 (Chapter 3)*
Γ	*angle subtended by the solid bed at the kiln axis*
$\Gamma Ieff$	*effective diffusion coefficient, m2 s-1*
ΓI	*Molecular diffusivity of species I, m2 s-1*

λ	*thermal conductivity, W m-1 K-1*
μ	*dynamic viscosity, Pa s*
μt	*turbulent viscosity, Pa s*
Φ	*mechanism factor in Gibb model*
Φv	*volumetric flow rate of the material through solid bed of the kiln, m3s-1*
ω	*kiln rotational speed, rad s-1*
Ω	*form factor for radiation*
σ	*Stephan Boltzmann constant, 5.67 x 10-8 W m-2 K-4*
σk, $\sigma \varepsilon$	*turbulence model constant*
σ_s	*gas-sold reaction modulus*
ρ	*density, kg m-3*
τ	*time required for complete conversion (Chapter 2)*

Subscripts

$cw \rightarrow cb$	*covered wall to covered bed*
$g \rightarrow ew$	*exposed wall to free-board gas*
$g \rightarrow eb$	*exposed bed to free-board gas*
$ew \rightarrow eb$	*exposed bed to exposed wall*
shell	*outer shell of kiln to surroundings*
w	*wall*
g	*Gas phase*
b	*Solid bed*
c	*Char*
p	*Particle*

PREFACE

Titanium metal and its alloys play a vital role in several industrial sectors such as chemical, metallurgical, aerospace, defence etc. including biomedical applications. Similarly TiO_2 finds wide application in paints, pigments, semiconductors and ceramic sectors. Kerala has extensive deposits of ilmenite mineral which is the basic raw material for the manufacture of Titanium and TiO_2. Several multiphase chemical reactors are involved in the processing of converting ilmenite mineral to TiO_2 and Titanium metal, most important among them being high temperature rotary kilns for carbothermal reduction of ilmenite mineral, fluidized bed for carbochlorination and aqueous leaching and high temperature aerosol reactors for the manufacture of nano-micron sized TiO_2 particles. Rotary kiln reactors involve a complex interplay of coupled heterogeneous reactions, conductive, convective and radiative heat transfer and complex solid and gaseous flows inside the reactor. In view of its extreme complexity, a comprehensive understanding of this process at various length and time scales has not yet been made and this work is aimed at closing this gap. This work presents a scientific basis for the design, scale up and optimization of the rotary kiln reactor for achieving a desired degree of reduction by carbothermal route for any give type of ilmenite and coal.

The objective of the present work is to develop a virtual simulator of the rotary kiln which will predict under steady state conditions the gas and solid flows, concentration profiles and thermal profiles along the axial length of the rotary kiln during the carbothermal reduction of ilmenite for a wide range of process conditions and reductant characteristics. The thesis is logically divided into the following three major modules.

1. A Mathematical model for the carbothermal reduction of ilmenite at conditions prevailing in a commercial rotary kiln reactor to arrive at appropriate rate equations for the reduction kinetics
2. A mathematical model of the pneumatic coal injection process from the discharge end of the kiln to arrive at the carbon load in the solid bed and thermal load in the free board of the rotary kiln
3. A comprehensive 1-D model for predicting the heat and mass flows along the axial length of the kiln by incorporating modules 1 & 2.

A lot of effort has been put in to apply various kinetic models to understand the mechanism of carbothermal reduction of ilmenite. Since the industrial rotary kiln reactor involves many complex physical and chemical processes apart from the reduction reaction, results from lab-scale experiments hardly can replicate the realistic process in the rotary kiln. As our aim is to model the actual rotary kiln processes we opted to use reported experimental data from industrial rotary kilns for validation and analysis of our proposed kinetics model.

The pneumatic coal injection and combustion process in the rotary kiln during carbothermal reduction of ilmenite is modeled using a multiphase Eulerian-Lagrangian CFD approach where the gas phase is treated as a continuous phase and the pulverized coal particles are tracked in the flow field in a Lagrangian way. All the relevant phenomena like coal devolatilization, homogeneous volatile combustion, heterogeneous char reaction, particle dispersion and radiation were included in the mathematical model proposed and the commercial CFD code ANSYS-CFX 11.0 was used to obtain the numerical results. The 3-D data for

carbon load and thermal load are radially and azimuthally averaged to yield axial profile.

These two modules are then incorporated in the 1-D comprehensive model of the heat and mass flows in the rotary kiln under steady state conditions. The model was built upon the basic principles of conservation of heat and mass along with solid and gas phase chemical reactions. Axial movements of the solid bed were assumed to be in plug flow and determined by the parameters of the kiln design and speed of rotation. Thermal energy conservation was fulfilled through a balance between various heat generation and heat losses coupled with conservation of the mass of various species.

In conclusion, we have developed a validated virtual simulator of the rotary kiln for carbothermal reduction process of ilmenite. The present model can be used for optimally fixing various process parameters such as type of coal used for reduction, coal/ilmenite ratio in the feed, amount of primary and secondary air supplied to the kiln, ratio of feed to discharge end coal, particle size distribution of the pneumatically injected coal and the temperature of inlet and wall. This can hardly be achieved using experimental techniques.

Chapter 1

INTRODUCTION

1.1 Introduction

A comprehensive mathematical model for the carbothermal reduction process of Ilmenite in a high temperature rotary kiln reactor is presented in this thesis. The process of carbothermal reduction of Ilmenite in a rotary kiln reactor is the first and foremost step in converting the low value Ilmenite ore to high value synthetic rutile. The present work aims to develop a virtual simulator of a high temperature rotary kiln which will predict under steady state conditions the gas and solid flows, concentration profiles and thermal profiles along the axial length of the rotary kiln during the carbothermal reduction of Ilmenite for a wide range of process conditions and reductant characteristics.

This Chapter gives an overview of the global resources of Ilmenite and the production steps involved in converting low grade Ilmenite to synthetic rutile. A detailed discussion of the Indian scenario in this context is also presented. Background of the present research as well as the framework of the thesis is elaborated subsequently.

1.2 Titanium – Metal and Alloys

Titanium is the ninth most abundant element, comprising 0.6% of the earth's crust. It is also the fourth most abundant structural material after aluminum (8.1%), iron (5.1%) and magnesium (2.1%). It offers an excellent set of properties, such as high strength-to-weight ratio, high strength at high temperatures, corrosion resistance, and thermal stability that makes it an ideal metal in the modern age of industrialization. Titanium metal is recognized for its ability to alloy with other metals to improve their strength, durability and

lightness. Thousands of titanium alloys have been developed and these can be grouped into four main categories. Their properties depend on their basic chemical structure and the way they are manipulated during manufacture. Some elements used for making alloys include aluminum, molybdenum, cobalt, zirconium, tin, and vanadium.

The applications of titanium and its alloys are numerous. The aerospace industry is the largest user of titanium products. It is useful for this industry because of its high strength-to-weight ratio and high temperature properties. It is typically used for airplane parts and fasteners. These same properties make titanium useful for the production of gas turbine engines. It is used for parts such as the compressor blades, casings, engine cowlings, and heat shields.

Since titanium has good corrosion resistance, it is an important material for the metal finishing industry. Here it is used for making heat exchanger coils, jigs, and linings. Titanium's resistance to chlorine and acid makes it an important material in chemical processing. It is used for the various pumps, valves, and heat exchangers on the chemical production line. The oil refining industry employs titanium materials for condenser tubes because of corrosion resistance.

Titanium is used in the production of human implants because it has good compatibility with the human body. One of the most notable recent uses of titanium is in artificial heart first implanted in a human in 2001. Other uses of titanium are in hip replacements, pacemakers, defibrillators, and elbow and hip joints.

Titanium materials are used in the production of numerous consumer products. It is used in the manufacture of such things as shoes, jewelry, computers, sporting equipment, watches, and sculptures. As titanium dioxide, it is used as a white pigment in plastic, paper, and paint. It is even used as a white food coloring and as a sunscreen in cosmetic products.

Its applications have spread through sports and automotive industries, industrial design and architecture. It is an effective catalyst in a number of commercially important chemical processes. It is also used in ceramics, coatings for welding rods, heavy aggregate, and steel furnace flux. Titanium is used in some construction projects and associated applications such as the 150-foot high Yuri Gagarin Memorial in Moscow, the Guggenheim Museum in Bilbao, Spain and others. The petroleum industry is a user for its off shore activities and pipe lines. Heat exchangers in desalination plants rely on Titanium for its non-corrosion properties and it is even used in heater-chillers in aquariums.

1.3 History of Titanium

Most historians credit William Gregor for the discovery of titanium. In 1791, he was working with menachanite (a mineral found in England) when he recognized the new element and published his results. The element was rediscovered a few years later in the ore rutile by M. H. Klaproth, a German chemist. Klaproth named the element titanium after the mythological giants, the Titans.

Both Gregor and Klaproth worked with titanium compounds. The first significant isolation of nearly pure titanium was accomplished in 1875 by Kirillov in Russia. Isolation of the pure metal was not demonstrated until 1910 when Matthew Hunter and his associates reacted titanium tetrachloride with sodium in a heated steel bomb. This process produced individual pieces of pure titanium. In the mid 1920's, a group of Dutch scientists created small wires of pure titanium by conducting a dissociation reaction on titanium tetra iodide.

These demonstrations prompted William Kroll to begin experimenting with different methods for efficiently isolating titanium. These early experiments led to the development of a process for isolating titanium by reduction with magnesium in 1937. This process, now called the Kroll process (Kroll 1940a,b) is still the primary process for producing titanium. The first products made from titanium were introduced around the 1940's and included such things as wires, sheets, and rods.

While Kroll's work demonstrated a method for titanium production on a laboratory scale, it took nearly a decade more before it could be adapted for large-scale production. This work was conducted by the United States Bureau of Mines from 1938 to 1947 under the direction of R. S. Dean. By 1947, they had made various modifications to Kroll's process and produced nearly 2 tons of titanium metal. In 1948, DuPont opened the first large scale manufacturing operation.

This large scale manufacturing method allowed for the use of titanium as a structural material. In the 1950's, it was used primarily by the aerospace industry in the construction of aircraft. Since titanium was superior to steel for many

applications, the industry grew rapidly. By 1953, annual production had reached 2 million lb (907,200 kg) and the primary customer for titanium was the United States military. In 1958, demand for titanium dropped off significantly because the military shifted its focus from manned aircraft to missiles for which steel was more appropriate. Since then, the titanium industry has had various cycles of high and low demand. Numerous new applications and industries for titanium and its alloys have been discovered over the years. Today, about 80% of titanium is used by the aerospace industry and 20% by non-aerospace industries.

1.4 Raw Materials

Rarely found in its pure form, titanium typically exists in minerals such as anatase, brookite, Ilmenite, leucoxene, perovskite, rutile and sphene. While titanium is relatively abundant, it continues to be expensive because it is difficult to isolate. The leading producers of titanium concentrates include Australia, Canada, China, India, Norway, South Africa and Ukraine.

The primary ores used for titanium production include Ilmenite, leucoxene and rutile. Other notable sources include anatase, perovskite and sphene. Ilmenite and leucoxene are titaniferous ores. Ilmenite ($FeTiO_3$) contains approximately 53% titanium dioxide. Leucoxene has a similar composition but has about 90% titanium dioxide. They are found associated with hard rock deposits or in beaches and alluvial sands. Rutile is relatively pure titanium dioxide (TiO_2). Anatase is another form of crystalline titanium dioxide and has just recently become a significant commercial source of titanium. They are both found primarily in beach sand deposits. The limited absolute and diminishing relative sources of natural rutile worldwide necessitated the development of processes for synthetic

rutile production. The emergence of the chloride process for the manufacture of Titanium dioxide pigment during the 1960's also augmented the demand for synthetic rutile. Synthetic rutile is largely produced from naturally occurring Ilmenite which is a complex oxide with iron. Ilmenite is the most widespread titanium mineral. It is named after its place of discovery at Ilmen Lake in the Ilmen Mountains, of Russia.

1.5 Ilmenite Reserves

The world reserve base for Ilmenite is estimated at 1,400 million tonnes in terms of TiO_2 content. Major resources occur in China (25%), South Africa (16%), India (15%), Australia (11%), Brazil (6%), Norway and USA (4% each), Mozambique (2%) and Ukraine (1%) and other countries (11%) as per the Mineral Commodity Summaries, 2008. The Ilmenite production worldwide is estimated to be Canada (20%), Australia (19%), South Africa (18%), China (10%), Norway (7%), India (6%), Ukraine (5%), USA (4%) and other countries (9%) as per the World Mineral Production 2007 (http://ibm.nic.in/Ilmeniteandrutile.pdf). The major Ilmenite production plants in the world are situated in Murray Basin and Queensland of Australia, Sorel of Canada and also in Madagascar, Mozambique, Sierra Leone etc.

India possesses the second largest Ilmenite reserves of the world next to China. As per Department of Atomic Energy, Mumbai, the total resources of Ilmenite in India are estimated at about 461 million tonnes and India's production of Ilmenite in 2005-06, 2006-07 and 2007-08 were 703,796 tonnes, 692,906 tonnes and 678,772 tonnes, respectively. Ilmenite and rutile along with other heavy minerals that form the ingredients of beach sand deposits are found right

from Ratnagiri coast in the west to Orissa coast in the east. These minerals are concentrated in three well defined zones:

- Over a stretch of 22 km between Neendakara and Kayamkulam, Kollam district, Kerala (known as 'Chavara' deposit after the main mining centre).
- Over a stretch of 6 km from the mouth of Valliyar River to Colachal, Manavalakurichi and little beyond in Kanyakumari district, Tamil Nadu (known as MK deposit).
- On Chatrapur coast stretching for 18 km between Rushikulya river mouth and Gopalpur light house with an average width of 1.4 km in Ganjam district, Orissa (known as 'OSCOM' deposit after IREL's Orissa Sands Complex).

In India, Tamil Nadu was the leading producer of Ilmenite contributing 46% of the total production followed by Orissa 30% and Kerala 24% as reported by Department of Atomic Energy during 2007-08. Mining and processing of beach sand is carried out by the Indian Rare Earths Limited (IREL), a Government of India undertaking, Kerala Minerals and Metals Limited (KMML), a Kerala State Government undertaking and two private sector producers viz. M/s. V. V. Mineral, Tuticorin (Tamil Nadu) and M/s Beach Minerals Co.Pvt. Ltd, Kuttam (Tamil Nadu). IREL is exploiting beach sand deposits located at Chavara in Kerala, Gopalpur in Orissa and Manavalakurichi in Tamil Nadu. Table 1.1 shows the Installed Capacity and Production of Ilmenite in India during 2005-2008. Table 1.2 depicts the quality aspects of Indian Ilmenite.

Table 1.1 Installed Capacity of Ilmenite Plants in India

Company/ Location	Specification	Installed capacity (TPA)	Production (Tonnes)		
			2005 -06	2006 - 07	2007 -08
Indian Rare Earths Ltd Manavalakurichi, Kanyakumari dist., Tamil Nadu	55% TiO_2	90 000	103 027	96 551	89 355
Chavara, Kollam dist., Kerala	58% TiO_2(min)	154 000	106 419	80 468	113 916
Orissa Sands Complex, Ganjam dist., Orissa	50.25% TiO_2(min)	220 000	244 160	207 795	200 845
Kerala Minerals & Metals Ltd Chavara, Kollam dist. Kerala	75.8% TiO_2	50 000	51 430	52 500	49 225
V.V. Mineral Tuticorin, Tamil Nadu.	46-56% TiO_2	392 000	144 953	196 427	165 541
Beach Minerals Co. Pvt. Ltd Kuttam, Tirunelveli dist., Tamil Nadu.	52% TiO_2	150 000	53 807	59 165	59 890

Table 1.2 Quality Aspects of Indian Ilmenite

Constituent	**% Composition**		
	Quilon	**Manavalakurichi**	**Orissa**
Heavy Minerals or grade	50	12	13.5
Ilmenite in heavy Mineral	70	64	43
Rutile+Zircon	0.17	0.12	0.08
Ilmenite			
TiO_2	60.0	55.0	50.2
Fe_2O_3	25.5	18.9	12.8
FeO	9.7	20.9	34.1
Al_2O_3	1.1	0.8	0.6
SiO_2	0.9	0.9	0.8
ZrO_2	0.4	0.06	0.01
MnO	0.4	0.06	0.55
Cr_2O_3	0.13	0.08	0.05
V_2O_5	0.15	0.22	0.24
MgO	0.6	1.0	0.6
P_2O_5	0.2	0.12	0.03
U+Th(ppm)	150	225	50-60

Indian Ilmenite due to their lower contents of Al_2O_3, MgO, Cr_2O_3, ZrO_2, V_2O_5, SiO_2, MnO and P_2O_5 are ideally suitable as chloride grade feed stocks (Doan(2003)) after beneficiation. In view of the excellent resource base and lower labor costs, Ilmenite mineral production in India is expected to be globally competitive (Walole (2004)) if logistics are met.

1.6 Synthetic Rutile manufacturing Process

Synthetic Rutile is a beneficiated product from Ilmenite ore ($FeTiO_3$) containing 92-96% TiO_2. The manufacture of Synthetic Rutile from Ilmenite is carried out through the chemical route of mineral beneficiation. The major steps involved in the beneficiation process include complete or partial carbothermal reduction of the iron oxide component of Ilmenite followed by some form of hydrometallurgical unit operation including leaching to remove the iron content. Various beneficiation technologies (both commercially proven and those under development) for the manufacture of Synthetic Rutile are depicted in Figure 1.1.

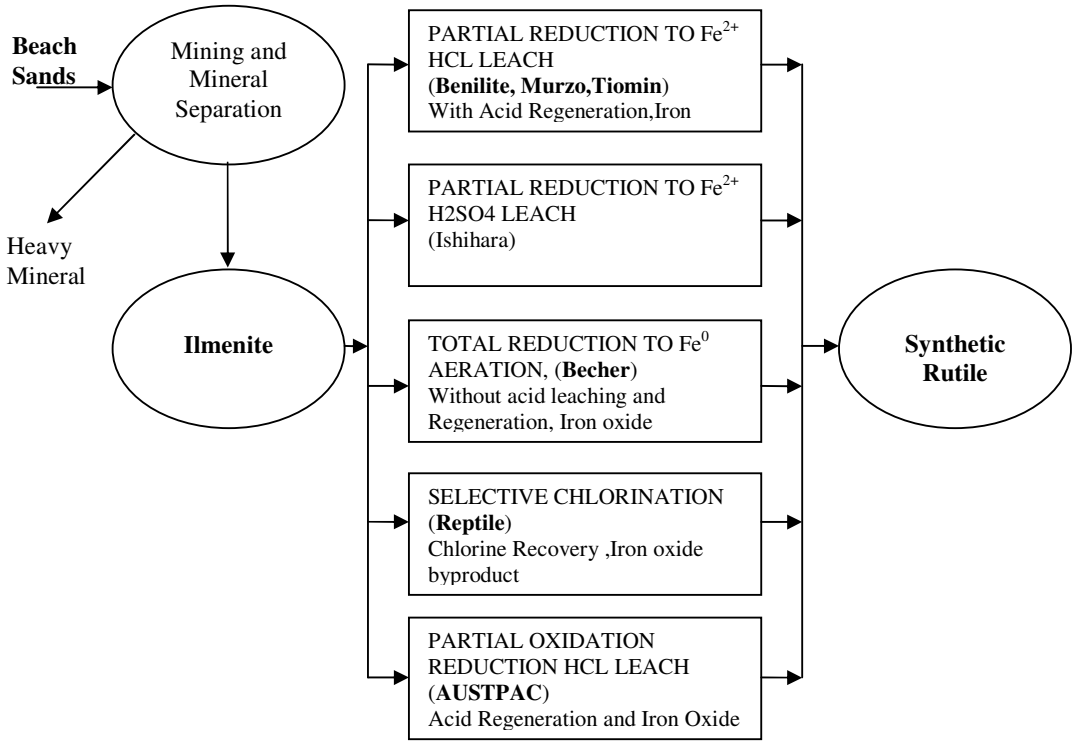

Figure 1.1 Beneficiation Technologies for Synthetic Rutile

The processes differ in the extent to which the Ilmenite particles are reduced and on the conditions used in the subsequent unit operations. The two major commercially available processes for the production of synthetic rutile from Ilmenite are the Becher process and the Benelite Process.

The Becher process (Becher 1963) involves reduction of the iron oxide content of Ilmenite to metallic iron using sub-bituminous coal at 1050^0C-1160^0C (carbothermal reduction) in a rotary kiln reactor. The metallic iron formed is then removed by accelerated corrosion (rusting). This gives rise to a product of around 90% TiO_2 content which is suitable as feedstock for TiO_2 pigment manufacture in the Chloride route. Becher's process is the well documented process, used extensively in Western Australia, which has an advantage of easier operability and reduced environment related problems compared to other beneficiation process of Ilmenite. This process works well but economic effectiveness is limited to treatment of high titanium – low iron oxidized ores and using a reactive coal as fuel. The process operates most effectively on Ilmenite with greater than 58% TiO_2 content, with the most suitable being Ilmenite with 62% TiO_2 content.

Synthetic Rutile is manufactured worldwide by other proven process viz., Benelite, Wah Chang, Ishihara processes. In Benelite Process acid leaching step follows roasting process. Other acid leaching processes such as Murso, Austpac ERMS, New Gen, Reptile, Dupont selective chlorination, CTL etc. are also in the development phase. Environmental impact and production costs had been crucial issues in all these processes. Overall performance data suggested that the Becher process has major attractive features in terms of reduced environmental impact and operating and capital costs.

Table 1.3 gives a brief account of the global Synthetic Rutile production as in 2004. In India there were four plants which manufactured Synthetic Rutile, with a total installed capacity of 1.6 lakh tonnes per annum (TPA). Due to the highly-corrosive nature of the acid leaching step, these plants faced major operational problems, which brought down the capacity utilization. As a result, the actual production in the country was around 60,000 TPA as against a projected demand of around three million worldwide.

Table 1.3 Global Synthetic Rutile Production as in 2004

Company	**Location**	**Process**	**Capacity (TPA)**	**Feedstock**
Iluka resources	Western Australia	Becher	480 000	Own sources and purchased 60% TiO_2 Ilmenite
TiWest Joint Venture	Western Australia	Becher	200 000	62%TiO_2 Cooljarloo Ilmenite
TOR Minerals	Ipoh, Malaysia	Benelite	50 000	Local 60 - 62% TiO_2 weathered Ilmenite
(KMML)	Kerala, India	Benelite	30 000	60% TiO_2 Chavara Ilmenite
Cochin Minerals and Rutiles Limited (CMRL)	Kerala, India	Benelite	15 000	60% TiO_2 Ilmenite from Indian Rare Earth's operation at Chavara
DCW Limited	Tamil Nadu, India	Wah Chang	20 000	55% TiO_2 Ilmenite from Indian Rare Earth's operation at Manavalakurichi
OSCOM	Orissa, India	Benelite	100 000	50% TiO_2 Ilmenite from OSCOM

1.7 NIIST Process for Synthetic Rutile Production

National Institute for Interdisciplinary Science and Technology (NIIST) of the Council of Scientific and Industrial Research (CSIR), India, has been striving hard to develop an indigenous environment-friendly technology suitable for the Indian raw materials for synthetic rutile manufacture, since 1986. A modified version of the Becher's process involving an additional thermal oxidation step prior to acid leaching step has been under development by NIIST. The major advantage of the NIIST process is the possibility of achieving higher grade of synthetic rutile (>95% TiO2) leading to higher value product. Following successful laboratory scale trials, a comprehensive program to optimize the process conditions at bench scale/micropilot plant scale was taken up during 1988. The process developed at NIIST can be broken up into two major process modules *viz*. carbothermal reduction step and iron removal step. The carbothermal reduction step, aims at converting the iron oxide component of Ilmenite into a metallic iron phase and rutile phase.

The carbothermal reduction step plays a crucial role due to the following reasons:

- The extent of iron removal by the rusting reaction depends on the extent of metallization under optimum conditions.
- Being a high temperature process with relatively slow kinetics, the productivity of the carbothermal reduction process has a direct bearing on the process economics.

The feasibility of the carbothermal reduction of Indian Ilmenite with Neyveli leco char has been established in laboratory scale static tube experiments at NIIST. The overall kinetics of the reaction has been found to be depending on both the

reducibility of Ilmenite as well as the reactivity of char. Thus, the raw material characterization such as degree of weathering, composition and rank of precursor coal play a vital role in deciding the overall kinetics and extent of metallization. For a given combination of Ilmenite char mixture, the reaction temperature and char/ore ratio play the most crucial role whereas minor effects are due to size distribution, mixing and segregation as well as reactor design and operating characteristics.

1.8 Background of the Thesis

The present work forms a part of the ongoing efforts of NIIST (CSIR) to scale-up and optimize the environment-friendly technology for manufacturing synthetic rutile from Ilmenite by modifying the Becher process. The carbothermal reduction reaction taking place in the rotary kiln reactors involve a complex interplay of coupled heterogeneous reactions, conductive, convective and radiative heat transfer and complex solid and gaseous flows inside the reactor. In view of its extreme complexity, a comprehensive understanding of this process at various length and time scales has not yet been made and the present work is aimed at closing this gap. This work presents a scientific basis for the design, scale up and optimization of the rotary kiln reactor for achieving a desired degree of reduction by Carbothermal reduction route for any given type of Ilmenite and coal.

1.8.1 Objective of the Thesis

The objective of the present work is to develop a virtual simulator of the rotary kiln which will predict under steady state conditions the gas and solid flows, concentration profiles and thermal profiles along the axial length of the rotary kiln

during the carbothermal reduction of Ilmenite for a wide range of process conditions and reductant characteristics. To achieve this objective it is essential to construct a comprehensive mathematical model of the carbothermal reduction of Ilmenite in the rotary kiln reactor. This can be logically divided into the following three major modules.

1. A Mathematical model for the carbothermal reduction of Ilmenite at conditions prevailing in a commercial rotary kiln reactor to arrive at appropriate rate equations for the reduction kinetics
2. A mathematical model of the pneumatic coal injection process from the discharge end of the kiln to arrive at the carbon load in the solid bed and thermal load in the free board of the rotary kiln
3. A comprehensive 1-D model for predicting the heat and mass flows along the axial length of the kiln by incorporating modules 1 & 2.

A quantum of effort has been put in to apply various kinetic models to understand the mechanism of carbothermal reduction of Ilmenite. Since the industrial rotary kiln reactor involves many complex physical and chemical processes apart from the reduction reaction, results from lab-scale experiments can hardly replicate the realistic process in the rotary kiln. As the aim of the present work is to model the actual rotary kiln process it was opted to use reported experimental data from industrial rotary kilns for validation and analysis of the proposed kinetics model. Practically, in the process of carbothermal Ilmenite reduction process carried out in a rotary kiln reactor, a kinetic equation with the best fit to experimental conversion data is essential for the process design and modeling. The first module is aimed at providing a simple model equation to describe the apparent kinetics of the carbothermal reduction of

Ilmenite in rotary kiln reactor, which in turn can be used in the comprehensive model of the kiln.

The pneumatic coal injection process from the discharge end of the rotary kiln is a significant feature of the industrial carbothermal reduction process. In this process, some part of the required coal is injected along with air from the discharge end of the kiln. This not only supplements the heat availability but also helps to maintain a reducing atmosphere to prevent reoxidation of the metallic iron and to control the degree of reduction and carbon content of the product. The optimum values for particle size distribution and the feed to discharge end coal ratio are essential for increasing the efficiency of this process. But no systematic study in this direction has been reported in the literature. In recent times, with the advances in computing power and numerical algorithms computational fluid dynamics (CFD) is becoming a feasible tool to analyze mathematically complicated processes like coal combustion in furnaces.

The objective of the second module is to model the pneumatic coal injection and combustion process in the rotary kiln during carbothermal reduction of Ilmenite using a multiphase Eulerian-Lagrangian CFD approach where the gas phase is treated as a continuous phase and the pulverized coal particles are tracked in the flow field in a Lagrangian way. All the relevant phenomena like coal devolatilization, homogeneous volatile combustion, heterogeneous char reaction, particle dispersion and radiation are included in the mathematical model proposed. The commercial CFD code ANSYS-CFX 11.0 is used to obtain the numerical results. The three dimensional results for carbon load and thermal load are radially and azimuthally averaged to yield axial profile.

These two modules are then incorporated in the one dimensional comprehensive model of the heat and mass flows in the rotary kiln under steady state conditions. The model is built upon the basic principles of conservation of heat and mass along with solid and gas phase chemical reactions. Axial movements of the solid bed are assumed to be in plug flow and determined by the parameters of the kiln design and speed of rotation. Thermal energy conservation is fulfilled through a balance between various heat generation and heat losses coupled with conservation of the mass of various species.

1.8.2 Thesis Framework

The thesis is divided into three sections based on the three major modules of the present work. Each section forms a separate chapter (Chapters 2, 3 & 4). Since the literature review for the three modules possess no interdependence as such, the exhaustive literature review for each module is presented as part of the corresponding Chapter, instead of compiling a separate chapter for literature review. Chapter 5 presents the concluding remarks of the present study and the scope for future work in this context.

Chapter 2

KINETICS OF CARBOTHERMAL REDUCTION OF ILMENITE

2.1 Introduction

This chapter includes the details of research work carried out to elucidate the reaction kinetics of the carbothermal reduction of Ilmenite in a rotary kiln reactor. The results of kinetic studies form major input to the comprehensive one dimensional model described in Chapter 4 of this thesis.

Carbothermal reduction is a desirable process for recovering metals from metal oxides and ores due to the low cost and availability of carbon. The metal oxides undergoing reduction should be less stable than CO according to thermodynamics, while the metal must be a weak carbide-former. An oxide of metals such as Iron, Magnesium and Manganese possesses these characteristics and hence are efficiently recovered from their oxides using the carbothermal route. The general carbothermal reduction equation can be written as

$$M_xO_y(s) + yC(s) \rightarrow xM(s) + yCO(g) \tag{2.1}$$

Carbothermal reduction of iron oxides is the oldest and historically important technological process. The mechanism of this reaction was a subject of numerous studies during the past few decades. Several mechanisms have been proposed so far but the oldest and most widespread is the mechanism of oxide reduction through gaseous intermediates CO and CO_2 in accordance with the following reactions:

Formation of the reducing gas:

$$CO_2 + C \rightarrow 2CO \tag{2.2}$$

Removal of oxygen from the ore:

$$Fe_nO_m + mCO \rightarrow nFe + mCO_2 \tag{2.3}$$

According to this two-stage mechanism, carbon must pass through the intermediate stage of carbon monoxide formation (Boudouard reaction). Since the carbon-oxide reaction proceeds by a CO gas generation and oxidation step, the environmental condition that influences the Boudouard reaction will have a significant effect on the reaction rate. Reduction was originally assumed to be governed by a chemical reaction on a narrow front separating iron, or an intermediate oxide, from a core of unreacted material (McKewan (1960)). Later the clear evidence of diffusion was reported (Olsson and McKewan (1970)). Although these earlier models fitted experimental data quite well, they were not good enough to predict the reduction in a porous pellet. The mathematical analysis of Sohn and Szekely (1972a) gave an expression where the overall reaction is controlled by the coupled reaction of the reduction of the oxide with CO together with the oxidation of carbon.

An empirical first-order rate expression for the reduction reaction was proposed by Von Bogdandy and Engell (1971) and later modified by Venkateswaran and Brimacombe (1977) as

$$r_R = 4.48 \times 10^{-2} A_p \exp(-E_R / RT_s)(1-F) M_{Fe} \frac{p^R_{CO_2} - p_{CO_2}}{p^R_{CO_2}} \tag{2.4}$$

The rate of oxygen removal as a function of the reactivity of the ore and fuel, and the temperature and degree of reduction was obtained by them. Fruehan (1977) determined the effect of pressure, particle size and the amount of carbon on the rate of reduction of iron oxide by different types of coal. He suggested that the type of carbon used greatly influences the rate of reduction.

The carbothermal reduction of Ilmenite is an extremely promising method for producing synthetic rutile from Ilmenite. Most of the studies on Ilmenite reduction kinetics show that problems faced by the researchers are more or less similar to those in iron oxide reduction studies. Rate of carbothermal reduction of Ilmenite carried out using various combinations of Ilmenite ore and coal has been reportedly dependent on the nature of the ore and coal used. Hence a technique to independently access the reactivity of the ore and coal is essential for the optimal selection and use of the raw materials.

2.2 Literature Survey

A considerable amount of literature has been published on the kinetics of Ilmenite reduction. A number of authors conducted experimental study using either pellets of Ilmenite and coal or graphite or mixtures of Ilmenite and coal/char in crucibles (Hussein, Kammel and Winterhager (1967), Donnelly *et al.* (1970), EI-Guindy and Davenport (1970), Wouterlood (1979), Sucre, Ablitzer and Brimacombe (1982), Gupta *et al.* (1987, 1989, 1990, 1991), El-Tawil, Morsi and Francis (1993)). These studies are of interest but of limited use in determining a true rate for Ilmenite reduction reaction.

Hussein and EI-Tawil (1967) studied the kinetics of reduction of Egyptian natural Ilmenite with H_2 in the temperature range 500^0C to 1000^0C. Donnelly *et al.* (1970) studied the reduction of natural Ilmenite with both H_2 and CO. They used samples of between 10 and 50 grams packed into the reaction tube. The reaction rate data reported was for the case where the reactant gas was passed down through the bed of Ilmenite. The reaction rate was determined from weight loss measurement as a function of time.

El-Guindy and Davenport (1970) carried out the solid state reduction kinetics of synthetic Ilmenite with Graphite by thermo gravimetric analysis. They observed that the reduction initiated around 860^0C at the contact points between Ilmenite and graphite. For temperatures up to 1200^0C the reduction was concluded to be primarily a result of solid-solid reaction between graphite and Ilmenite. Above 1020^0C, the reduction rate increased dramatically. The increased rate was concluded to be the result of dominance of gaseous reduction of Ilmenite by CO. The reduction rate was then related to the rate of CO supply to the Ilmenite by the Boudouard reaction.

Poggi, Charette and Rigaud (1973) studied the kinetics of reduction of synthetic and natural Allard Lake Ilmenite using H_2 and CO. The samples were cut into various shapes and polished. Reduction was carried out using CO and H_2. The rate of reaction was determined by observation of the advance of the reaction interface and measurement of progressive weight loss using a micro balance. They concluded that the reaction was controlled by chemical kinetics at the reaction interface.

Jones (1975) studied the reduction of natural Ilmenite using flowing CO and CO/CO_2 gas mixtures. Their conclusion was that, within the accuracy of the

experimental results, gas-film diffusion control could account for the observed rate values as a function of gas flow rate. They also found that when some natural Ilmenite samples were subjected to pre oxidation prior to reduction, the subsequent reduction rate increased.

Wouterlood (1979) conducted experiments to investigate the reduction of natural and pre-oxidised Ilmenite with carbon at temperatures between 1173K and 1473K (900^0C-1200^0C). The reaction was carried out in the atmosphere produced by the gaseous reaction products and the degree of reduction was determined from the CO and CO_2 contents of the product gas, as measured by chemical absorption and continuous infrared analysis. Solid reaction products were analyzed chemically, by X-ray diffraction and by magnetic balance. The reaction was found to consist of a fast first stage representing the reduction of ferric to ferrous iron, and a slower second stage in which ferrous iron was reduced to metallic iron.

Hammond and Taylor (1982) observed the reduction of synthetic Ilmenite-hematite and spinel-magnetite solid solutions using CO/CO_2 gas mixtures between 900^0C and 1100^0C. Sucre, Ablitzer and Brimacombe (1982) studied the reduction of a New Zealand and a Florida sample of natural Ilmenite and a New Zealand sample of titaniferous iron sand in a rotary reactor using pre-charred coal. The tests were designed to simulate reduction in a rotary kiln. The kinetics of the reaction was modeled on the basis of the rates of Boudouard and Reduction reactions. Gupta *et al.* (1987, 1989) investigated the reduction of Ilmenite with carbon.

Gupta *et al.* (1990) studied the effect of preheating on the kinetics of reduction of Ilmenite with carbon at 1000^0C and 1050^0C. Preheating changed the Ilmenite and pseudorutile phases into pseudobrookite solid solutions and rutile which as in the case of Ilmenite being oxidized to rutile, increased the subsequent reduction rate considerably.

Merk and Pickles (1988) studied the reduction of natural Allard Lake Ilmenite by carbon monoxide. The Ilmenite was crushed and ground to less than 44 *μm* and then briquetted into 13 *mm* diameter cylinders. The briquettes were then sintered and a single pellet was suspended in a vertical tube furnace within a chromel basket. A gas flow rate of 0.8 litre min^{-1}, at NTP, was used. This was considered sufficient to overcome any mass transport resistances at the particle surface. The gas flow rate was no greater than that used by number of other workers. The influence of the wire basket is likely to have caused some mass transport problems. They found that the rate of reduction increased with temperature to a maximum value at around 1000^0C. At the higher temperatures the metallic iron was observed to migrate to the Ilmenite grain boundaries and retard further reduction of Ilmenite.

Briggs and Sacco (1991) studied the reduction of synthetic Ilmenite in H_2 gas at temperature between 550 and 1080 ^{0}C. The sample was prepared as disks with a diameter of 12.7 mm. These disks were suspended in nichrome wire basket within a vertical tube furnace. Gas flow rate of up to 4.5 litre min^{-1}, at NTP, were used. When Briggs and Sacco (1991) studied their rate data they found that the low temperature initial rate values fell on a line of higher activation energy than the high temperature initial rate data.

The initial reduction rate was used for activation energy determination in order to avoid the influence of intra particle diffusion on the reduction rate. They showed, by temperature measurements of reacting pellets, that the endothermic heat of reaction decreased the temperature of the reacting disks by only 4^0C to 5^0C at the highest reduction rate. Temperature differences were thereby eliminated as a possible cause of the non-linearity in the activation energy plots. The use of binary reduction gas mixtures to infer effective diffusion coefficients within the particle was a significant advance. Ilmenite reduction has the added complexity of the porous titanate matrix. Significant error was reported for Briggs and Sacco's porosity measurements in the iron film.

Zhao and Shadman (1990), Satoshi and Atsushi (2001), Eungyeul and Oleg (2003) *etc.* carried out investigations of Ilmenite reduction by carbon monoxide. They observed that the reduction rate increased with increasing temperature. Though the rate and the degree of reduction depended on the formation of a metallic shell of iron which inhibited the transfer of CO to the reaction zones, titanium had a strong effect on the mechanism and rate of reduction of iron oxides.

Carbothermic reduction of Ilmenite and rutile was investigated by Welham and Williams (1999) at temperatures up to 1500^0C in which the reduction of rutile was found to proceed through a series of oxides until the formation of Ti_3O_5 which was described as a stable oxide phase. El-Tawil, Morsi and Francis (1993) studied the solid state reduction of Ilmenite by carbon under nitrogen at temperatures upto 1200°C. They suggested that the reduction of titanium dioxide towards its lighter oxides occurs in parallel with the reduction of iron oxides.

Welham and Williams (1999) suggested that the dissolution and rapid diffusion of carbon in the metallic iron will ensure an abundance of carbon at the interface and the solid state diffusion of oxygen from unreacted Ilmenite to the reaction interface becomes the rate controlling step.

Pesl and Eric (2002) investigated carbothermic reduction of Fe_2O_3–TiO_2–M_xO_y oxide mixtures under both Ar and CO atmospheres at smelting temperatures. Wang and Yuan (2006) investigated the reduction of Ilmenite by graphite under argon atmosphere using thermo gravimetric analysis at temperatures from 850^0C to 1400^0C. They observed the reaction rate and degree of reduction increasing with temperature. Iron, Ilmenite, rutile, reduced rutiles and carbon were the phases of reduced products below 1200^0C except that the reduced rutiles were absent at 900^0C. The kinetics was also investigated and it was found that the rate-controlling steps were different in the different temperature ranges.

Kucukkaragoz and Eric (2006) studied the solid state reduction of a natural Ilmenite at 1250^0C to 1350^0C. Experiments were conducted using a thermo gravimetric analyzer and samples at different stages of reduction were examined using optical microscopy, image analyzer, X-ray diffraction studies and Scanning Electron Microscopy. Reduction was found to take place topochemically from Fe^{3+} to Fe^{2+}, Fe^{2+} to Fe and Ti^{4+} to Ti^{3+} and from Ti^{3+} to Ti^{2+}. They observed the metallic phase consisting mainly iron as globules dispersed within the simultaneously formed secondary oxide phase at 16% reduction.

Sai (2008) used the experimental data of Sucre (1979) to identify the controlling mechanisms of reduction reaction of Ilmenite. The five models chosen for evaluation are the unreacted core model for spherical particles of unchanging size, Ginstling model, Jander's model, Prout Tompkin model and Avarami model.

The results indicated that the rate controlling steps are solid-solid reaction during initial stages and diffusion of carbon monoxide through product layer during later stages of reaction. The activation energies for the two heterogeneous reactions are estimated to be 25 and 35 kcal/mol for solid-solid and gas solid reactions, respectively.

X-ray diffraction and spectroscopic studies of the Carbothermal reduction of Ilmenite has been conducted by many researchers such as El-Tawil *et al.* (1993), Jones (1973), Merk and Pickles, (1988), Zhang and Ostroviski, (2002), Zhao and Shadman, (1990). Fe-Mössbauer spectroscopy was employed to analyse the feedstock and product of the carbothermal reduction of ferrous pseudobrookite (Teller *et al.* 1990). Saensunona *et al.* (2008) has demonstrated ^{57}Fe-Mössbauer spectroscopy as a sensitive phase analysis tool for control of the Ilmenite reduction process in a commercial rotary kiln. He showed that the feed material is predominantly Pseudo rutile and rutile and the key phases are confirmed to evolve in two stages, namely the formation of Ilmenite from Pseudo rutile ($Fe^{3+} \rightarrow Fe^{2+}$) followed by the reduction of Ilmenite into metallic iron and rutile ($Fe^{2+} \rightarrow Fe$) via ferrous Pseudo brookite

Recently Dewan *et al.* (2010) carried out investigation on the Carbothermal reduction of a primary Ilmenite in different gas atmospheres like hydrogen, argon, and helium. Ilmenite and graphite were uniformly mixed and pressed into pellets. Reduction was studied in isothermal and temperature-programmed reduction experiments in a tube reactor with continuously flowing gas. CO, CO_2, and CH_4 contents in the off-gas were measured online using infrared sensors. The phase composition of reduced samples was characterized by X-ray diffraction (XRD). Oxygen and carbon contents in reduced samples were determined by LECO

analyzers (LECO Corporation, St. Joseph, MI). The main phases in the Ilmenite concentrate were Ilmenite and Pseudo rutile. The reaction started with the reduction of Pseudo rutile to Ilmenite and Titania, followed by the reduction of Ilmenite to metallic iron and Titania. Titania was reduced to Ti_3O_5 and even more to Ti_2O_3, which was converted to titanium oxycarbide. Reduction was faster in hydrogen than in helium and argon, which was attributed to involvement of hydrogen in the reduction reactions.

The review of the literature on Ilmenite reduction kinetic studies shows that problems similar to those experienced by researchers in Iron oxide reduction have been experienced in measuring the reduction rate of Ilmenite. The reduction of natural Ilmenite has been demonstrated to be complicated by a number of factors. Samples of natural Ilmenite contain a wide variety of individual particle morphologies. They are much less homogeneous than pellets of iron oxide. The weathering process also results in extensive pitting and crackling of some particles. Particle shape factors are variable within a typical sample. Morphology of the reduced Ilmenite particle is dependent on the morphology of the parent Ilmenite particle. Transport of iron during reduction adds complexity to the reduction process. Iron tends to migrate to the outside of the grain as reduction progresses.

Modeling of carbothermal reduction of Ilmenite in commercial kiln also requires an understanding of the processes occurring in the solid bed of the kiln. All these complexities point to the fact that developing a phenomenological model of Ilmenite reduction is extremely impractical and it requires customization from process to process and reductant to reductant. Therefore, an alternative is the construction of semi-empirical model tailored to kinetic data representative of the

conditions prevailing in a commercial Ilmenite reduction process. Practically, in the process of carbothermal reduction of Ilmenite in a rotary kiln reactor, a kinetic equation with the best fit to experimental conversion data is very useful for the process design and modeling.

Therefore in the present work, it is aimed to arrive at a simple model equation to describe the apparent kinetics of carbothermal reduction of Ilmenite, by determining the kinetic parameters using the conversion data available in literature. This is achieved by applying various kinetic models to the reported data for Ilmenite reduction in commercial rotary kilns. A considerable amount of experimental reduction data for Ilmenite reduction in commercial rotary kiln reactor had been summarized by Nicholson (1995). Initially selected solid state kinetic models for gas solid reactions were tested using these data. Since any one of these models does not give an appreciable fit to the experimental data, other models based on various mechanisms were developed and results compared with the experimental data (Nicholson (1995)).

2.3 Model Development

2.3.1 Identification of Control Mechanism for Kinetics

From the literature survey, it can be observed that two broad classes of reactions are possible for carbothermal reduction of Ilmenite in a rotary kiln reactor *viz.*,

(a) Reaction through solid-solid contacts

$$FeTiO_3 + C \rightarrow Fe + TiO_2 + CO \tag{2.5}$$

(b) Reaction through gaseous intermediates CO and CO_2

$$FeTiO_3 + CO \rightarrow Fe + TiO_2 + CO_2$$

$$C + CO_2 \rightarrow 2CO \qquad (2.6)$$

In literature there are two methods available in understanding the reactions kinetics: (i) at investigating reaction sequence and (ii) kinetics of reduction. Kinetic analysis of experimentally determined reaction rate data often provides a simple and effective model equation for representing the reaction. Carbothermal reduction of Ilmenite comes under the class of non catalytic gas solid reactions. In general these reactions can be represented as:

$$aA(g) + bB(s) \rightarrow cC(g) + dD(s) \qquad (2.7)$$

The overall fluid-solid reaction involves a combination of the following individual steps:

- Transfer of the fluid reactants and the fluid products between the bulk fluid and the external surface of the solid particle.
- Diffusion of the fluid reactants and the fluid products within the pores of the solid, if the solid contains open porosity.
- Chemical reaction between the fluid reactant and the solid at the fluid-solid interface.
- Transfer of the reaction heat within the solid.
- Transfer of heat between the external surface of the solid and the surroundings by convection and radiation.
- Changes in the structure of the solid due to chemical reaction and heat.

The rate-controlling step can change depending on reaction conditions, and thus the rate information obtained under a given set of conditions may not be applicable under another set of conditions. Furthermore, there may not be a single rate-controlling step because several steps may have comparable effects on

determining the overall rate. The relative importance of these steps could also change in the course of the reaction. Therefore, understanding how the individual reaction steps interact with each other is important in determining not only the rate-controlling step under given reaction conditions but also whether more than a single step must be considered in expressing the rate over the entire duration of the reaction.

The global kinetics of non-catalytic gas solid reactions is determined by the interaction of resistances associated with surface kinetics, product layer diffusion, pore diffusion, and mass transfer between the bulk gas and external surface of the solid. The reaction system is complex because the relative importance of these resistances may change during the reaction. For example, the mass transfer resistance is most important at the start of the reaction when the global rate is maximum. However, there are many instances in which the mass transfer resistance is negligible throughout the reaction. In contrast, the product layer diffusion resistance, which must be zero at the start of the reaction, increases as the reaction progresses. Under appropriate conditions, this resistance may also be negligible throughout. In terms of single resistances, only the surface reaction resistance can dominate throughout the reaction.

As a first step, the unreacted core model for spherical particles of unchanging size as developed by Yagi and Kunii (Levenspiel (1999)) is used in the present work to understand the kinetics of carbothermal reduction of Ilmenite. According to this model, if diffusion through gas film controls, then

$$\frac{t}{\tau} = X \tag{2.8}$$

If diffusion through the product layer controls then

$$\frac{t}{\tau} = 1 - 3(1 - X)^{2/3} + 2(1 - X) \tag{2.9}$$

If chemical reaction at interface controls then

$$\frac{t}{\tau} = 1 - (1 - X)^{1/3} \tag{2.10}$$

The experimental reduction data reported by Sucre (1979) for the solid state reduction of Ilmenite using coal as reductant in a rotary kiln reactor is used in the above equations to determine the rate limiting step. In the above equations, X denotes the conversion, and τ denotes the time required for complete conversion. Figures 2.1 and 2.2 show the kinetic plots for equations (2.9) and (2.10) respectively for a typical data of Sucre (1979).

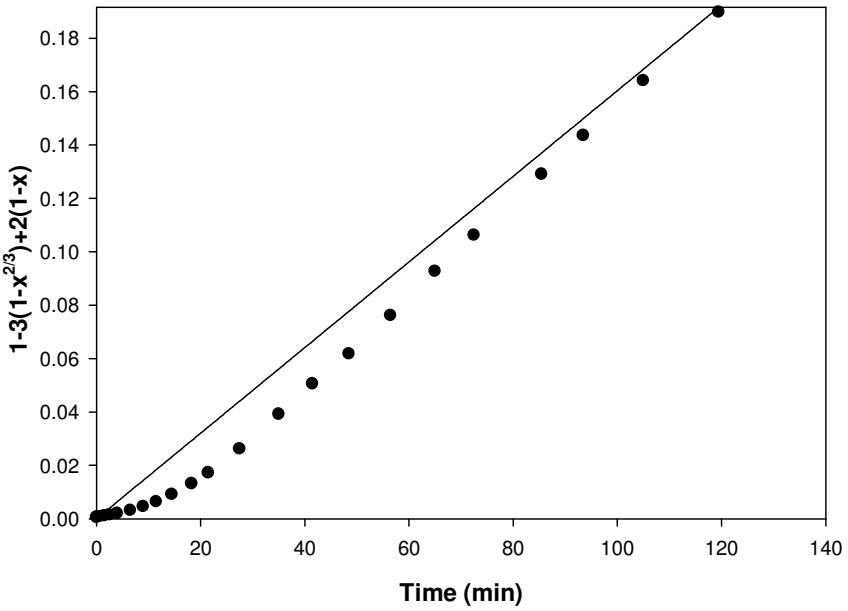

Figure 2.1 Kinetic Plot Corresponding to Equation (2.9)

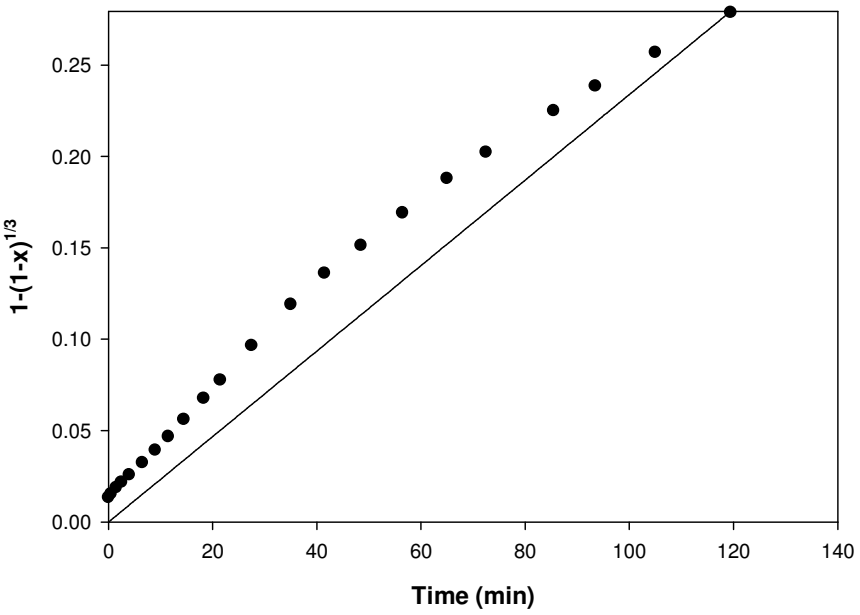

Figure 2.2 Kinetic Plot Corresponding to Equation (2.10)

The above figures show that the kinetics models based on the shrinking unreacted core mechanism do not fit to the experimental data considerably. Hence it would be appropriate to consider other mechanisms and kinetic models to simulate the carbothermal reduction of Ilmenite. In all the above plots, it can be noted that the reaction reaches a stage after which the mechanism changes altogether. In other words, the results of such studies lead to the conclusion that any single controlling step cannot be attributed to the reduction reaction as a whole. Thus the overall controlling mechanism of the reaction remains unclear.

Sohn and Szekely (1972b) developed a general structural model for the description of non-catalytic gas solid reactions, which allows for spherical and flat plate like pellets, made up of spherical or flat plate-like grains. The numerical solution of the dimensionless form of the governing equations results in a plot of the dimensionless time to achieve complete reaction against a gas solid reaction modulus, which is valid for all the geometries considered. They formulated the

following equation incorporating chemical kinetics, diffusion through porous product layer, and external mass transfer as well as the three basic geometries of the solid:

$$g_{F_p}(X) + \sigma_s^2 \left[p_{F_p}(X) + 4X / Sh^* \right] = t^* \tag{2.11}$$

where F_p is the shape factor (=1,2 or 3 for a slab, a long cylinder or a sphere) and t^* and σ_s are the dimensionless time and gas solid reaction modulus respectively. The expressions for g_{F_p} and p_{F_p} are given as

$$g_{F_p}(X) = 1 - (1 - X)^{1/F_p} \tag{2.12}$$

$$p_{F_p}(X) = \begin{cases} X^2 & \text{for } F_p = 1 \\ X + (1 - X)\ln(1 - X) & \text{for } F_p = 2 \\ 1 - 3(1 - X)^{2/3} + 2(1 - X) & \text{for } F_p = 3 \end{cases} \tag{2.13}$$

It has been shown by Szekely *et al.* (1976) that chemical reaction controls the overall rate when $\sigma_s^2 <$ 0.1 or 0.01 depending on the range of tolerable error (<10% or <1%, respectively). On the other hand, pore diffusion and external mass transfer control the overall rate (g*Fp*(X) becomes negligible) when $\sigma_s^2 >$ 10 or 100. The asymptotic expression for a spherical pellet can be written as

$$1 - (1 - X)^{1/3} + \sigma_s^2 \left[1 + 2(1 - X) - 3(1 - X)^{2/3} \right] = kt \tag{2.14}$$

The parameter σ_s^2 is defined as

$$\sigma_s^2 = \frac{k_c}{2D_e}\left(\frac{V}{A}\right) \tag{2.15}$$

where k_c is the interface reaction constant, D_e is the effective diffusivity of the reactant through the product layer, V and A are the volume and surface area of the pellet. Here k can be treated as the apparent rate constant. As there is little or no information regarding the product morphology, it is not feasible to evaluate the actual effective diffusivity and hence the value of σ_s^2. Therefore the method of curve fitting was used for finding the approximate values of σ_s^2. In the present study, sets of experimental data for Ilmenite reduction reported by Sucre (1979) and Nicholson (1995) are fitted to equation (2.14) by varying the values of σ_s^2. The results obtained are shown in Figures 2.3 and 2.4. The slope of the curve gives the apparent reaction constant.

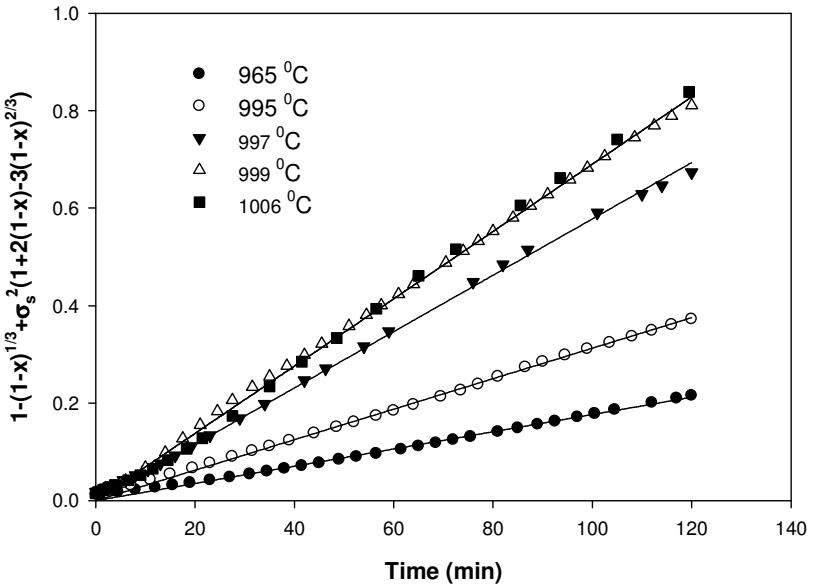

Figure 2.3 Conversion Data of Sucre (1979) Fitted to Equation (2.14)

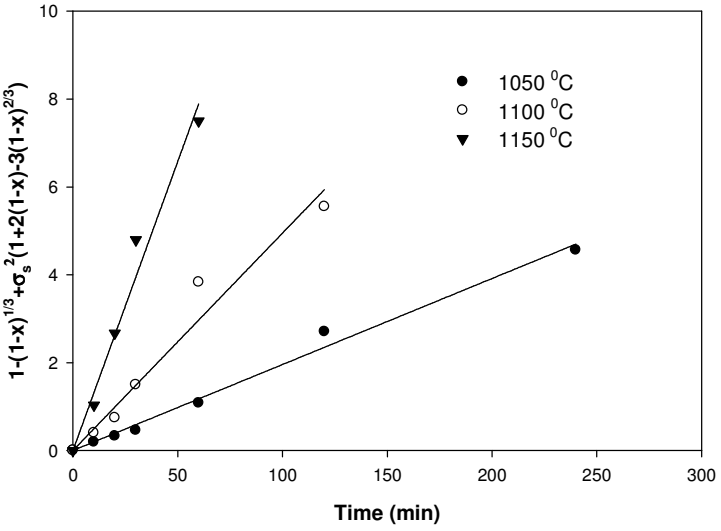

Figure 2.4 Conversion Data of Nicholson (1995) Fitted to Equation (2.14)

The values of σ_s^2 and k along with the corresponding regression coefficient are depicted in Table 2.1 for both the sets of data. The reduction data reported by Sucre (1979) lies in a more or less lower temperature range of 965^0C to 1006^0C. It can be noted that in this temperature range, the reduction data gives perfect fit to the mixed control equation.

Table 2.1 Fitting Parameters for Mixed Control Mechanism.

Nicholson (1995)	Temperature (^{0}C)	σ^2	k	R^2
	1050	5.02	0.008	0.973
	1100	7.02	0.049	0.960
	1150	11.02	0.131	0.973
Sucre (1979)	965	0.17	0.001	0.996
	995	0.10	0.003	0.997
	997	0.71	0.005	0.998
	999	2.69	0.006	0.999
	1006	2.96	0.007	0.997

The values of σ_s^2 also lie in the ranges of chemical reaction and pore diffusion control range. The reduction data of Nicholson (1995) which is in a higher temperature range of 1050^0C to 1150^0C, also fits to the mixed control equation but to a lesser degree as compared to the low temperature data. The value of σ_s^2 is also towards the higher side indicating product layer diffusion taking control of the reaction. This can be explained by the comparatively higher reduction rate at this temperature, which in term augments the formation of a less pervious metallic iron layer (Welham and Williams (1999)) as compared to the iron globule formation (Kucukkaragoz and Eric (2006).

Many researchers (Donnelly *et al.* (1970), El-Guindy and Davenport (1970), Gupta *et al.* (1989, 1990), Kucukkaragoz and Eric (2006)) observed the formation of iron globules during Ilmenite reduction and noted that as reduction progresses the iron globules tend to coalesce and segregate to the particle surface thus forming a metallic iron shell covering the oxide phase. This process of coalescence of iron globules followed by segregation to the boundary through the titanate matrix is the process which differentiates Ilmenite reduction from iron oxide reduction.

The activation energy values calculated using from the apparent reaction constants of the above sets of data are 32.76 and 45.53 kcal/mol respectively which also supports the above inference. Figure 2.5 shows the variation of reduction rate constant k_{ore} with respect to the coal/Ilmenite ratio β.

The linear dependence of k_{ore} on β corroborates the significance of coal/Ilmenite ratio in carbothermal reduction of Ilmenite in rotary kiln reactors. It

indicates that the dependency equation can be judiciously used for fixing the coal/ore ratio at a given temperature for the industrial rotary kiln reactors.

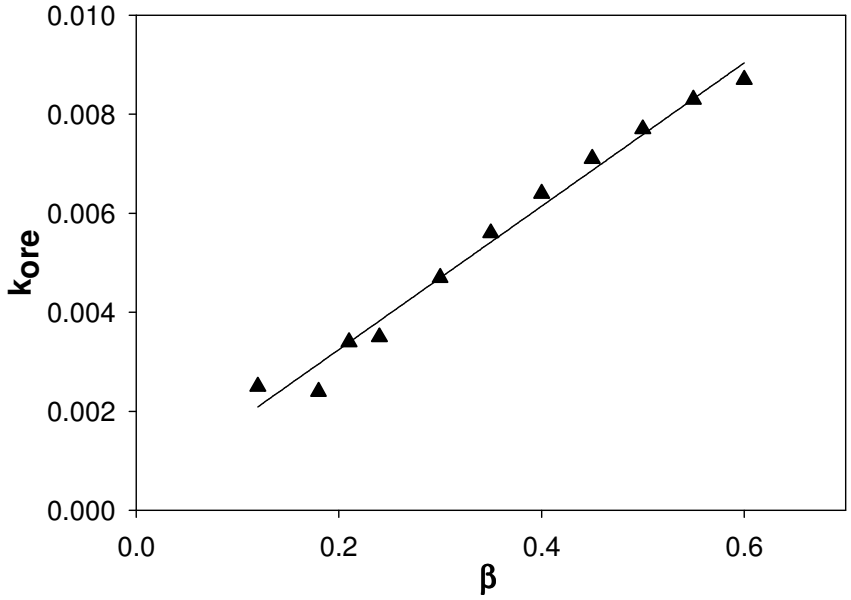

Figure 2.5 Variation of reduction rate constant k_{ore} with coal/Ilmenite ratio β

2.3.2 Mathematical Model for the Carbothermal reduction of Ilmenite

Though the above described procedure gives an apparent reaction constant for carbothermal reduction of Ilmenite, the factors such as the role of Boudouard reaction in the overall rate of reduction cannot be assessed based on this. There is a consensus among researchers that the Boudouard reaction is the controlling step on the overall carbothermal reduction of metal oxides like Iron oxide and Ilmenite. However, the overall rate of reduction has been observed to increase with increasing carbon content, increasing carbon surface area, and presence of Boudouard reaction catalyzing agents (including metallic iron). These effects suggest that there is a limitation to the degree of control of the Boudouard reaction, which is not yet fully understood. Thus it is still difficult to kinetically describe the reaction system. Though there have been tremendous amount of

research work carried out in the areas of iron ore reduction as well as Ilmenite reduction, the dependence of reduction rate on factors such as coal/ore ratio and type of carbon source used has not yet been explained satisfactorily.

The overall kinetics of the carbothermal reduction reaction has been found to depend on both the reducibility of Ilmenite and the reactivity of coal. The raw material characterization such as degree of weathering, composition, rank of precursor coal plays a vital role in deciding the overall kinetics and extent of reduction. For a given Ilmenite/coal combination, the reaction temperature and Ilmenite/coal ratio plays the crucial role whereas minor effects are due to size distribution, mixing and segregation as well as reactor design and operating characteristics. In the present work these issues are addressed by modeling the overall reduction reaction using two independent approaches viz. the Combined Reaction Model and the Semi empirical Model.

2.3.2.1 Experimental Work

The experimental studies on Ilmenite reduction at lab scale are aimed at prototyping the physical condition prevailing in a commercial Ilmenite reduction kiln and thereby predicting the kinetic data with minimum error. Hence the design of a test procedure is of prime importance. Different test procedures were developed by researchers all over the world. CSIRO developed the Boat Reducibility Test (Nicholson (1995)), in which a molybdenum boat was used to hold Ilmenite and char within an alumina work tube with one open end and one quenched end. The open end was placed in a furnace tube heated by silicon carbide elements. CO gas was purged over the surface of the charge. The sample could be allowed to react for different lengths of time by arresting the reaction by

rapid cooling of the sample upon rapidly withdrawing the boat from the hot open end to the quenched end of the work tube. Good reproducibility of results was achieved with this procedure. But the disadvantage of the procedure was its lack of simplicity.

To overcome this, the Rotating Pot Test procedure was developed (Nicholson 1995). The procedure was carried out in a top loading muffle furnace. A cylindrical pot, rotating at a set speed on two rollers, was used to hold Ilmenite and char. Furnace was heated by silicon carbide elements. A sample of about 3 g of solid was taken from the flowing bed by inserting a lance and rapidly cooled upon removing from the furnace to prevent oxidation of metallic iron. The sample is screened to separate from char and analyzed for extent of metallisation. Sampling of the bed done in every 15 minutes after the furnace temperature reached 950 ^{0}C. 12 to 13 samples were taken during one reduction run.

For the present study, electrically heated salvis tube reactor is used as a simulator for the carbothermal reduction behavior of Ilmenite in a commercial rotary kiln. The reactor tube is fabricated out of SS 316 steel and has an effective volume of 2240 cc for the charge. The reactor tube after loading is fastened to a rotating assembly with an inner rigid tube frame work with provision for temperature measurements and purging inert gas. The entire set up rests on a movable platform on rails and is capable of moving such that it dovetails into a horizontal tube furnace. Adequate set point control is provided to maintain temperature at ± 5 ^{0}C. After the end of the preheating and reaction period, the carriage containing the reactor tube withdraws from the furnace and reaches the farthest point so that water quenching may be carried out. In this manner, the entire operation is programmed and repeated with high accuracy. Advanced

features inherent in the design include programmed logic for heating and water quenching automatically, provision for gas sparing during and after the reduction reaction.

A suitable combination of leco char and fresh Ilmenite ore was loaded in the rotary salvis tube reactor. The reactor tube after loading is fastened to a rotating assembly with an inner rigid tube framework. The entire setup was moved into a furnace at 1000^0C. After the reactor reached 1000^0C the reduction of Ilmenite was recorded for every 30 minutes up to 2 hours. After the reaction, the furnace is switched off and the carriage containing the reactor is taken out of the furnace and quenched with water in order to bring the reactor to room temperature.

After water quenching, the contents of the reactor tube are removed and by employing a magnetic separator, metalized Ilmenite is removed from the reacted coal and weighed. Metalized Ilmenite is then subjected to chemical analysis to obtain total iron and percentage of metallisation. The conversion data obtained by these experiments are used for arriving at appropriate rate equations for overall reduction equation for carbothermal reduction of Ilmenite.

2.3.2.2 Combined Reaction Model

The first approach for modeling the overall reduction reaction is a combined reaction model for the coupled reactions of Ilmenite reduction and Boudouard reaction. The model is inspired by the combined reaction model used by Fortini and Fruehan (2005) for studying the rate of reduction of ore carbon composites. The apparent reaction rate constants calculated using the mixed control mechanism as depicted in Table 2.1 are used as the rates of reduction

reaction in this model. Gaseous reduction and gasification were assumed to follow simple first-order kinetics, as follows:

Reduction rate of ore in *g/s* is expressed using equation (2.16) as

$$\frac{dm_{ore}}{dt} = k_{ore} m_{ore} \left(p_{CO} - p_{co}^{ore} \right) \tag{2.16}$$

where k_{ore} is the reaction rate constant (in *g/g.s.atm*), m_{ore} is the amount of unreacted ore, p_{CO} is the local partial pressure of CO (in *atm*), p_{CO}^{ore} is the equilibrium partial pressure of CO for the reduction reaction.

Similarly the rate of Boudouard reaction in g/s is expressed as

$$\frac{dm_c}{dt} = k_c m_c \left(p_{CO\,2} - p_{co_2}^{c} \right) \tag{2.17}$$

where k_B is the rate constant (in *g/g.s.atm*), m_c is the amount of un reacted carbon, p_{CO_2} is the local partial pressure of CO_2 (in *atm*) and $p_{CO_2}^{c}$ is the equilibrium partial pressure of CO_2 for gasification.

A combined rate equation for the overall reaction in a mixture of Ilmenite and coal can be written as

$$\frac{dm}{dt} = \frac{M_o}{M_{ore}} k_{ore} m_{ore} \left(p_{CO} - p_{co}^{ore} \right) + k_c m_c \left(p_{CO\,2} - p_{co_2}^{c} \right) \tag{2.18}$$

where M_O, M_{ore} are the atomic weight of oxygen and molecular weight of ore respectively.

The local partial pressures of CO and CO_2 are evaluated by the equations (2.19) and (2.20) respectively.

$$p_{CO}^2 / p_t - p_{CO}(2 + \phi + p_{CO}^C / pt) = -(2 p_{CO}^C + \phi p_{CO}^{ore}) \quad (2.19)$$

$$p_{CO_2}^2 / p_t + p_{CO_2}(1 + \phi - p_{CO2}^C / pt) = p_{CO2}^C + \phi p_{CO_2}^{ore} \quad (2.20)$$

The parameter ϕ represents the relative importance of the two elementary steps of carbon oxidation and ore reduction to the overall rate of reaction.

$$\phi = \frac{M_C k_{ore} m_{ore}}{M_{ore} k_C m_C} \quad (2.21)$$

where M_c is the molecular weight of carbon.

Equations (2.17) and (2.18) are solved numerically using Runge Kutta method. From these results the rate of conversion with respect to time is obtained. The parameters required for the simulation are the equilibrium partial pressures of CO and CO_2 with carbon and Ilmenite at the desired temperature. The equilibrium partial pressure for the Boudouard reaction is calculated from equilibrium constants given by Coetsee *et al.* (2002). A total pressure of 1 atm was assumed. The question of pressure buildup during reduction is ignored as suggested by Fortini and Fruehan (2005).

Figure 2.6 shows the conversion data simulated using the combined reaction model and are compared with experimental data of Nicholoson (1995) for three different temperatures. The k_{ore} value used here, are the apparent reaction rate constants obtained by fitting the respective data to the mixed control equation mentioned in Section 2.3.1.

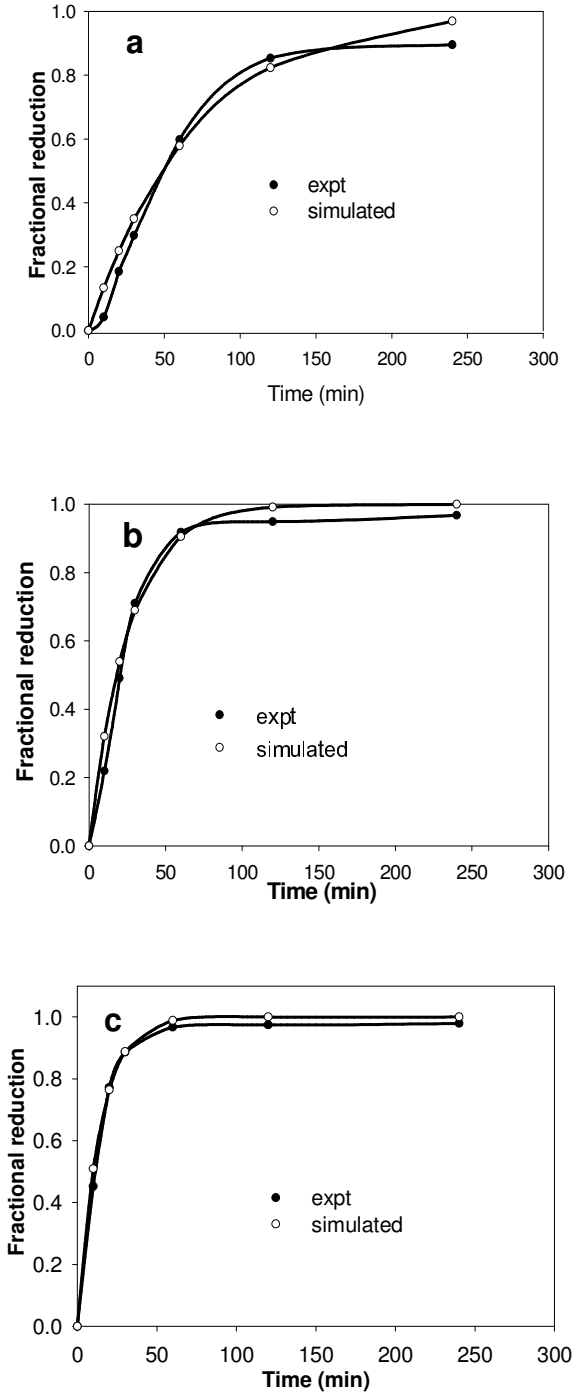

Figure 2.6 Comparison of Combined Reaction Model with Conversion Data of Nicholson (1995) (a) at 1050 ^{0}C (b) at 1100 ^{0}C (c) at 1150 ^{0}C.

Figure 2.7 shows the conversion data simulated using the combined reaction model compared with experimental data of Sucre (1979) for different coal to Ilmenite ratios.

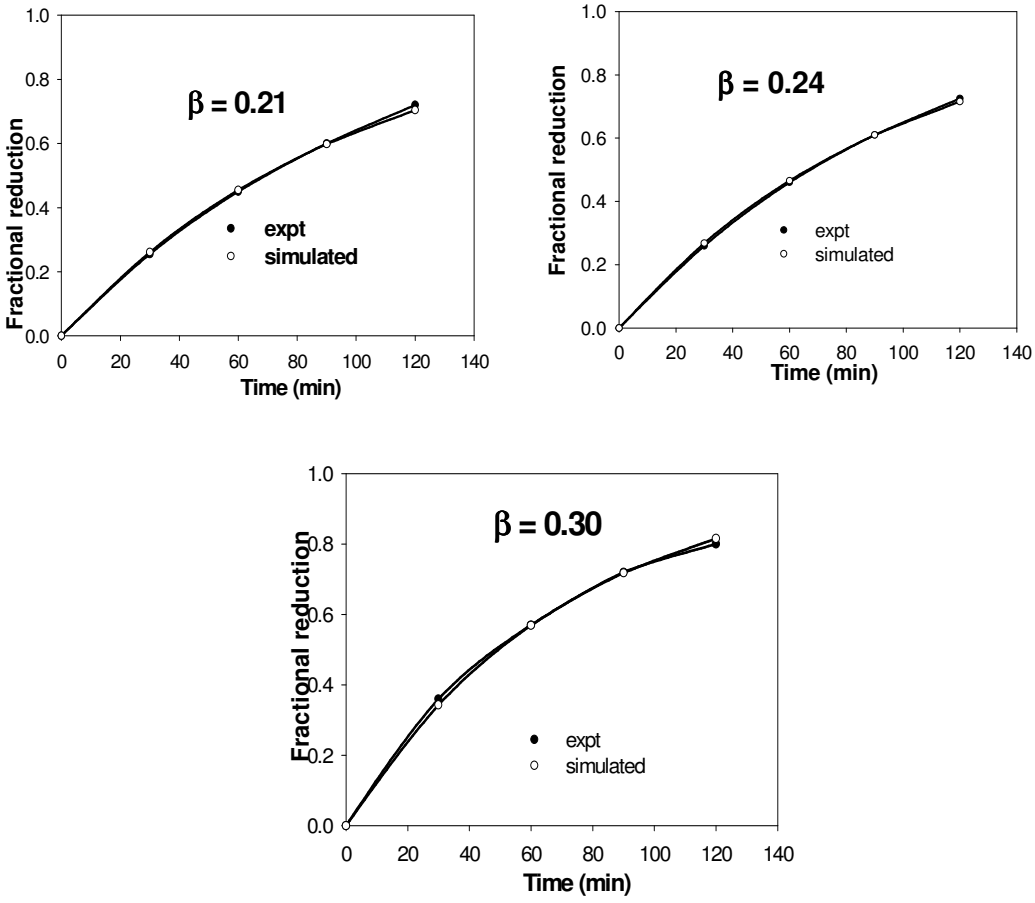

Figure 2.7 Comparison of Combined Reaction Model with Conversion Data of Sucre (1979) (a) at $\beta = 0.21$ (b) at $\beta = 0.24$ (c) at $\beta = 0.30$

From these results it can be observed that the combined reaction model is able to predict the conversion of carbothermal reduction of Ilmenite for different reduction temperatures and for different coal to Ilmenite ratios. Combined reaction model is found to be suitable when carbothermal reduction of Ilmenite coal mixtures is carried out. But converting this equation to a simpler equation to

take care of carbothermal reduction kinetics of Ilmenite in a rotary kiln is difficult and hence it was decided to develop a semi empirical model for the carbothermal reduction of Ilmenite in a rotary kiln reactor.

2.3.2.3 The Semi Empirical Model

A semi empirical model is developed to obtain reactivity parameters directly from the data obtained from salvis tube batch reactor for a given coal/Ilmenite mixture at a given temperature. A novel concept is introduced wherein carbon activity is the thermodynamic driving force for the reduction reaction. A unique relationship of carbon activity to the coal/ore ratio β is obtained which in turn is related to the partial pressure of carbon monoxide in the solid bed of the rotary kiln. The approach is similar to the approach used by Von Bogdandy and Engell (1971) for arriving at a reduction rate equation for Iron oxide reduction. Their derivation of rate equation is based on the assumption that the rate of carbon removal through Boudouard reaction is equal to the rate of oxygen removal from Iron oxide at steady state conditions. It follows, from this assumption, that only CO is produced as a result of the overall reaction. However, it is known that CO_2 is always present and is evolved as well. Hence in the present work, an empirical relation is proposed between the amount of carbon removed from coal and the amount of oxygen removed from the ore at any instant of reduction.

$$\frac{\text{Rate of Oxygen Removed from Ilmenite per unit Weight of Ilmenite}}{\text{Rate of Carbon Removed from Coal per unit Weight of Coal}} = \alpha \quad (2.22)$$

where α is ratio of oxygen removal rate to carbon removal rate and can be obtained as

$$\alpha = p_{CO} + 2p_{CO_2} \quad (2.23)$$

In equation (2.23) p_{CO}, p_{CO_2} are the partial pressures of CO and CO_2 respectively.

$$\text{Rate of oxygen removed from Ilmenite} = -\frac{\text{d[O]}}{dt} = k_R a_c \tag{2.24}$$

where a_c is the carbon activity and is related to the Boudouard reaction rate as

$$a_c = \frac{1}{k_B}\frac{P_{CO}^2}{P_{CO_2}} \tag{2.25}$$

Similarly the carbon removal rate is given by the expression

$$\text{Rate of carbon removed from Coal} = -\frac{\text{d[C]}}{dt} = k_B[C] \tag{2.26}$$

At steady state, making use of equation (2.22) the following expression can be obtained

$$k_R \frac{P_{CO}^2}{P_{CO_2}} F(X_o) = \alpha\beta \frac{k_B p_{CO_2}}{1 + k_1 p_{CO}} F(X_c) \tag{2.27}$$

In equation (2.27) k_R, k_B are the rate constants for reduction of Ilmenite by CO and Boudouard reaction respectively. k_1 is the inhibition rate constant which represents the inhibiting effects of CO on the Boudouard reaction. $F(X)$ is the conversion function which forms part of the rate equation. Initially at $X = 0, F(X) = 1$. Further it can be assumed that $p_{CO} + p_{CO_2} = 1$ which signifies the fact that the reaction proceeds entirely in an atmosphere of CO/CO_2.

With these simplifications the coupled overall rate constant can be defined as

$$k_{obs} = k_R \frac{p_{CO}^2}{p_{CO_2}} = \alpha\beta \frac{k_b p_{CO_2}}{1 + k_1 p_{CO}} \quad (2.28)$$

The overall rate constant k_{obs} is obtained from the experimental data by fitting the experimental data with the following equation for each β value

$$\frac{dX}{dt} = k_{obs}(1 - X) \quad (2.29)$$

For any β value, k_{obs} value is first obtained equation (2.29). From the corresponding β, k_{obs} values the value of partial pressure of CO is obtained using equation (2.28). Then a linear relationship between the carbon activity value and β is obtained. Once this relationship is established, for any given β value, carbon activity value is obtained from the linear relationship and then this value is used in equation (2.25) to obtain the value of p_{CO}. From this p_{CO} value, α value is obtained using equation (2.23) and these values are substituted back in equation (2.28) to calculate the k_{obs} value from equation (2.28). This procedure is repeated until the k_{obs} value matches with the experimental fitted value. The final value of p_{CO} is equal to the value of p_{CO} for which matching has been obtained between calculated and experimental k_{obs} values.

The validity of this reduction rate equation is checked against the experimental results of NIIST for carbothermal reduction of Ilmenite with leco char, Wouterlood's reduction data (1979) for Western Titanium Ilmenite ore, Sucre's reduction data (1979) for Westport Ilmenite ore and are presented in Figures 2.8 to 2.10

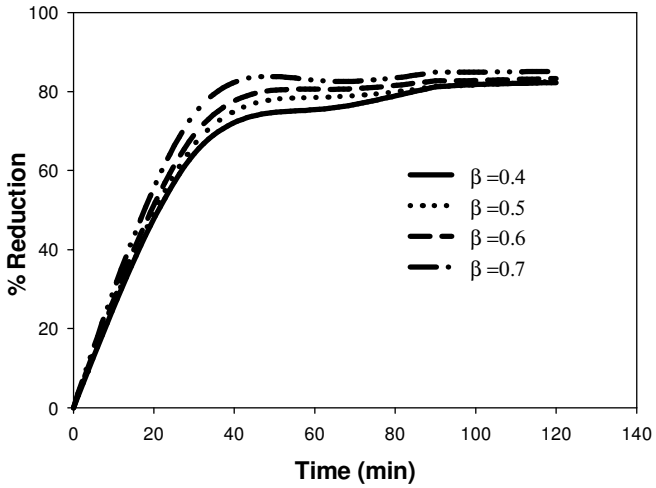

Figure 2.8 Experimental Reduction Data (Present Work) at 1000 ^{0}C for varying Coal/Ilmenite ratio (β)

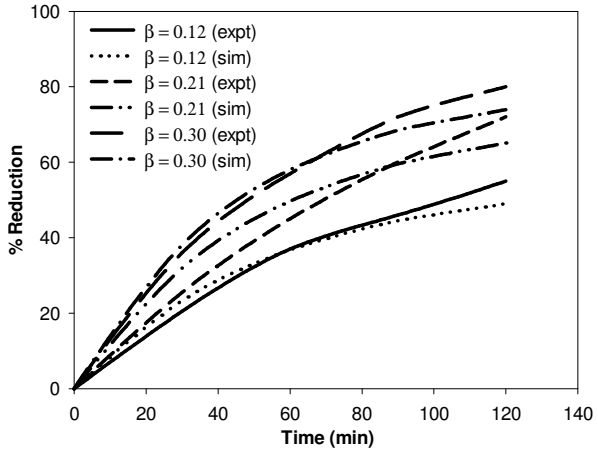

Figure 2.9 Comparison of Experimental and Simulated Reduction Data (Sucre (1979))

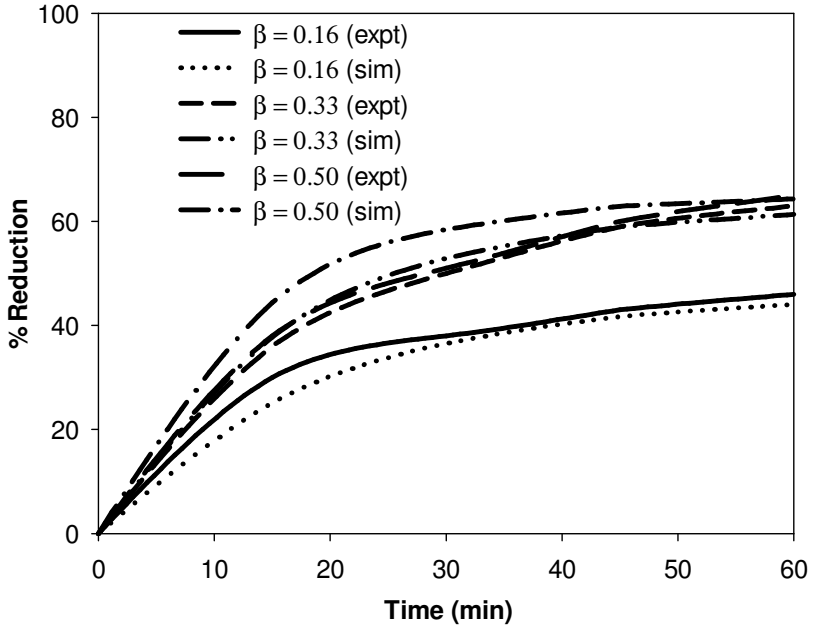

Figure 2.10 Comparison of Experimental and Simulated Reduction data (Wouterlood (1979))

Figure 2.11 shows plot of carbon activity calculated based on the semi-empirical model against coal/ore ratio for each set of reduction data (present work, Sucre(1979) and Wouterlood(1979)). For each set of data carbon activity varies linearly with the coal/Ilmenite ratio, giving rise to a unique equation between them. The considerable increase in carbon activity as the coal/ore ratio increases suggests that the carbon activity has a significant role in the rate of carbothermal reduction of Ilmenite. This is in agreement with the findings of Abril(2002) for Iron Oxide reduction.

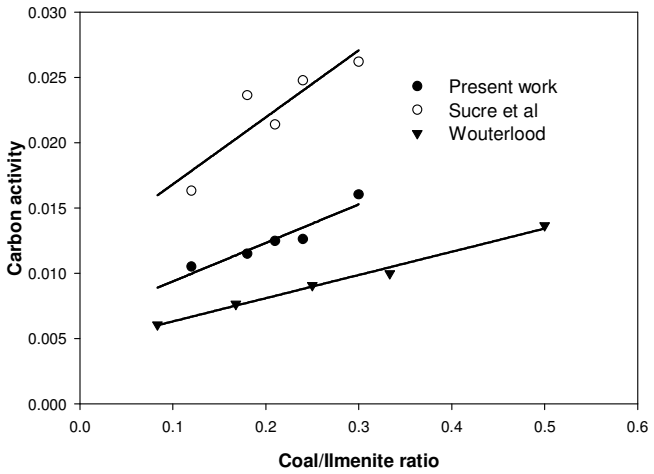

Figure 2.11 Variation of Carbon Activity with respect to Coal/Ilmenite ratio (β)

Hence for any given input values for Ilmenite and Coal feed rate along with experimental conversion data, the semi empirical approach can be used to obtain the reaction rate constant, p_{CO} value etc**.** This equation is used in our one dimensional comprehensive heat and mass balance model which is presented in detail in Chapter 4.

2.4 Conclusions

In this chapter, various aspects of the carbothermal reduction process of Ilmenite in a rotary kiln reactor are discussed in detail. The kinetics of the carbothermal reduction follows a mixed mechanism where both diffusion and chemical reaction controls the overall conversion. Two different kinetic models based on two independent approaches taking into account various aspects of the reduction process are presented and the results are compared with experimental data. Both the models proved to be powerful tools to study the reduction kinetics of Ilmenite with various parameters such as coal to Ilmenite ratio, partial pressure data, carbon activity etc. Since the semi empirical model provides a pseudo first order equation of the form equation (2.29), it can be directly used for modeling the carbothermal reduction of Ilmenite in the rotary kiln. This equation is used in the comprehensive one dimensional heat and mass balance model described in Chapter 4 of this thesis.

Chapter 3

CFD SIMULATION OF PNEUMATIC COAL INJECTION PROCESS

3.1 Introduction

This chapter deals with the modeling of the pneumatic coal injection process from the discharge end of an Ilmenite reduction rotary kiln reactor. The results from simulation of this model is given as input to the Ilmenite reduction simulator developed based on one-dimensional modeling which is detailed in Chapter 4 of this thesis. In Ilmenite reduction rotary kilns, coal serves the purpose of both fuel and reducing agent. The kiln is basically divided into two zones, *viz.,* the preheating zone (near the feed end) and the reduction zone (towards the discharge end). The solid bed gets preheated in the preheating zone and the reduction is effected by reducing gases derived from coal gasification. As the reaction taking place in the bed is highly endothermic, bed temperature remains almost constant in the reduction zone. The heat required is produced by the combustion of volatiles released and excess carbon monoxide. Air is blown into a countercurrent freeboard with onboard fans located at several positions along the kiln axial direction.

Tremendous improvements were made in the design of direct reduction rotary kilns based on systematic investigations through modeling and mechanistic investigations by several authors like Venkateswaran and Brimacombe (1977), Barr *et al.* (1989 a,b), Boateng and Barr (1996), Nicholson (1995) *etc.* One such improvement, which is widely used in the present day direct reduction kilns is the pneumatic coal injection process from the discharge end of the rotary kiln as patented by Hockin (1975) where some part of the required coal are injected along with air from the discharge end of the kiln in such a manner that it is distributed along the length of the kiln to within the feed end zone of the kiln and

so that substantially no coal is incorporated in the bed within at least the last 15% of the kiln length. The coal pneumatically injected from discharge end of the kiln, not only supplements the heat availability but also helps to maintain a reducing atmosphere to prevent reoxidation of the metallic iron and for controlling degree of metallization and carbon content of the product.

When coal is injected with air from the discharge end into the rotary kiln in a continuous operation, the coal particles get dispersed due to turbulent nature of hot gases in the freeboard and simultaneously undergo devolatilization releasing volatiles and combustion of volatiles which provides the heat source for the entire process. The optimum values for particle size distribution and the feed to discharge end coal ratio are essential for increasing the efficiency of this process. But no systematic study on the advantages of this process has been reported in the literature except that of Ramakrishnan and Sai (1999) where they have developed a simple and yet comprehensive model for direct reduction process coupled with particle dynamic equations given by Biswas (1993). In their work they predicted the influence of coal/char injection on the performance of a direct reduction rotary kiln. That is the only reported literature, where some preliminary investigations have been directed towards the pneumatic coal injection process in a direct reduction rotary kiln.

In recent times, with the advances in computing power and numerical algorithms computational fluid dynamics (CFD) is becoming a feasible tool to analyze mathematically complicated processes like coal combustion in furnaces. Several authors have used CFD techniques to numerically simulate coal combustion process in boilers, blast furnaces *etc.,* since 1980's but so far there

has been no reported work on the CFD modeling of the pneumatic coal injection process in a direct reduction rotary kiln. Hence the objective of the present work is to develop a three-dimensional CFD model of the pneumatic coal injection and combustion process in the direct reduction rotary kiln.

Lack of experimental and/or reported data for the complete validation of the model makes it necessary to use some indirect methods to carry out model validation. The validation of the present model is thus carried out in two ways. The first set of validation is against empirical particle dynamics calculations of pneumatically injected coal particles under cold conditions in a rotary kiln of Biswas (1993). The second set of validation is for coal combustion process under hot conditions and for this purpose the work of Guo *et al.* (2005) is chosen where they have reported experimentally validated results for pulverized coal injection in the tuyere and raceway of a blast furnace. After these validation tests, the results obtained for CFD modeling of pneumatic coal injection process in Ilmenite reduction kiln is presented in terms of particle trajectories, particle and gas temperature and mass fraction of various gas components. The effect of various process parameters like initial particle velocity, initial particle size distribution and wall temperature on the coal combustion process is presented.

3.2 Description of the process and mathematical model

When pulverized coal particles of different sizes are injected with air from the discharge end into the rotary kiln in a continuous operation, the coal particles get dispersed due to the turbulent nature of hot gases in the freeboard and they reach the solid bed by a projectile path under the influence of gravity. While they are traversing the projectile path, the coal particles get heated up due

to the hot gases in the freeboard region of the rotary kiln and once the temperature reaches around 350^0C, they undergo devolatilization releasing volatiles. The released volatile gases undergo homogeneous combustion and the remaining char in the coal particles undergoes heterogeneous combustion at a higher temperature. Hence they provide both heat and carbon source in the reduction zone of the rotary kiln and serves two purposes: one providing heat to freeboard gas and the other maintaining a reducing atmosphere in the reduction zone of the kiln. The schematic representation of pneumatic coal injection process is shown in Figure 3.1.

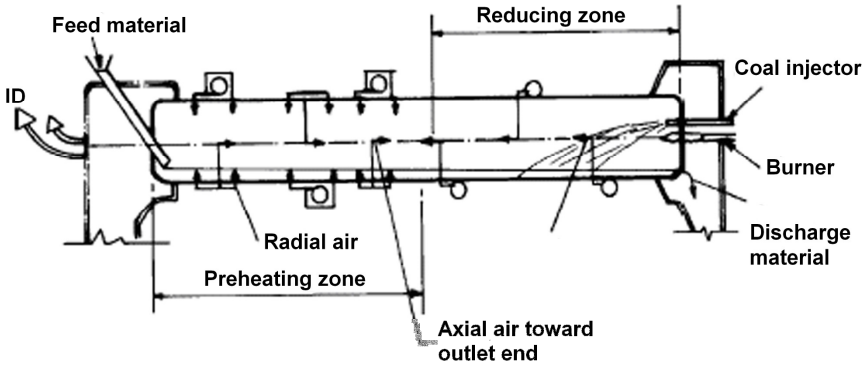

Figure 3.1 Schematic Diagram of Pneumatic Coal injection Unit In a Direct Reduction Rotary Kiln (Biswas (2003))

The coal particles injected into the hot freeboard of the rotary kiln get heated up and start releasing volatiles which then undergo both homogeneous and heterogeneous combustion depending upon the availability of oxygen in the system. Moreover the rotary kiln is rotating and hot freeboard gases flow in a counter current fashion to the solid bed. Modeling the pneumatic coal injection process involves modeling the complex processes like two phase turbulent flow which involves heat transfer including conduction, convection and radiation and

reactions. Hence modeling the whole physical process is a formidable task and certain simplifications are assumed in the present analysis while modeling the pneumatic coal injection process in a direct reduction rotary kiln using 3-diemnsional CFD.

3.2.1 Assumptions/Simplifications

As pneumatic coal injection involves many complex processes certain simplification assumptions are required for constructing a robust mathematical model. The following are the assumptions used for the present model:

- The free board region of the kiln alone is taken as the model domain and hence the upper surface of the solid bed is considered as a wall. This tends to be valid as the objective of the model is to simulate the pneumatic coal injection and the influence of the solid bed on this process is negligible.
- The rotary kiln is considered as stationary. As the free board region alone is modeled and the speed of rotation is considerably low, the kiln rotation might not have any significant effect.
- Pneumatically injected coal particles are assumed to be spherical in shape and have a specific mean diameter.
- The wall is assumed to be at a uniform static temperature (1000^0C for the present simulation).
- At the inlet the coal particles and air are at room temperature and the kiln wall is around 1000^0C.

The pneumatically injected coal particles along with air enter into the rotary kiln from the discharge end as a turbulent free jet. Hence we have adapted a two phase flow approach where the air is considered as a continuous phase and the coal particles are considered as the dispersed phase.

3.2.2 Governing Equations

The pneumatic coal injection process from the discharge end of the rotary kiln is a typical gas solid two phase turbulent flow with chemical reactions. Hence the simulation of pneumatic coal injection process in a rotary kiln is based on the comprehensive representation of the features of gas phase fluid dynamics, combustion of coal particles, heat transfer including radiation and chemical reactions to investigate the velocity profile, temperature and emissions at various locations in the rotary kiln. The mathematical model is based on the numerical solution of three-dimensional differential equations for conservation of mass, momentum and energy.

The gas phase is treated as a continuous phase and is solved using RNG time averaged k-ε turbulent equations. The solid phase which consists of pneumatically injected coal particles is solved using particle transport model where particles are tracked through the computational domain in a Lagrangian way. Both these phases are coupled by homogeneous gas phase volatile combustion and heterogeneous combustion of solid coal particles. Coal combustion is calculated by combining a particle transport model of the coal particles with a combined eddy dissipation/finite rate chemistry model for the combustion of volatile gases in the gas phase. Coal particles are treated as non-interacting spheres with internal reactions and heat transfer and full coupling of mass, momentum and energy with the gaseous phase.

3.2.2.1 Gas phase

The gaseous field is described by the transport equations of the continuum phase. Three-dimensional, steady-state Reynolds averaged Navier-Stokes

equations closed by the k-ε turbulence model are solved for the turbulent gas flow, including mass, momentum, turbulence kinetic energy, turbulent dissipation rate, enthalpy, and a number of gaseous species mass fractions. The gas phase flow in the furnace is taken as a gas mixture consisting of all the gaseous components, such as O_2, H_2O, CO_2, N_2, and volatiles. These components are assumed to mix at the molecular level, sharing the same mean velocity, pressure, and temperature fields.

The mass conservation equation is solved for each component '*I*' in the gas mixture is given by equation (3.1)

$$\frac{\partial}{\partial x_j}\left(\rho_g u_j^g y_I\right) = \frac{\partial}{\partial x_j}\left(\Gamma_{Ieff}\frac{\partial y_I}{\partial x_j}\right) + S_I \tag{3.1}$$

where y_I is the mass fraction of the component I and ρ_g is the density of gas mixture. Gas mixture properties such as density ρ_g, molecular viscosity μ_g, thermal conductivity λ_g and specific heat capacity C_v are defined by equations similar to equation (3.2).

$$\alpha_g = \sum_{I=1}^{N_c} y_I \alpha_I \tag{3.2}$$

where α_I is the corresponding property of the component gas and N_c is the number of components in the gas mixture.

Effective diffusion coefficient Γ_{Ieff} is defined as

$$\Gamma_{Ieff} = \Gamma_I + \frac{\mu_t}{Sc_t} \tag{3.3}$$

where the molecular diffusion coefficient Γ_I is equal to $\rho_I D_I$ where D_I is the kinematic diffusivity of component I. Sc is the turbulent Schimidt number μ_t / Γ_t

where μ_t and Γ_t are turbulent viscosity and diffusivity respectively. The source term S_I in equation (3.1) is due to the chemical reaction rate involving the component I. Each gas component except the constraint gas N_2 has its own conservation equation.

The mass fraction of N_2 is determined by solving the constraint equation

$$\sum_{I=1}^{N_c} y_I = 1 \tag{3.4}$$

The bulk motion of gas mixture is determined by solving the conservation equation for momentum

$$\frac{\partial}{\partial x_j}(\rho_g u_i^g u_j^g) = -\frac{\partial p_g}{\partial x_j} + \frac{\partial}{\partial x_j}\left[\mu_g\left(\frac{\partial u_i^g}{\partial x_j} + \frac{\partial u_j^g}{\partial x_i}\right)\right] + \frac{\partial}{\partial x_j}(-\rho_g \overline{u_i' u_j'}) \tag{3.5}$$

Here p_g is the gas mixture pressure. The terms $-\rho_g \overline{u_i' u_j'}$ are Reynold's stresses and are modeled based on Boussinesq hypothesis as

$$-\rho_g \overline{u_i' u_j'} = \mu_t\left(\frac{\partial u_i^g}{\partial x_j} + \frac{\partial u_j^g}{\partial x_i}\right) - \frac{2}{3}\left(\rho_g k_g + \mu_g \frac{\partial u_i^g}{\partial x_i}\right)\delta_{ij} \tag{3.6}$$

3.2.2.2 Standard k-ε Model for Turbulence

The turbulent viscosity is computed from

$$\mu_t = \frac{C_\mu \rho_g k_g^2}{\varepsilon_g} \tag{3.7}$$

Here k_g is the gas mixture turbulence kinetic energy and ε_g is the gas mixture turbulence eddy dissipation rate. The governing equation for turbulence kinetic energy is given by

$$\frac{\partial}{\partial x_j}(\rho_g u_j^g k_g) = \frac{\partial}{\partial x_j}\left[\left(\mu_g + \frac{\mu_t}{\sigma_k}\right)\frac{\partial k_g}{\partial x_j}\right] + P_k - \rho_g \varepsilon_g \tag{3.8}$$

where P_k is the turbulence production due to viscous forces and is given by

$$P_k = -\rho_g \overline{u_i' u_j'} \frac{\partial u_i^g}{\partial x_j} \approx \mu_t \left(\frac{\partial u_i^g}{\partial x_j} + \frac{\partial u_j^g}{\partial x_i}\right)\frac{\partial u_i^g}{\partial x_j} - \frac{2}{3}\left(\rho_g k_g + \mu_g \frac{\partial u_i^g}{\partial x_i}\right)\frac{\partial u_i^g}{\partial x_i} \tag{3.9}$$

For incompressible flow, the second term on the right hand side does not contribute significantly and hence can be neglected.

The governing equation for the turbulence eddy dissipation rate ε is given by

$$\frac{\partial}{\partial x_j}(\rho_g u_j^g \varepsilon_g) = \frac{\partial}{\partial x_j}\left[\left(\mu_g + \frac{\mu_t}{\sigma_\varepsilon}\right)\frac{\partial \varepsilon_g}{\partial x_j}\right] + C_{1\varepsilon}\frac{\varepsilon_g}{k_g}P_k - \rho_g C_{2\varepsilon}\frac{\varepsilon_g^2}{k_g} \tag{3.10}$$

These equations contains five constants C_μ, σ_k, σ_ε, $C_{1\varepsilon}$, $C_{2\varepsilon}$ and their values are given by Launder and Spalding(1974) as

$$C_\mu = 0.09,\ \sigma_k = 1.0,\ \sigma_\varepsilon = 1.3,\ C_{1\varepsilon} = 1.44,\ C_{2\varepsilon} = 1.92$$

The energy equation is represented as

$$\nabla \bullet \left[\rho U H - \left(\frac{\lambda}{C_P} + \frac{\mu_t}{\sigma_H}\right)\nabla H\right] = S_E \tag{3.11}$$

where λ is the thermal conductivity C_p is the mass fraction weighted specific heat, H is the mean enthalpy and S_E is the heat source term from the particle phase and radiation. The temperature in the rotary kiln is high and radiation heat transfer is dominant. In this work thermal radiation through the gas phase is modeled using a discrete transfer model. In discrete transfer model, the scattering is assumed to be isotropic and is based on tracing multiple rays from the bounding surfaces through the domain. Discrete transfer model is found to be economical and

efficient method for determining thermal radiation within combustion chambers (Yamamoto *et al.* (2005)). The heat source term due to particle phase combustion is given in detail in the Section 3.2.2.3.

3.2.2.3 Particle Phase

Particle transport modeling is used to track the coal particles through the continuous flow in a Lagrangian way during pneumatic coal injection process in a rotary kiln. The coal particles are separated into a number of groups depending on their size range and Lagrangian equations of motion are solved for a representative number of coal particles for each size range and the total flow of the particle phase is modeled by tracking a representative number of particles through the continuous fluid. The tracking of each coal particle is carried out by solving a set of ordinary differential equations in time for position, velocity, temperature and mass. The calculation also takes into account the interactions between the gas and particle mass, momentum and energy by treating the coal particles as non-interacting spheres with internal reactions and heat transfer and full coupling of mass, momentum and energy with the gas phase. The governing equations for the particle phase are given below:

Momentum transfer equations:

$$m_p \frac{du_p}{dt} = F_{all} \tag{3.12}$$

where F_{all} denotes the sum of all forces acting on the particles. The forces acting on the particles are due to the difference in velocity between the particle and fluid (drag force), buoyancy force due to gravity, virtual mass force, pressure gradient

force, Basset force, turbulent dispersion force *etc.* In the present simulation only the drag force has been considered and is given by the expression

$$F_D = \frac{1}{2} C_D \rho_F A_F \left| u_F - u_p \right| \left(u_f - u_p \right) \tag{3.13}$$

where C_D is the drag coefficient and the value is based on modified Schiller Naumann drag model and is given by

$$C_D = \max\left(\frac{24}{\mathrm{Re}} \left(1 + 0.15\,\mathrm{Re}^{0.687} \right),\ 0.44 \right) \tag{3.14}$$

A_F is the effective particle cross sectional area. The particle displacement is calculated by integrating the particle velocity equation and is given by

$$\frac{dx_i}{dt} = u_{p_i} \tag{3.15}$$

3.2.2.4 Heat Transfer Equations

The rate of change of particle temperature is governed by three physical processes: convective heat transfer, latent heat transfer associated with mass transfer and radiative heat transfer and is given below as

$$\sum \left(m_c c_p \right) \frac{dT_p}{dt} = Q_C + Q_M + Q_R \tag{3.16}$$

In equation (3.16) Q_c denotes the convective heat transfer term and is given by

$$Q_c = \pi d_p \lambda Nu \left(T_g - T_p \right) \tag{3.17}$$

where λ is the thermal conductivity of the continuous gas phase, T_g and T_p are the temperatures of the continuous gas phase and particle respectively. Nu denotes the Nusselt number and is given by

$$Nu = 2 + 0.6\,\mathrm{Re}^{0.5}\left(\mu\frac{c_p}{\lambda}\right) \tag{3.18}$$

Q_M is the heat transfer term associated with mass transfer and is given by the expression

$$Q_M = \sum \frac{dm_c}{dt} V \tag{3.19}$$

where the sum is taken over all the components of the particle on which heat transfer is taking place and V is the latent heat of vaporization which is a temperature dependent value.

Q_R is the heat transfer term associated with radiative heat transfer and is given by the expression

$$Q_R = \pi d_p^2 \varepsilon_p \left(\pi I - \sigma n^2 T_p^4\right) \tag{3.20}$$

where I is the radiation intensity on the particle surface at the location of the particle, n is the refractive index of the continuous phase and σ is the Stefan Boltzmann constant and ε_p is the particle emissivity.

3.2.2.5 Coal Devolatilisation and Combustion

The coal particles are assumed to undergo a three-step process during combustion in the rotary kiln:

- Devolatilisation of raw coal particles producing volatiles and residual char.
- Gaseous combustion of the volatiles.
- Residual char oxidation.

Devolatilisation can be modeled by one or more reaction steps and in literature several types of Devolatilisation models are available such as single

reaction model of Badzioch and Hawksley (1970), two step reaction model of Ubhayakar *et al.* (1977) and multiple reaction model (Distributed Activation Energy Model) of Anthony and Howard (1976). The first-order single-reaction model offers a simple but effective mathematical description of coal Devolatilisation. Hence for the present simulation we have used the model of Badzioch and Hawksley (1970). The model states that the rate of production of volatile gases is first order, dependent on the amount of volatiles remaining in the particle.

Accordingly the devolatilization rate can be expressed as:

$$-\frac{dm_p}{dt} = k\left(m_p - (1 - f_{v0})m_{p0}\right) \tag{3.21}$$

Where m_p is the mass of coal particle at time t, f_{v0} is the initial volatile mass fraction and m_{p0} the initial mass of the coal particle. k is the first order reaction constant which can be expressed in the Arrhenius form as:

$$k = A\exp\left(-\frac{E}{RT}\right) \tag{3.22}$$

The values of parameters A and E used in the present simulation are given in Table 3.1. During coal combustion two separate gases are given off by the coal particles, the volatiles and char products that come from the burning of carbon within the particles.

The volatile matters evolved during coal particle devolatilization react with O_2 in the air forming CO_2 and H_2O. This reaction is calculated by a single step combustion model using the combined eddy dissipation/finite rate chemistry model. The Eddy dissipation model (Magnussen and Hjertager (1976)) is based on the concept that the chemical reaction is fast relative to the transport

processes in the flow, whereas the finite rate chemistry model assumes that the rate of progress of elementary reaction *k* can be reversible only if a backward reaction is defined. The effective rate for the combined model is computed to be the minimum of the Finite Chemistry Rate and the Eddy Dissipation rate. These reaction rates contribute to the source term S_I in the gas phase equations. The source term S_I is summed from the contributions of the reaction rates by

$$S_I = W_I \sum_{J=1}^{N_r} n_{IJ} R_J \tag{3.23}$$

Where W_I is the molecular weight of the component *I*, n_{IJ} is the difference of the stoichiometric coefficients for reactants and products and N_r is the number of reactions. The rate of reaction *J*, R_J can be calculated either using the Eddy Dissipation Model and/or the Finite Chemistry model.

In the Eddy dissipation model the reaction rate R_J is calculated as

$$R_J = A \frac{\varepsilon_g}{k_g} \min\left(\frac{[I]}{\upsilon_I'} \right) \tag{3.24}$$

where [*I*] is the molar concentration of reactant component *I*, υ_I' is the stoichiometric coefficient for *I* and *A* is a constant with value equal to 4. In the finite rate chemistry model, the rate of reaction is given by

$$R_J = F_J \prod_{I=A,B,\ldots}^{N_c} [I]^{r_{kl}'} - B_J \prod_{I=A,B,\ldots}^{N_c} [I]^{r_{kl}''} \tag{3.25}$$

where [*I*] is the molar concentration of reactant component *I* and F_J and B_J are the forward and backward reaction rate constants respectively and *r* represents the reaction order of component *I* in the elementary reaction *J*. The effective rate

for the combined model is computed to be the minimum of the Finite Rate and the Eddy Dissipation rate.

The char oxidation can be modeled either as a global reaction, or by using an analytical solution for the diffusion of oxygen within the pores of the char particle. The char combustion model proposed by Gibb (1985) is used in the current work. Gibb's model takes into account the diffusion of oxygen within the pores of the char particle as well as boundary layer diffusion and reaction kinetics. The oxidation mechanism of carbon can be characterized by the molar ratio Φ of carbon atom/oxygen molecules, so that oxides are produced according to the equation:

$$\Phi C + O_2 \rightarrow 2(\Phi - 1)CO + (2 - \Phi)CO_2 \tag{3.26}$$

where the value of Φ is assumed to depend on the particle temperature T_p and is given by the expression

$$\frac{2(\Phi - 1)}{2 - \Phi} = A_S \exp\left(-\frac{E_V}{RT_p}\right) \tag{3.27}$$

where the constants are given by A_s = 2500 and T_s = 6240K. By solving the oxygen diffusion equation analytically, the following equation is obtained for the rate of decrease of char mass

$$\frac{dm_c}{dt} = -\frac{3\Phi}{1-\varepsilon}\frac{M_c}{M_{O_2}}\frac{\rho_\infty}{\rho_c}\left[k_1^{-1} + (k_2 + k_3)^{-1}\right]^{-1} m_c \tag{3.28}$$

where ρ_∞ is the far filed oxygen concentration and is taken to be the time averaged value obtained from the gas phase calculation and ρ_c is the density of char. k_1 is the rate of external diffusion, k_2 is the surface reaction rate and k_3

represents the rate of internal diffusion and surface reaction. These are defined as follows

$$k_1 = \frac{D_{ref}}{\rho_g}\left[\frac{T_p + T_g}{2T_{ref}}\right]^{\alpha} \tag{3.29}$$

D_{ref} is the dynamic diffusivity, T_{ref} is the reference temperature and α is the exponent with value 0.75

$$k_2 = (1-\varepsilon)\frac{k_c}{R} \tag{3.30}$$

where k_c is the carbon oxidation rate and is given by

$$k_c = A_c T_p \exp\left(-\frac{T_c}{T_p}\right) \tag{3.31}$$

With values Ac = 14 $ms^{-1}K^{-1}$ and T_c =21580 K

$$k_3 = k_c \frac{(\beta \coth \beta - 1)}{\beta^2 a} \tag{3.32}$$

$$\beta = R\left(\frac{k_c}{D_p \varepsilon a}\right)^{0.5} \tag{3.33}$$

Where D_p is the pore diffusivity

3.2.3 Geometry and Simulation Conditions

The model developed is used to simulate the gas-particle flow during pneumatic coal injection process in a rotary kiln and the commercial CFD software ANSYS CFX 11.0 is used to solve the governing equations for mass, momentum and energy. The rotary kiln used for the present simulation is of inner diameter 2.6 m and length 40 m and the schematic view of the kiln along with the pneumatic coal injection tube is shown in Figure 3.2. The diameter of the coal

injector tube is 80 mm. The rotary kiln is assumed to be filled by solids by a fill fraction of 18 %. From the fill fraction value the height of the solid bed is calculated to be 760 mm. The top surface of the solid bed is considered as a wall for the simulation purposes. Hence the cylindrical geometry of entire rotary kiln was created first, and then the solid bed portion was removed. Boundary-fitted multi-block unstructured tetrahedral finite volume mesh was generated as shown in Figure 3.3.

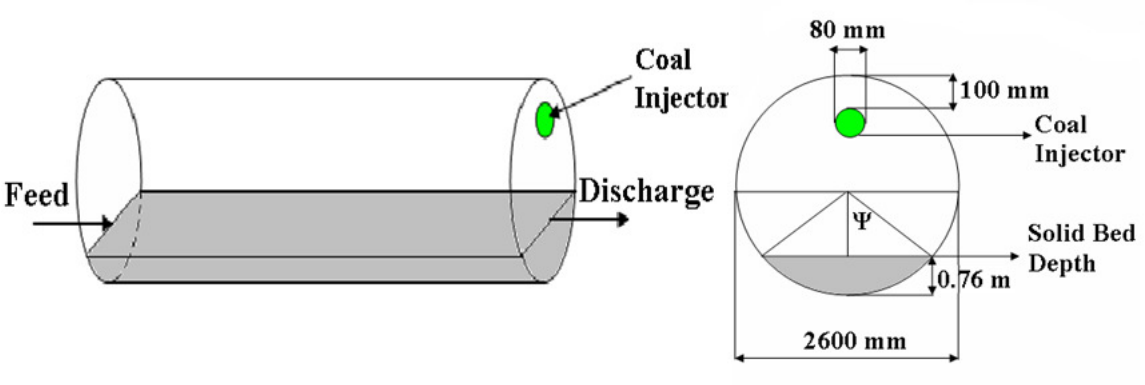

Figure 3.2 Schematic View of the Rotary Kiln along with Coal Injector Tube

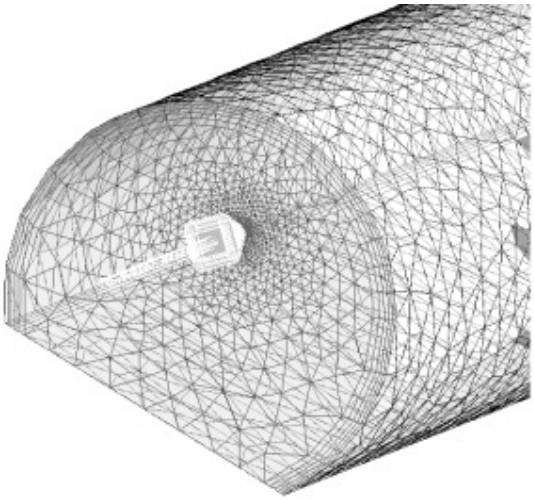

Figure 3.3 Computational Mesh Created for Coal Injection Simulation

The coal injector tube is considered as the coal inlet and both air and coal mass flow rate values are given normal to the coal inlet surface. Coal particle

initial velocity is also specified at the inlet. The coal particles are divided into discrete size ranges and are uniformly injected from the coal injector tube. In the present simulation we have used two different sets of particle size distribution for evaluating the effect of particle size distribution on particle trajectory and combustion process. Also separate runs for each individual particles size are carried out to study the effect of injected particle size on various process parameters. The representative number of coal particles chosen for particle transport simulation is 1000. The inner surface of the kiln along with the top surface of the solid bed is taken as a wall and the boundary conditions applied are no-slip flow and specified wall temperature conditions for heat transfer. An element based finite volume method is used to obtain the discrete algebraic governing equations. The second order equivalent to high-resolution discretization scheme is applied for obtaining algebraic equations for momentum, turbulent kinetic theory and turbulence dissipation rate because of accuracy and stability. Pressure velocity coupling was achieved by the Rhie Chow algorithm. The governing equations are solved using the advanced coupled multi grid solver technology of CFX-11. A residual convergence criterion for RMS mass-momentum equations of 10^{-4} was used in all simulations which is the factor by which the initial mass flow residual reduced. The simulations are carried out on the 12 node, 32 processor AMD64 cluster with clock speed of 2.55GH and 8 GB memory with each node.

Since any simulation has to be validated first and since there is no data available for direct validation of pneumatic coal injection process we have done the validation in two ways. The first set of validation deals with cold model

simulation where only the velocity and displacement equations are solved for gas phase and particle phase. The results obtained for the trajectories of the coal particles are validated with the data of Biswas (1993). The second set of validation deals with hot model simulation where coal combustion and heat transfer simulation are included. For this purpose we have taken the geometry given by Guo et. al (2005), where they have simulated coal flow and combustion in the tuyere and raceway of the blast furnace. The schematic view along with the dimensions of the computational geometry used by these authors and the cross section of the injection lance through which coal along with conveying gas and also the cooling gas are introduced into the combustion chamber are depicted in figure 3.4. The lance enters the blowpipe with an inclination angle of 10°. The lance is coaxial, with the coal and conveying gas (nitrogen) in the inner tube, and a cooling gas(air) in the annular region. The cooling gas protects the coal from excessive heating in the blow pipe, to prevent in-lance coking. The raceway is modeled as a tube of 1 m length with a divergence angle of 3°. To simplify the geometry further, we have excluded the injection lance from our model and hence the inflow boundary is defined at the lance tip. This simplification is valid as the results reported by Guo *et al.* (2005) is based on such a simplified geometry.

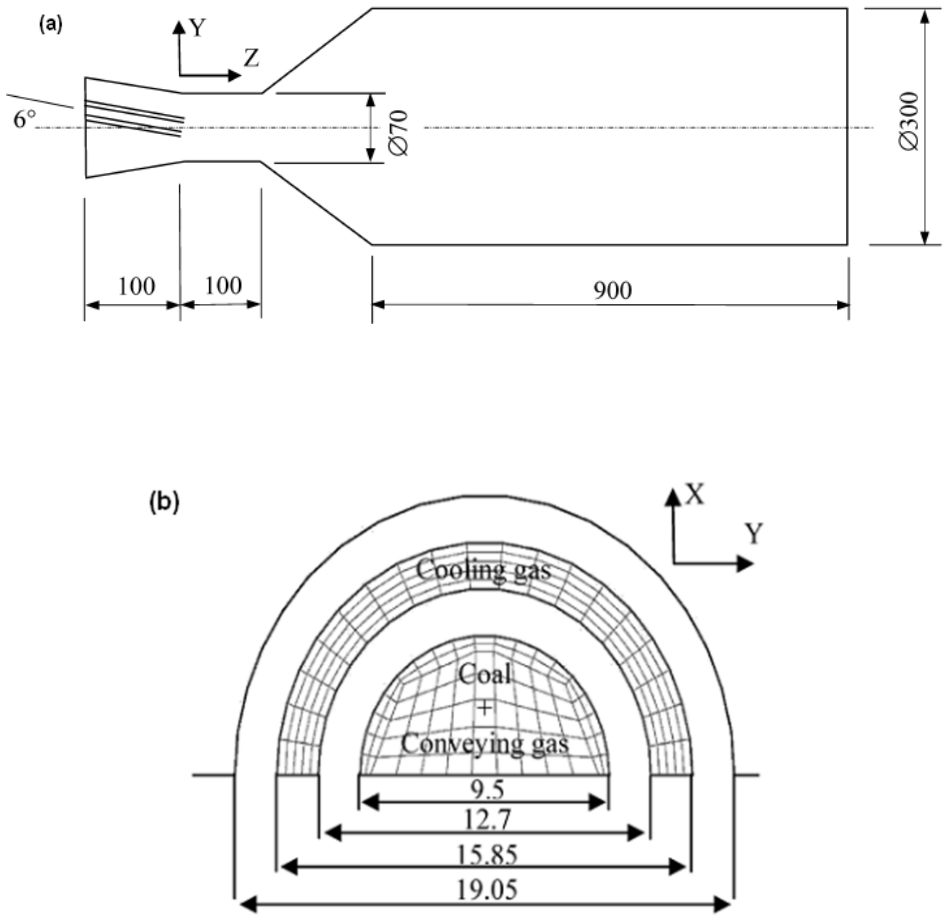

Figure 3.4 Main Dimensions (in mm) of the Geometry used for Validation (a) coal combustor (Guo et al (2005)) and (b) injection lance (Shen(2008))

Tetrahedral mesh with 127508 nodes as shown in Figure 3.5 is used for the combustor model.

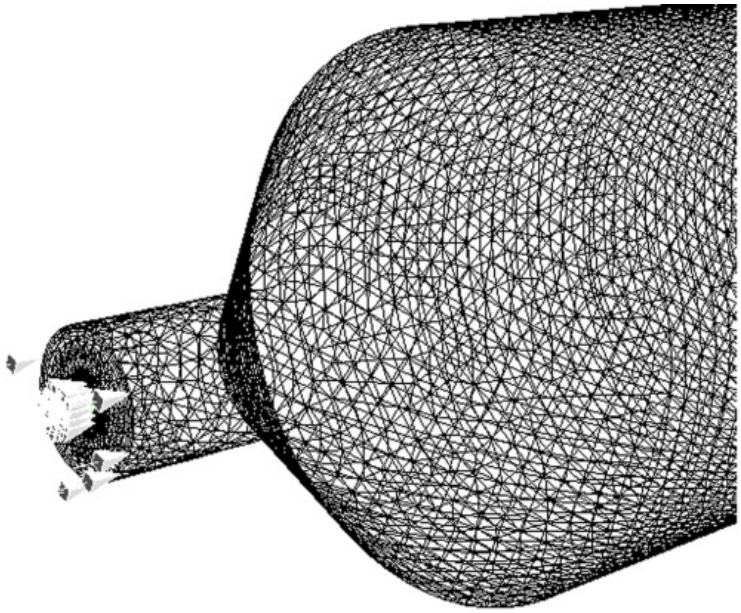

Figure 3.5 Computational Mesh for Validation

The physical, and process parameters used for the present simulation study along with the corresponding parameters for validation study are given in Table 3.1. The proximate and ultimate analysis of the coal used along with their size distributions, mass fraction and kinetic parameters used in the present study are depicted in Table 3.2.

Table 3.1 Physical Dimensions and Process Parameters

Hot model validation – process parameters		**Cold model validation – process parameters**	
Length of the combustor, m	1.115	Length of the kiln, m	40
Diameter of combustion	0.3	Degree of fill,%	18
chamber, m	600	Outer Shell diameter, m	3.1
Wall Temperature, K		Inner Shell diameter, m	2.6
Input Parameters		**Input Parameters**	
Blast flow rate, Nm^3/hr	300	Pneumatic coal injection rate, t/h	1.8
Coal flow rate, kg/hr	40	Air rate, Nm^3/hr	1275
Conveying gas flow rate, Nm^3/hr	2	Static inlet temperature, K	303
Cooling gas flow rate, Nm^3/hr	3.2		
Blast temperature, K	1473		
Coal temperature, K	323		
Conveying gas temperature, K	323		
Cooling gas temperature, K	600		

Table 3.2 Proximate and Ultimate Analysis of Coal with Size Distribution and Reaction Parameters

Coal Proximate analysis		**Coal Proximate analysis**	
Fixed Carbon, %	54.5	Fixed Carbon %	58.1
Volatile Matter, %	32.5	Volatile Matter%	35.2
Ash, %	9.8	Ash%	2.4
Moisture, %	1.2	Moisture%	4.3
Sulphur, %	0.58		
Coal Ultimate analysis		**Coal Ultimate analysis**	
Carbon%	83.5	Carbon%	79.37
Hydrogen%	5.3	Hydrogen%	5.69
Nitrogen%	1.95	Nitrogen%	0.31
Sulphur%	0.6	Oxygen%	14.57
Oxygen%	8.6		
Coal Size Distribution		**Coal Size Distribution**	
		Mean Diameter, mm	Mass fraction
Minimum diameter, μm	1		I II
Maximum diameter, μm	200	0.5	0.385 0.025
		1.5	0.1 0.1
		2.5	0.14 0.5
		4.0	0.19 0.19
		6.5	0.13 0.13
		10.0	0.055 0.055

Coal Combustion Reactions and Rate Constants

	Pre-exponential factor	Activation Temperature
Coal Devolatilization	134000 s^{-1}	8852 K
Char oxidation field	497 $kg/m^2/s$	8540 K
Fuel Gas Oxidation	132.8E6 s^{-1}	15098 K

3.3 Results and discussion

3.3.1 Validation Results

3.3.1.1 Cold Model Validation

The only work which deals with dynamics of the injected particles and air flow requirements during pneumatic coal injection is by Biswas (1993) where the design requirements of the coal injector tube are discussed in detail. Hence in the present study, the simulation is first carried out for cold conditions where only the hydrodynamic equations are solved for both the gas phase and the particle phase. The physical and process parameters used for the simulations are presented in Table 3.3.

Table 3.4 shows the comparison of results obtained from the present CFD simulation with the values reported by Biswas (1993) for the trajectories of coal particles of different sizes. The CFD simulation results shows that coal particles reaches the solid bed in the horizontal range of 25-35 m in the axial direction from the feed end. It can also be observed that even though the projectile trajectory of the coal particle is matching between the present CFD simulation and the empirical results presented by Biswas (1993), there is a discrepancy between the two results at which axial location the coal particle reaches the solid bed. This may be due to the reason, that in the present CFD simulation full gas-particle coupling is incorporated whereas Biswas (1993) has taken the gas phase as a turbulent free jet and has used an empirical equation to calculate the gas velocity which is then used to calculate particle horizontal and vertical acceleration. It can also be observed that coal particles of size less than 1 mm reaches the solid bed in the

horizontal range of 30 to 35 m whereas coal particles of size greater than 1 mm reaches the soli bed in the horizontal range of 25-30 m.

Table 3.3 Dimensions and Process Parameters for Cold Model Validation (Biswas (1993))

Kiln Diameter, m	2.6
Kiln Length, m	40
Fill fraction, %	18
Coal injection rate, tpd	35
Air rate, m^3/h	1100
particle injection velocity, m/s	60

Table 3.4 Comparison of Simulated Particle Trajectory Data with The Data of Biswas (1993)

Size of particles (mm)	Time (s)	Axial Distance (m)		Radial Distance (m)	
		Biswas (1993)	Present Simulation	Biswas (1993)	Present Simulation
6.0	0.08	4.8	4.6	0.03	0.04
	0.16	9.3	8.3	0.12	0.11
	0.24	13.8	11.4	0.27	0.24
	0.32	17	14.1	0.49	0.45
	0.39	20.5	14.7	0.54	0.51
3.0	0.08	4.7	4.2	0.03	0.03
	0.16	8.2	7.1	0.12	0.11
	0.24	11.8	8.9	0.27	0.23
	0.32	14.4	9.9	0.47	0.38
	0.39	15.5	10.4	0.54	0.53
0.5	0.08	4	3.6	0.03	0.03
	0.16	6.2	4.7	0.11	0.1
	0.24	8	5.3	0.24	0.2
	0.32	9.6	5.6	0.39	0.32
	0.39	10.6	5.7	0.57	0.49

3.3.1.2 Hot Model Validation

Though there are numerous studies reported for devolatilization and combustion of pulverized coal particles injected in the raceway of blast furnace, the data for validation is selected distinctively based on certain criteria. Since the present model requires experimental validation, the reported data required is to be based on combustion experiments. Another requirement is that the geometry should not be too complicated to be created and discretized using the available modeling tools. With this specification, the data reported by Guo *et al.* (2005) is chosen for validation of coal combustion data of the present CFD simulation, because these authors have validated their simulation results with the experimental measurements obtained from a pilot scale test rig. The comparison of our results with their results is shown in Figure 3.6. The qualitative agreement with the reported results validates the devolatilization and combustion reaction implementation scheme implemented in the present CFD simulation.

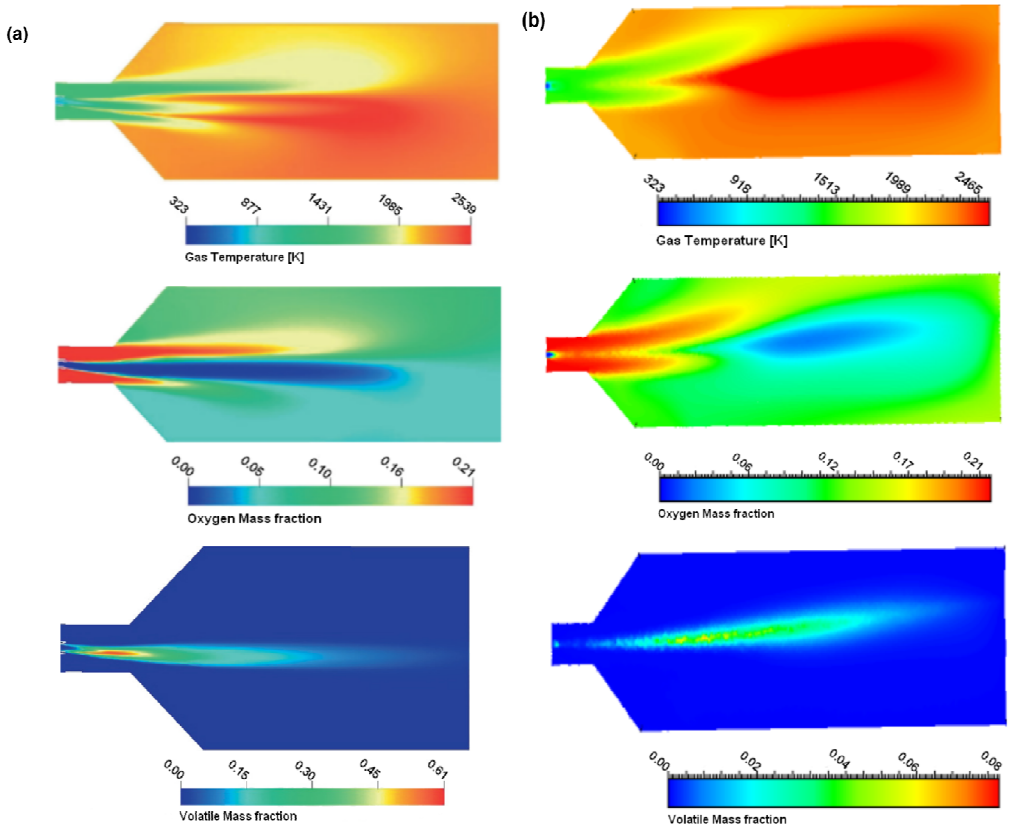

Figure 3.6 Temperature and species mass fraction isopleths in Y-Z plane for (a) results reported by Guo *et al. (*2005) (b) present CFD simulation

3.3.2 Pneumatic Coal Injection Simulation Results

3.3.2.1 Grid Resolution Study

The accuracy of the numerical computations depends on the mesh density. Grid independence test is thus necessary, as it allows the optimum mesh grid size to be determined. In this study, this is achieved by comparing the prediction of numerical results presented based on different mesh sizes. The computational geometry chosen is the rotary kiln of inner diameter 2.6 m and length 40 m. All the relevant processing parameters are shown in Table 3.1 & 3.2. Three different tetrahedral meshes are chosen for this analysis: mesh 1 is the coarser mesh with 16513 nodes where as mesh 2 is finer with 30448 nodes and mesh 3, the finest with 53015 nodes. The variation of particle and gas velocity along the axial

distance is shown in Figure 3.7. It can be observed that the results obtained using mesh1 (coarser) deviates more from the results obtained using either mesh 2 or mesh 3. Hence for want of computational power mesh 2 is chosen for all the simulations reported in this work.

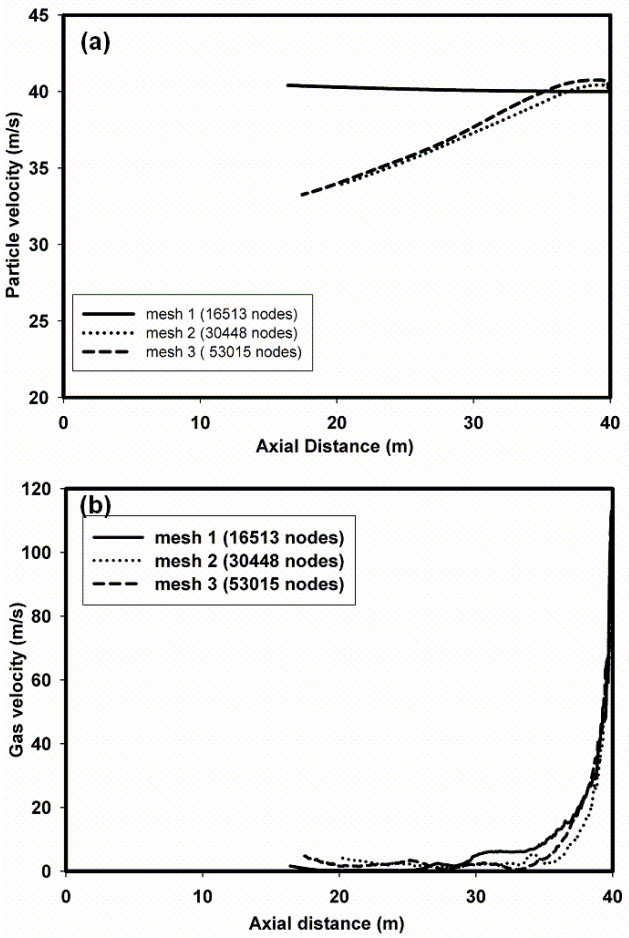

Figure 3.7 Variation of (a) Particle velocity and (b) Gas velocity along the Axial Distance for Three Different Meshes

3.3.2.2 Effect of Particle Size Distribution

After the validation and grid resolution studies, numerical simulations are carried out for pneumatic coal injection process from the discharge end of the

rotary kiln of inner diameter 2.6 m and length 40 m. The process parameters and size distribution chosen for the present simulation are given in Tables 3.2 and 3.3. Figures 3.8 and 3.9 shows the particle trajectory data based on (a) particle temperature and (b) particle mean diameter for the two particle size distributions as given in Table 3.2. The initial particle velocity chosen for both the particle size distribution is 40 m/s and the particles are injected from the same locations. The kiln wall temperature is kept at 1000^0C. The results show that the particles in the size range of 0.5-1 mm falls near the discharge end of the kiln than the bigger size particles. Also smaller size particles gets combusted quickly thus providing heat load to the freeboard. It can be seen from these figures that depending on the particle size distribution, the heat load varies along the axial kiln length.

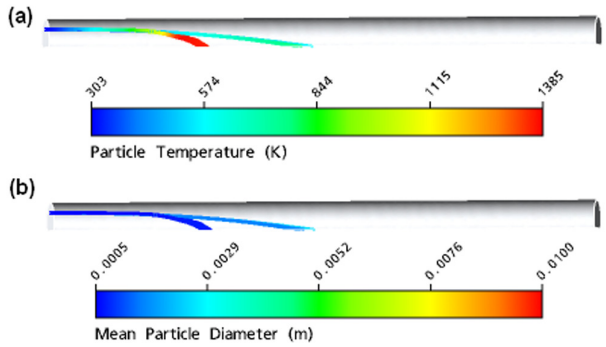

Figure 3.8 Distribution of (a) Particle Temperature and (b) Mean Particle Diameter along the Particle Trajectories for Particle Size Distribution I.

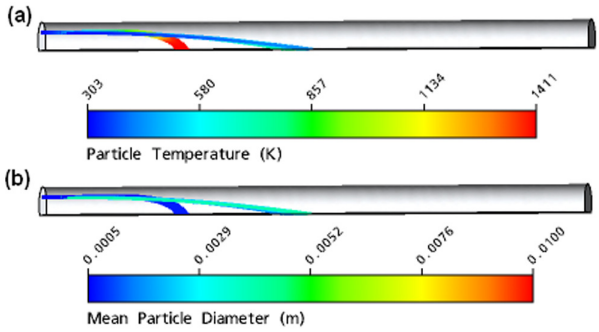

Figure 3.9 Distribution of (a) Particle Temperature and (b) Mean Particle Diameter along the Particle Trajectories for Particle Size Distribution II.

Figures 3.10 and 3.11 show the gas temperature and species mass fraction contours on a plane perpendicular to the solid bed surface along the axis of the kiln for the two particle size distributions.

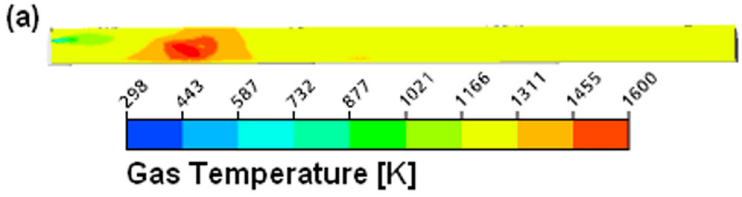

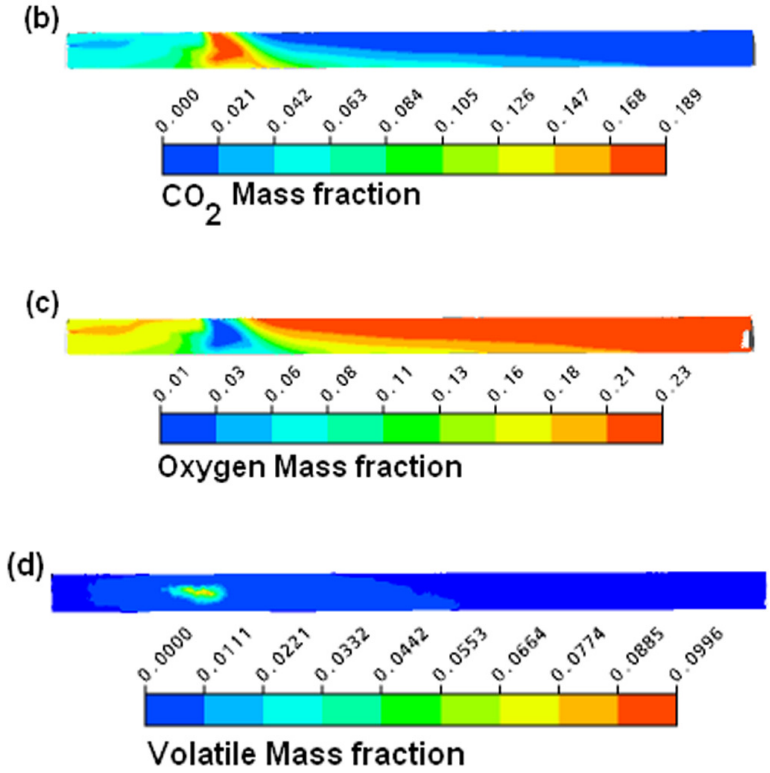

Figure 3.10 Distribution of (a) Gas temperature (b) CO_2 mass fraction (c) O_2 mass fraction and (d) Volatile mass fraction in plain perpendicular to the solid bed surface, along kiln axis for particle size distribution I.

It can be seen clearly from Figure 3.10(a), that for the particle size distribution I, where the mass fraction of particles less than 1 mm size is around 38%, the maximum gas temperature reaches around 1700K and this occurs near the solid bed where the smaller size particles get combusted just before reaching the solid bed. This is also confirmed by the CO_2 and O_2 profiles shown in Figures 3.10(b) and (c). Since smaller size particles gets burned off easily, the CO_2 mass fraction is also higher for this size distribution and the mass fraction of volatiles released is around 0.07.

Similar type of results is presented in Figures 3.11(a) to (d) for the second particle size distribution where the mass fraction of 2.5 mm particles is 50%. It can be seen from Figure 3.11(a), that for the particle size distribution II, the maximum gas temperature reaches around 1600 K at a very small region and the temperature reaches around 1200 K in most part of the freeboard in the kiln. The CO_2 mass fraction is also less for this size distribution and the mass fraction of volatiles released is around 0.003. From these results it can be concluded that particle size distribution plays a major role in distribution of heat load and volatile release and combustion.

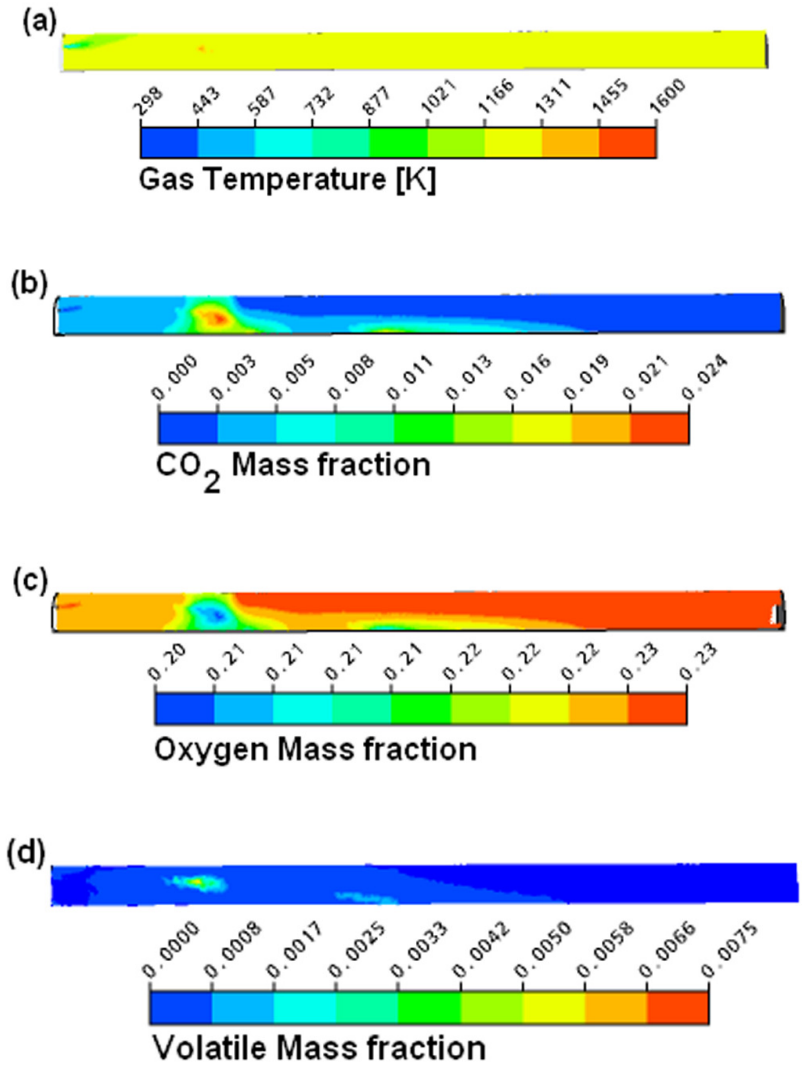

Figure 3.11 Distribution of (a) Gas temperature (b) CO_2 mass fraction (c) O_2 mass fraction and (d) Volatile mass fraction in plain perpendicular to the solid bed surface, along kiln axis for particle size distribution II.

Factors such as the location where each particle size group fall down on the solid bed, the point where the maximum temperature is attained, maximum temperature to which they are heated up etc. play vital role in determining the efficiency of the pneumatic coal injection process in a direct reduction rotary kiln. The results of the present simulation indicate that by properly designing the particle size distribution of the pneumatically injected coal particles, we can control

and optimize the various process conditions of the direct reduction kiln appropriately.

3.3.2.3 Effect of Particle Size

The next set of numerical simulations is carried out for pneumatic coal injection process with single particle size to determine the effect of particle size on the process. Figure 3.12 shows the variation of species mass fraction with varying particle sizes.

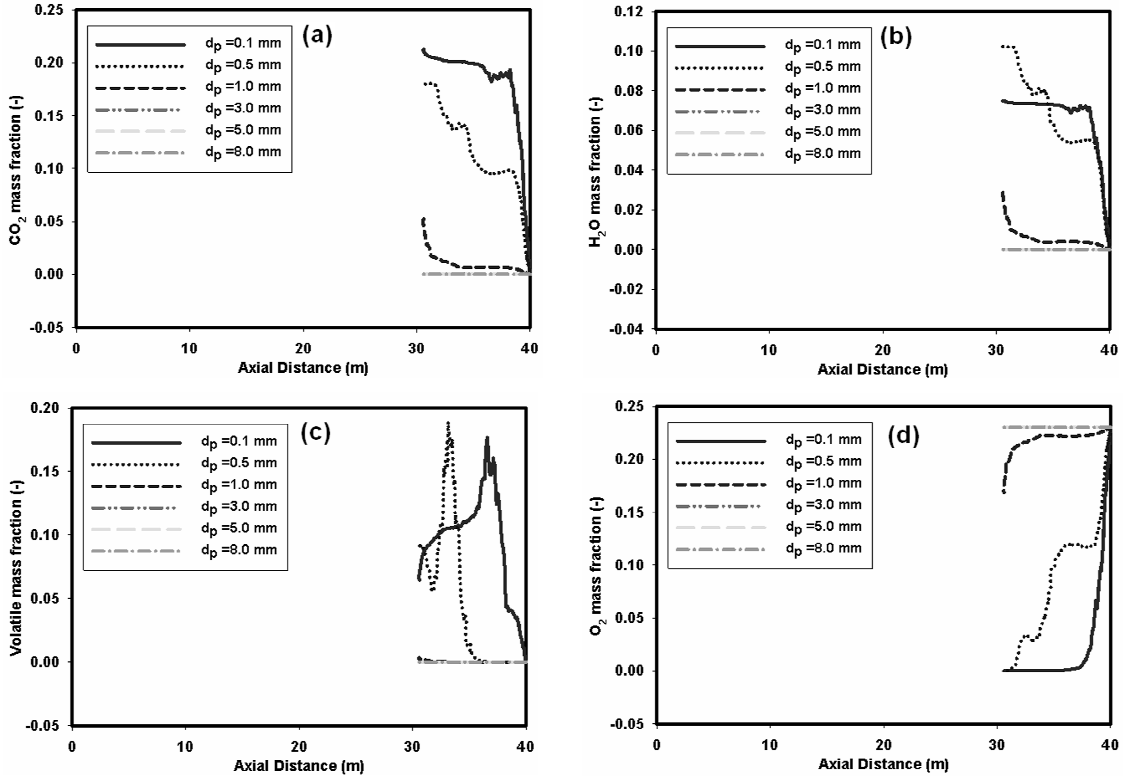

Figure 3.12 Variation of (a) CO_2 Mass Fraction (b) H_2O Mass Fraction (c) Volatile Mass Fraction and (d) O_2 Mass Fraction for different Particle Sizes

CO_2 and H_2O mass fraction indicates that the particles of diameter less than 3 mm only undergo combustion in the freeboard. Volatile mass fraction indicates that particles of diameter greater than 5 mm do not undergo even devolatilisation.

Coal burnout is evaluated according to an ash balance, which represents the total weight loss of the organic fraction of the coal due to volatile release and char oxidation and gasification reactions:

$$\%\,Burnout = \frac{1 - X_{a,0} / X_a}{1 - X_{a,0}} \times 100 \qquad (3.33)$$

where $X_{a,0}$ is the original ash content of the coal used and X_a is the ash content of the burnt out char. The effect of particle size on the heating up and burnout of the injected coal particles are shown in Figure 3.13. Particles of diameter 3 mm and more just get heated up to around 700K but smaller particles get heated up rapidly to around 1700K and undergo combustion and hence they act as a heat source. Also the rapid increase in percentage burnout at distinct distances from the injection point clearly indicates the onset of char oxidation for different particle sizes. Also it can be noticed that particles of diameter 3 mm and above do not undergo char oxidation at all.

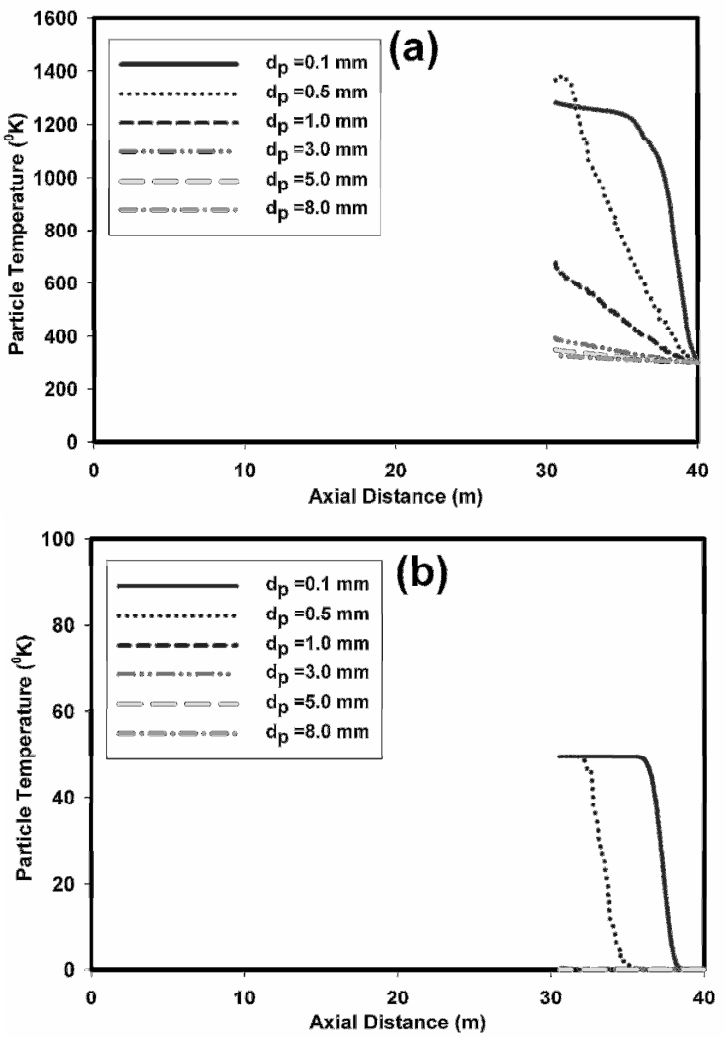

Figure 3.13 Influence of Particle Size on (a) Particle Temperature (b) Char Burnout

3.3.2.4 Effect of Initial Particle Velocity

Figures 3.14(a) and 3.14(b) show the effect of initial coal particle injection velocity on the particle dynamics for two particle sizes of 0.5 mm and 3 mm respectively. It can be seen that for 3 mm particle size there is an increase in the axial distance travelled by the particles in the range of 2 to 5 m but in the case of 0.5 mm particles particle velocity does not have any noticeable effect. As particle of bigger size travel farther distance by increasing the injection velocity, to study the effect of coal injection emphatically in the reduction zone of the kiln, the

particle injection velocity for all the runs has been fixed to be 40 m/s. Also it can be observed that 0.5 mm coal particles reach the solid bed at an axial distance of 35 m from the feed end of the kiln whereas the 3 mm coal particles reach the solid bed at an axial distance of 25 to 30 m for different initial particle velocities.

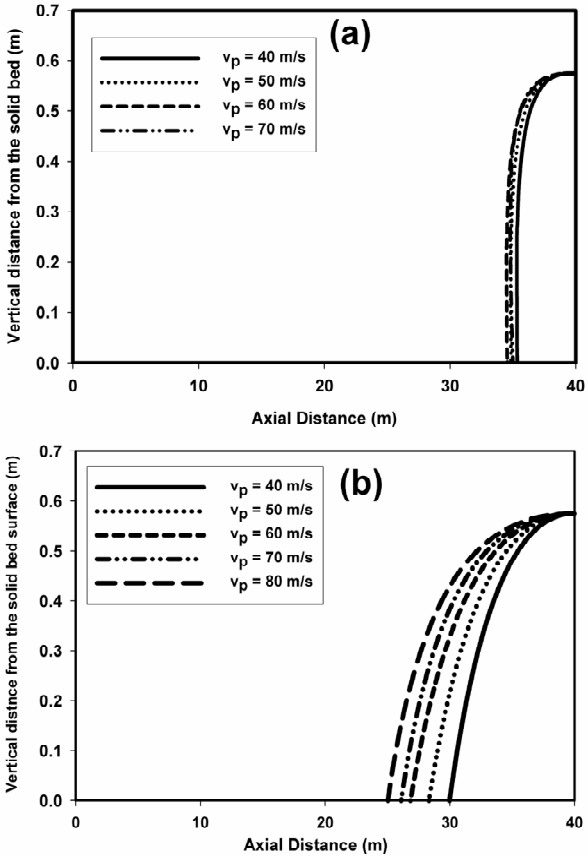

Figure 3.14 Effect of Particle Velocity on the Particle Dynamics for (a) Particle size 0.5 mm (b) Particle size 3 mm

3.3.2.5 Effect of kiln wall temperature

Figures 3.15 shows the variation of coal particle temperature at two different kiln wall temperatures for coal particles of size 0.5 mm and 3 mm. The kiln wall temperatures of 1000^0C and 1400^0C are chosen for this analysis. It can be noted that the particle temperature are immensely affected by the increase in the kiln wall temperature. The effect is more intense in the case of bigger size particles.

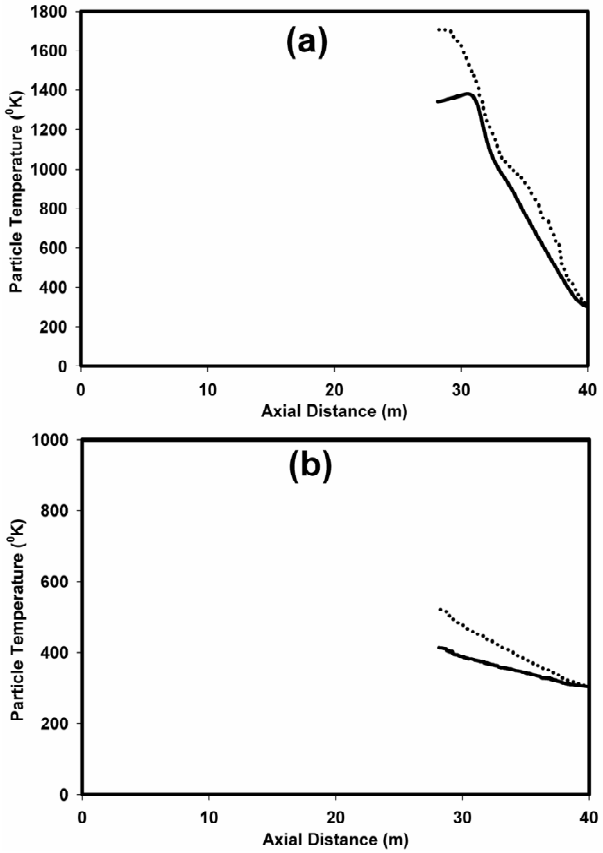

Figure 3.15 Variation of Particle Temperature with Wall Temperature (a) Particle size 0.5 mm (b) Particle size 3 mm

3.4 Integrating to the overall one-dimensional simulator

3.4.1 Axially Averaged Species Concentration

Results of the CFD simulation of pneumatic coal injection from the discharge end of the kiln forms part of the one dimensional model o the overall carbothermal reduction process taking place in the kiln. Figure 3.16 gives an account of the axially averaged species concentration profiles. These values are given as input to the carbothermal reduction simulator as described in chapter 4 of this thesis.

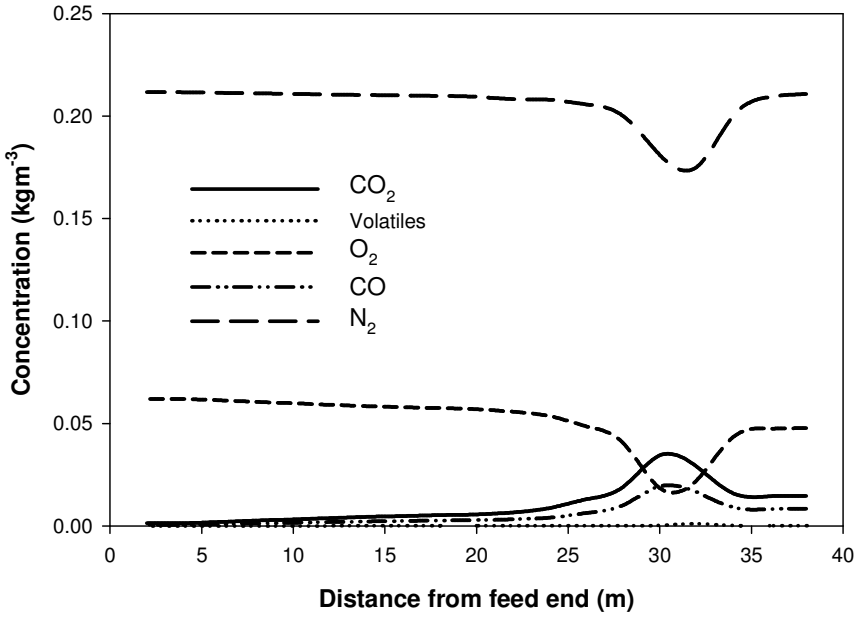

Figure 3.16 Axial Profile of Free Board Gases Resulting from Pneumatic Coal Injection Process

3.4.2 Carbon Load to the Solid Bed

As a result of the combustion of pneumatically injected coal particles, carbon load is added to the solid bed mostly in the reduction zone of the kiln thus balancing the carbon depletion towards the discharge end. The percentage of char

in the falling particle as well as the location where the particle falls on the bed are strongly influenced by the particle size and the initial particle velocity as discussed in the previous section. This data forms a key input for the one dimensional model o the overall carbothermal reduction process taking place in the kiln. Table 3.5 shows the char percentage and location of falling for particles of different sizes. These values are given as input to the carbothermal reduction simulator as described in Chapter 4 of this thesis.

Table 3.5 Carbon Load Provided to the Solid Bed by Pneumatic Coal Injection Process

Particle size (mm)	% Fixed Carbon	Falling distance from feed end (m)
0.5	0.226	31.41
1	0.9	31.82
3	0.95	28.58
5	0.95	27.05
8	0.95	25.34
10	0.95	24.54

3.5 Conclusions

In this chapter the pneumatic coal injection and combustion process in a commercial rotary kiln is modeled using a three dimensional steady state multiphase Eulerian-Lagrangian CFD approach where the gas phase is treated as a continuous phase and the pulverized coal particles are tracked in the flow field in a Lagrangian way. The CFD simulation results are validated under cold and hot conditions with the data reported in the literature by Biswas (1993) and Guo *et al.*

(2005). After the validation the numerical results of CFD simulation of pneumatic coal injection for different particle size distribution are presented. The effect of initial particle velocity, particle size and kiln wall temperature on the particle dynamics and char burnout are investigated. The results indicate that the injection velocity and particle size has profound influence on determining the efficiency of the pneumatic injection in supplementing the reduction process. The effect of particle size distribution on the thermal and carbon load added to the bed was also studied. The present model is thus useful in predicting the optimum particle size distribution and injection velocity for any given operating and physical conditions of the kiln. The particle size distribution show profound influence on the coal devolatilization and combustion reaction as the particle temperature is controlled by the particle size. Particles of size more than 5 mm just get heated up and they reach the solid bed almost unburnt, thus providing the carbon load for the reduction process. Smaller particles burn off completely in the free board and they contribute only to the thermal load which supplements the heat availability in the free board region. By simulating combustion and devolatilization reactions of different types of coals, the present model helps in selecting the suitable type of reductant for improved efficiency of the industrial reduction processes.

Chapter 4

STEADY STATE SIMULATION OF ROTARY KILN

4.1 Introduction

In Chapter 2 of this thesis we have seen a detailed analysis of the kinetics of carbothermal reduction of Ilmenite taking place in the high temperature rotary kiln reactor. In Chapter 3 a three dimensional model of the pneumatic coal injection process from the discharge end of the kiln is given in which the concentration of various species and the gas temperature profile have been axially averaged. In the present chapter, the models given in Chapters 2 and 3 are incorporated in to a comprehensive one dimensional steady state model which serves as the overall process model for the carbothermal reduction of Ilmenite in the rotary kiln reactor.

4.2 Literature Survey

The rotary kiln is a widely used reactor in chemical and metallurgical industries. It is basically a long steel cylinder lined with refractory on the internal surface. The cylinder is mounted on rollers and is rotated *via* a drive motor and gearbox assembly. The elevation of one roller with respect to the other fixes the slope of the kiln. The solids flow down the kiln under the influence of gravity and kiln rotation. Dams located along the length hold back the flow of the solids. This results in the buildup of a bed of solids. The kiln geometry and operating conditions and physical characteristics of the solids determine the bed volume and residence time of solids within the kiln. Transverse segregation within the solids bed occurs as a result of particle size and density differences. The temperature of the solids bed increases as it travels the length of the kiln. Heat is supplied to the kiln bed via various heat transfer pathways. Heat is consumed within the kiln bed due to endothermic reduction reactions.

Numerous chemical reactions occur within the kiln bed. When solid reductant such as coal is used, loss of volatiles and combustion of carbon from the coal must be considered. Reduction of the ore takes place with the associated complex reaction chemistry. Homogeneous gas reactions occur within the voids between particles in the bed, determining the interstitial gas composition. The rates of various heterogeneous reactions are dependent upon the interstitial gas composition, mass transfer conditions and the temperature distribution within the bed.

In spite of the commercial significance of the usage of rotary kiln reactors, very little work has been done on the important aspects of its operation like axial and transverse bed motion, heat transfer etc. For this reason the design and scale-up of rotary kilns is based heavily on experience rather than fundamental principles.

4.2.1 Literature survey for solid-hold up and residence time distribution

The motion of the solid bed can be resolved into the axial as well as transverse components. The former takes care of the shape of the solid bed and the residence time of the particles whereas the latter is responsible for the homogeneity of the solid bed. Depending on the speed of rotation of the kiln, the motion of the bed of granular solid in the transverse plane of the kiln has been observed to take a number of forms, *viz.*, slipping, slumping, rolling, cascading, cataracting and centrifuging as described by Henein *et al.* (1983) and depicted in Figure 4.1. In the slipping mode, speed of rotation is the lowest and there is no shear rate in the bed. As speed increases, the bed enters into the slumping mode with discontinuous bed motion at the free surface of the bed. Further increase in

speed takes the bed to the rolling mode where there is continuous bed motion at the free surface of the kiln and all particles are in the lower half of the transverse plane of the kiln. Beyond this speed the bed attains the cascading motion and some particles are in the upper half of the transverse plane of the kiln. Further increase in speed leads to cataracting where particles are rejected to the free board and finally to centrifuging of the solid bed inside the kiln wall.

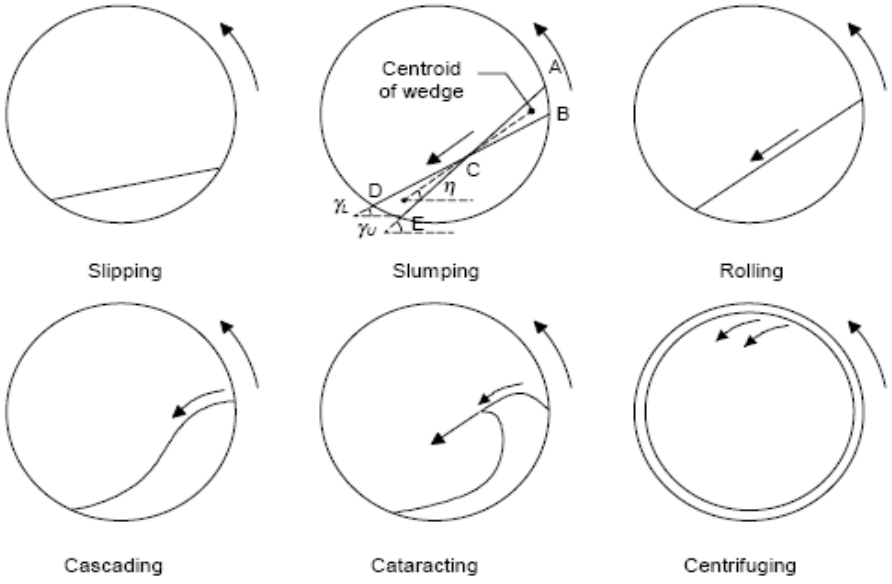

Figure 4.1 Granular Flow Patterns of the Solid Bed in a Rotary Kiln

Rolling is the most preferred mode of solids motion as it provides better mixing of particles and improved heat transfer in solid bed and between the bed and the hot free board gas thereby ensuring better product quality. Solid bed in rolling mode is characterized by a thin active layer (shear layer) in which particles flow down the sloping free bed surface and a thick passive layer (plug flow region). Particle mixing mainly occurs in the active layer where particles are

carried upward by the cylinder wall. Particle mixing is negligible in the passive layer.

The solid motion in the transverse view has been deeply investigated by Mellmann (2001). Different forms of solid motions, such as sliding, slumping, rolling, and the transition behavior between these motions are well described. The solid transverse motions are found to influence the solid axial motion in the kiln. Furthermore, it is also found that the change of the bed depth in axial direction inversely influences the solid transverse motion (Liu *et al.* (2005)), as well as the residence time of the particles in the active layer (Liu *et al.* (2006)), and the hold up of solids in kilns (Liu and Specht (2006)).

Axial motion of solids in the kiln is dependent on the mass flux of solids, speed of rotation, height of solid bed (percentage fill), particle size, angle of repose and kiln tilt (Kramers and Croockewit (1952), Lebas *et al.* (1995) and Spurling *et al.* (2001)). The changes in these operating parameters cause variation in bed height along the kiln length. This not only changes the area of solids that are exposed to freeboard for energy exchange but also influences residence time of solids in the kiln. Obviously, this has effect on kiln performance. It is therefore essential to use accurate models of axial motion of solids while developing reaction engineering model of a kiln.

The bulk motion of the granular bed in steady state operation of a rotary kiln has been investigated experimentally by a large number of authors in laboratory and pilot plant scale devices, commencing with the work of Sullivan *et al.* (1927). Several numerical models are available to predict the depth profile (Saeman (1951), Gupta *et al.* (1991), Hogg *et al.* (1974) and Sai *et al.* (1992)). Modeling of the solids motion observed is of two principal types: (i) empirical

correlations in terms of dimensionless parameters, for example Chaterjee *et al.* (1983), and (ii) mechanistic models, as first proposed by Saeman (1951) and Kramers and Croockewit (1952). The latter approach proposes a mechanism for the granular flow through the kiln based on a simple average particle motion. The model calculates the axial hold-up profile and particle mean residence time as a function of the kiln diameter, length, discharge dam height, axis inclination and rotation speed, the mass feed rate, and the bulk density and dynamic angle of repose of the granular solid. Generally, good qualitative agreement, and reasonable quantitative correlation, has been found between the experimental measurements and the model calculations; for example, Lebas *et al.* (1995) have shown that the model agrees with their experiments on bed depth in a cylinder with no end dam. For a review, see Spurling (2000). A recent paper by Liu and Specht (2006) agrees with the conclusions regarding residence time distributions. However, when these models are coupled with modeling of heat transport, these numerical models often lead to a complex system of differential equations that is rather difficult to solve or even unsolvable. Such models are incapable of predicting influence of key design and operating parameters of kiln on its performance.

4.2.2 Literature Survey on Heat Transfer

Heat transfer from the free board to the solid bed needs to be modeled accurately since this drives the chemical reactions in the bed. The mechanism of heat transfer in the rotary kiln is very complex because it involves not only the gas and solids but also the rotating kiln wall. The various modes by which heat transfer takes place in kiln are shown in Figure 4.2. Q_{RWB} and Q_{CWB} are heat

transfer rates due to radiation and conduction respectively between kiln internal wall and bed. Q_{RGB} and Q_{CGB} are heat transfer rates due to radiation and convection between gas and bed. Q_{RGW} and Q_{CGW} are heat transfer rates due to radiation and convection between the kiln freeboard gas and internal wall. Q_{REF} and Q_{STL} are heat transfer due to conduction in refractory and steel shell respectively. Q_{LOSS} is loss of heat from steel shell by radiation and convection.

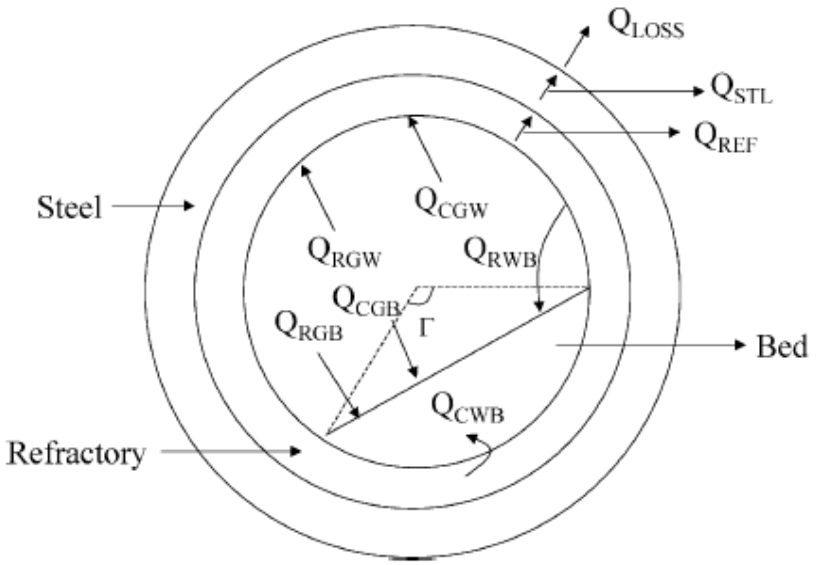

Figure 4.2 Various Heat Transfer Paths in a Rotary Kiln (Boateng (1996))

Many mathematical models have been proposed for operations in rotary kilns dealing with heat transfer to the solid bed (Imber and Paschkis (1960), Sass (1967) and Gorog *et al.* (1981, 1982,1983). Brimacombe and Watkinson (1978a) investigated the characterization of heat flow process in direct fired rotary kilns with detailed experimentation and modeling. Brimacombe and Watkinson (1978b) proposed methods of calculating heat flows among solids, wall and gas from the measured axial and radial temperature and also a simple radiative model. Gorog *et*

al. (1982) studied the radiative heat transfer between a nongray free board gas and the interior surfaces by evaluating the fundamental radiative exchange integrals using numerical methods. Gorog *et al.* (1983) proposed a mathematical model to determine the temperature distribution in the wall of rotary kiln incorporating a detailed formulation of the radiative and convective heat transfer coefficients. Ferron and Singh (1991) predicted wall-to-bed heat transfer coefficients by penetration model. For operating conditions prevailing in direct reduction kilns, radiation dominates the heat transfer process (Boateng and Barr (1996), Mastorakos *et al.* (1999) and Karki *et al.* (2000)).

4.2.3 Literature Survey on Steady State Models for Rotary Kilns

To simulate steady state heat and mass balance in an Ilmenite reduction rotary kiln, material conservation equations have to be written to describe the flow of solids. These equations have to take into account the loss of volume from the bed due to reaction of the solids at points along the length of the kiln. Ilmenite reduction kilns are operated with a secondary injection of coal from the discharge end of the kiln, *via* a pneumatic coal injection system from the discharge end of the rotary kiln. This plume of coal will be distributed along the kiln bed depending on the velocity and momentum of the injected particles. The temperature of the solids bed increases as it travels the length of the kiln. Heat is supplied to the kiln bed *via* various heat transfer pathways. Heat is consumed within the kiln bed due to endothermic reduction reactions.

The heat transfer within the reduction kiln is complex. Radiative transfer dominates in the high temperature zones of the kiln. Various heat transfer paths require consideration. Radiative transfer to and from the gas phase and to the exposed wall and exposed bed surface is important. Convective heat transfer

between the counter current flow of the gas and the solids bed must be considered. As the kiln rotates, periodic changes in temperature within the refractory wall occur. Heat may be transferred to and from the covered wall and the underside of the solids bed by conductive of radiative heat transfer. Motion of the solids bed induces transfer of heat throughout the bed by conduction or possibly radiation. Heat is also conducted through the refractory wall and steel shell. Radiative and convective losses from the outside shell of the kiln are important.

The nature of the solids transport problem in the Ilmenite reduction kiln will require a comprehensive approach to modeling the bed volumetric flow characteristics. The Ilmenite reduction kiln is operated with at least one dam ring. Solids are held back by the dam ring and the dimensions of the dam rings have a significant influence on the kiln filling profile. The model should take into account the influence of kiln geometry, solids flow characteristics and kiln operating conditions.

In the SL/RN (Stelco-Lurgi / Republic National) iron oxide reduction process and the Becher Ilmenite reduction process, a carbonaceous reductant is used. To support the endothermic reduction process, a large bed heat input is required. This heat input is provided principally by burning the combustible gases released from the bed in the gas zone. Shell tubes are placed at various axial positions and air is injected into the gas zone through these tubes. Because the injection of this air is critical to control of the kiln temperature profile (Venkateswaran and Brimacombe (1977)), it is important to include a more detailed model of the gas transport than those used in models of other rotary kiln processes.

Direct reduction process of iron ore in rotary kilns have been modeled by Wingfield *et al.* (1974), Venkateswaran and Brimacombe (1977) and Mukopadhyay *et al.* (1984). Of these models Wingfield's model is for a gaseous reductant while the other two are for coal based reduction process. Wingfield *et al.* (1974) and Iyer *et al.* (1983) both developed steady state models for rotary kilns used for partial reduction of iron ore. The reductant was a mixed atmosphere of CO and H_2 flowing counter currently over the surface of the bed. The reaction kinetics was represented using the model of Themelis and Gauvin (1963).

The SL/RN direct reduction process has been modeled by Venkateswaran and Brimacombe (1977) and the TDR process has been modeled by Mukopadhyay *et al.* (1984). Venkateswaran and Brimacombe (1977) modeled the gas flow in the SL/RN kiln as plug flow. The reaction in the solids bed was modeled using rate expressions for the Boudouard and reduction reactions and the reduction kinetics coupled through gas composition driving force terms. They calculated the evolution of CO from the bed into the gas zone from the iron oxide reaction rate. For every mole of CO consumed by the iron oxide reduction reaction, one mole of CO was assumed to escape to the gas zone.

In contrast to the work of Venkateswaran and Brimacombe (1977), Mukhopadhyay *et al.* (1984) made no attempt to model flame behavior in the TISCO iron-oxide direct reduction rotary kiln. They made the assumption that the flame length at the discharge end of the kiln could be neglected. From the description given, no shell tubes were present in the kiln.

Ramakrishnan (1996) studied the influence of operating parameters such as iron and carbon concentration in the charge, oxide and coal reactivity and kiln holdup and analyzed the process behavior. The model was also extended for the

Ilmenite reduction reaction. Watkinson and Brimacombe (1982) studied the limestone calcinations in a rotary kiln and related the observed temperature and calcinations patterns to the heat transfer process which governs the performance of the kiln.

In recent years, computational fluid dynamics (CFD) based models are being applied to simulate rotary kilns (Mastorakos *et al.* (1999) and Ranade *et al.* (2003)). It is possible to simulate pneumatic coal injection and the free board region of rotary kiln fairly accurately using the state of the art CFD models. It is however difficult to model motion of solid particles in a conventional CFD framework. Therefore, a one-dimensional model is required for simulating the various chemical and physical processes taking place in the Ilmenite reduction rotary kiln.

4.3 Process Description

Rotary kilns used for carbothermal reduction of Ilmenite involve a complex interplay of coupled heterogeneous reactions, conductive, convective and radiative heat transfer and complex solid and gaseous flows inside the reactor. A comprehensive understanding of the process at various length and time scales is necessary to obtain optimum kiln throughputs, air requirements, thermal load distributions, and carryover of solids as a function of kiln process design variables. This understanding can be achieved only through modeling and simulation as experimental investigation of a commercial kiln is not feasible. Since the carbothermal reduction of Ilmenite in the rotary kiln reactor is the most important step in the Becher Process of Ilmenite beneficiation, it is quite important to develop a comprehensive model for this process. In spite of the commercial

significance of the Ilmenite reduction process in rotary kiln reactor, which has been practiced for quite a long time now, reported modeling studies of this process are very few.

The carbothermal reduction of Ilmenite is carried out in the rotary kiln reactor by feeding the desired portion of Ilmenite ore and coal to the refractory lined rotary kiln inclined from the feed end to the discharge end. It is to be noted that both reducing (in the solid bed) and oxidizing atmosphere (in the freeboard) prevail side by side in the rotary kiln. Within the material charge a reducing atmosphere accompanied with endothermic reaction prevails while in the freeboard above oxidizing conditions with exothermic reactions prevail.

The kiln can be divided into a pre-heating and reduction zone. In the pre-heating zone, the charge is dried and volatilization of coal takes place and the charge is heated to the reducing temperature. The heating medium is normally a gas stream flowing through the free board in a counter current way to the solids bed. The schematic view of the carbothermal reduction process in a rotary kiln is shown in Figure 4.3.

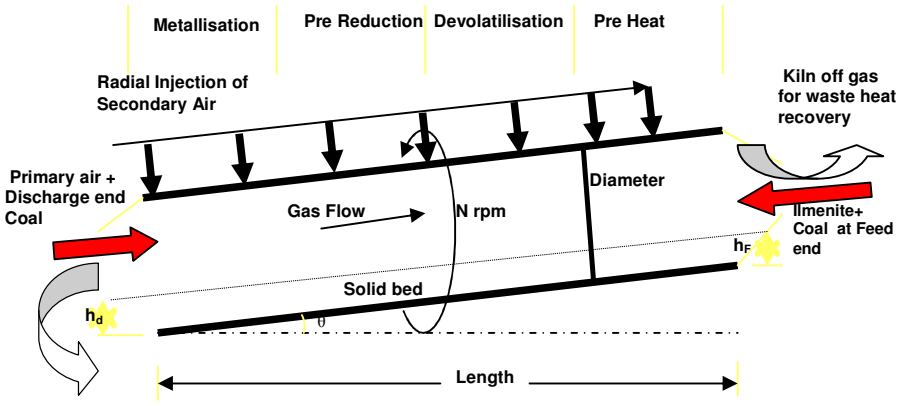

Figure 4.3 Schematic View of the Ilmenite Reduction Kiln

Within the gas phase, above the solid bed (freeboard gas region) various combustion reactions occur. Air is injected at fixed points along the length of the kiln, counter current to the bulk gas flow and through the coal fireman, co-current to the bulk gas flow, resulting in the formation of flames. An induced draft fan provides the pressure gradient for the bulk flow of gas towards the feed end of the kiln. Because the air injection is crucial to control the kiln temperature profile, it is important to include a more detailed model of the gas transport than those used in models of other rotary kiln processes.

The temperature of the solids bed increases as it traverses the kiln length. Heat is supplied to the kiln bed via various heat transfer pathways. Heat is consumed within the kiln bed due to endothermic reduction reactions. Numerous chemical reactions occur within the kiln bed. Devolatilization and volatile combustion along with combustion of carbon from the coal must be considered. Reduction of Ilmenite takes place with the associated complex reaction chemistry. A suitable kinetic model is essential to take into account the influence of different factors on the important bed reactions. Heat and mass balances on the solids and gas species determine the instantaneous bed phase composition and temperature

distribution. Boudouard Reaction is highly endothermic and the solid bed temperature thus becomes almost constant in the reduction zone. The heat required is produced by the combustion of the CO released from the solids bed. The desired temperature is attained by the controlled addition of the combustion air along the length of the kiln. Coal particles are injected pneumatically in the rotary kiln through the discharge end to supplement the heat availability in the kiln and also to maintain a reducing atmosphere. The mechanism of heat transfer in the kiln is very complex because it involves not only the gas and solids but also the rotating kiln wall.

In addition to these, heat is also generated in the free board by the combustion of volatiles escaping from coal and any unreacted CO carried over to the free board. Major chemical reactions in the reduction zone include reduction of Ilmenite by CO gas and gasification of carbon by CO_2 as given by equations (4.1) and (4.2) respectively.

$$FeTiO_3(s) + CO(g) \rightarrow FeTiO_2(s) + CO_2(g) \tag{4.1}$$

$$C(s) + CO_2(g) \rightarrow 2CO\ \ (g) \tag{4.2}$$

On summarizing we get the overall chemical reactions involved in the reduction process as

$$FeTiO_3(s) + C(g) \rightarrow FeTiO_2(s) + CO(g) \tag{4.3}$$

4.4 Challenges involved in Modeling

Modeling of rotary kiln involves three different parts: the gas phase, the solid phase and the kiln wall. Interactions between all these parts have to be taken into account. First step is to identify the significant process variables. Extent

of accuracy for each component modeled should be understood. In the gas phase concentration profile of various gas species, pressure, temperature and flue gas composition are important variables. In the solid phase the phase composition of the Ilmenite ore, composition of coal and release of volatiles and solid bed temperature are important variables. The temperature of the kiln wall is essential for closing the energy balance equation in the rotary kiln.

In order to develop a robust model of kiln, it is extremely essential to carefully evaluate the various sub-processes occurring in kiln. It is important to develop appropriate models to estimate average residence time of solids in the kiln and variation of solid bed height within the kiln as a function of solids flow rate, kiln rotational speed, tilt angle and so on. Hence parameters like rotational speed, angle of inclination, dam height and discharge end coal injection ratio form the critical design parameters of the kiln. Velocity and enthalpy of exhaust gases, enthalpy of solid product, percentage entrainment in the free board gas etc. also are of prime significance in the design of kilns. The bed motion poses major design issues as rolling mode is the most desirable in commercial rotary kilns. Major design parameters include thickness of the active layer, particle velocities in the active layer and particle residence time on the bed surface.

Another major design consideration is the chemical reactions taking place in the solid bed. The most important of these, the kinetics of Ilmenite reduction by coal has been extensively studied by researchers all over the world and a detailed account of the same is given in Chapter 2 of this thesis. By analyzing the reported reduction data for a commercial Ilmenite reduction kiln and by applying classical models of reaction kinetics, we have developed a semi empirical model and formulated an overall rate constant which takes care of various controlling factors

such as the coal/Ilmenite ratio in the feed, CO/CO_2 in the kiln etc. Coal requirement is determined by carbothermal reduction reaction requiring endothermic heat, heat losses in the exhaust gases, heat in products, wall losses and sensible heat requirements of gases and solids. Energy required for the reactions taking place in the bed is solely from the free board gas.

The residence time of the solid bed within the kiln should be evaluated for accurate simulation of chemical reactions occurring in the bed. Axial velocity of solids varies along the kiln length causing variation in height of the solid bed. Models which do not take into account the variation in bed depth along the axis of the kiln fails to predict realistic performance of the kiln. In industrial kilns, parameters like rotational speed and angle of inclination largely affect the bed depth profile. This causes considerable changes the area of solid bed exposed to freeboard for energy exchange and influences the residence time of solids in the kiln. It is therefore essential to incorporate robust models of axial motion of solids while developing reaction engineering model of a kiln.

Heat transfer within the kiln has a profound impact on the rate of various chemical reactions taking place in the slid bed. Therefore it is essential to model the heat transfer with utmost care. Key parameters appearing in heat transfer models are: emissivity of gas, absorption coefficient of gas, conductivity of gas and solid. Estimation of these properties is not straightforward. Because of the counter current gas flow, solids will get entrained from bed to freeboard region. The extent of solid entrainment will influence the effective emissivity as well as conductivity of gas. Hence effective thermal properties of dust-laden gas need to be estimated to model heat transfer in transverse direction accurately.

Apart from all these critical issues, there are certain constraints specific to the Ilmenite reduction process taking place in the kiln. These include the requirement of at least seven hours of residence time for the Ilmenite coal mixture in the kiln, desired fractional degree of conversion of 85%. Rotational Speed is fixed by the requirement of rolling mode for granular solid flow and residence time required for preheating and reduction reaction. Thus the kiln Inclination, rotational speed and height of dams are to be judiciously fixed to adjust the holdup and residence time of solids. Adequate Radial Mixing is ensured by rolling mode operation. Coal particle sizes must be selectively chosen to prevent segregation of Ilmenite-coal mixtures.

4.5 Mathematical Model

4.5.1 Modeling of the Holdup Profile of the Solid Bed

The mathematical model proposed by Spurling (2000) for solid hold-up and axial velocity is used in the present work for predicting the axial profiles of bed depth. The mechanism by which the granular solid moves through the cylinder is made up of a simple average particle motion, where the main body of the granular bed rotates as a rigid body about the cylinder axis with the same angular speed of the cylinder and particles follow circular tracks from the lower half of the free surface to the upper half of the free surface. On the free surface there is a thin layer of particles falling under gravity. Particles fall rapidly from the upper half of the bed, following the steepest line of descent in the surface. On reaching the lower half of the free surface, they come to rest relative to the cylinder and re-enter the solid body motion. This is schematically shown in Figure 4.4.

The main assumptions of the model are:

- In a cross-section of the bed perpendicular to the cylinder axis, the free surface of the bed is a straight chord
- On an average the trajectory of a particle in a falling layer is straight and inclined to the horizontal plane at the dynamic angle of repose of the granular solid.
- It is simplified by combination of the above to assumptions that a plane tangent to the bed surface is representative of the true shape of the bed surface over the axial distance traveled by a particle in a single fall.

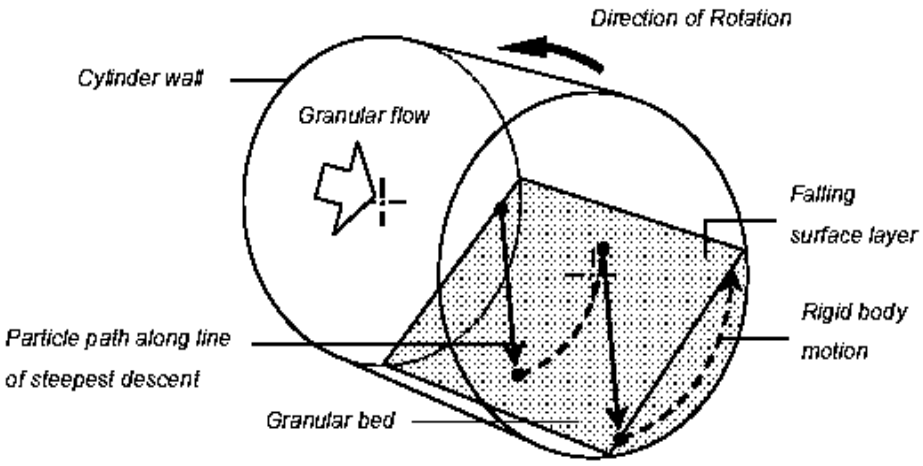

Figure 4.4 Schematic View of the Granular Material Motion in a Rotating Cylinder (Spurling (2000))

.

Using the geometric relationships and the assumptions, the variation of bed height along the length of the kiln is represented by the following equation by Spurling (2000) using the model of Kramers and Croockewit (1952).

$$\frac{dh}{dx} = \tan\gamma\left[\frac{\tan\beta}{\sin\gamma} - \frac{3\phi_v}{4\pi nR^3}\left(\frac{2h}{R} - \frac{h^2}{R^2}\right)^{-3/2}\right] \qquad (4.4)$$

where x is the axial position of solids in kiln, β is the kiln inclination with respect to horizontal, γ is the angle of repose of solids Φ_v is the volumetric flow rate of the

material, *n* the kiln rotational speed and *R* is the kiln radius. The above model is based on mechanism of transportation put forward by Saeman (1951). This model was shown to predict the height variation of solid bed along the kiln length for a wide range of operating conditions and kiln dimensions by Spurling (2000).

This is a non linear first order differential equation with constant coefficients. This equation is integrated with appropriate boundary condition from the cylinder discharge end up to the feed end to calculate the axial bed depth profile. Cross sectional area of the solid bed at various axial locations can then be calculated using equation (4.5). Here Γ is the angle subtended by the solid bed at the kiln axis and *h* is the height of the solid bed.

$$A_s = \frac{1}{2} R^2 \Gamma - \frac{1}{2} L_s (R - h) \tag{4.5}$$

Hold-up profile is integrated along the length of the cylinder to calculate the total hold-up and then divided by the volumetric flow rate to give the mean particle residence time.

4.5.2 Steady State Heat and Mass Balance

The process simulation is based on a one-dimensional steady state model in which the rotary kiln is divided into a number of segments or cells discretized in the axial direction. Each cell is subdivided into a gas phase and a solid phase. Mass and energy transfer between the phases are taken into consideration. Input and output mass and energy flows for each cell is identified. Conservation equations for mass and energy are formulated and solved for each cell. The formulated balance equations of each cell depend on the adjacent cells. Therefore, the equations of each balance segment are linked with one another according to the direction of gas and solid flows. In the solid phase, solid–solid reactions and

heterogeneous gas solid reactions occur, while in the gaseous phase only homogeneous gas reactions have to be considered (Figure 4.5).

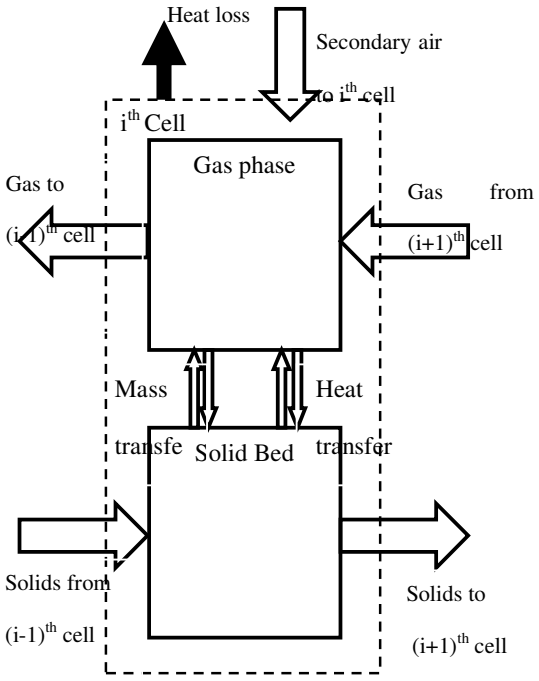

Figure 4.5 Material and Energy Flows in a Control Volume

4.5.3 Assumptions/Simplifications

The assumptions used for developing the one dimensional mathematical model of the Ilmenite reduction kiln are given below:

i. The process operates under steady state conditions.

ii. The flow of solids and gases in the kiln are in plug flow i.e., the radial gradients in each phase and axial dispersion is neglected.

iii. The axial mixing in the solid bed is neglected.

iv. The combustion in the freeboard gas is instantaneous.

v. Individual particles in the solid bed have a uniform temperature

vi. Dusting and entrainment of particles are not taken into account

vii. Variation of kiln wall temperature in the azimuthal direction is neglected. (The regenerative effect of the wall is not taken into account.)

viii. The contribution of radiative transfer over axial distances is neglected.

4.6 Governing Equations

The kiln is divided into thin slices of differential length dx as shown in Figure 4.5. Mass and heat balances are performed on such a slice and it leads to the following set of equations

4.6.1 Mass Balances

(a) On the solids Bed

The mass conversion equation for species *i* in the solid bed can be written as

$$\frac{dG_{si}}{dx} + \sum r_{gi} - \sum r_{ci} = 0 \tag{4.6}$$

where the terms r_g and r_c represent the rate of generation and consumption per unit volume respectively of individual components due to chemical reactions. The term G_{si} represents the mass flux of solids and is given by

$$G_{si} = \rho_{si} V_s Y_{si} \tag{4.7}$$

Where Y_{si} is the mass fraction of species i. V_s is the velocity of the solid bed, ρ_{si} is bulk density of the solids. From the bed depth profile, we calculate the kiln solid hold-up as

$$M = \rho_s R^2 \int_0^L (\Gamma - \sin\Gamma\cos\Gamma) dx \tag{4.8}$$

where Γ is the local fill angle of the solid bed and is defined as

$$\Gamma = \arccos\left[1 - \frac{h(x)}{R}\right] \tag{4.9}$$

With known hold-up M, the mean residence time of the solids in the bed is calculated as

$$MRT = \frac{M}{\dot{m}} \tag{4.10}$$

where $\dot{m}$ is the mass feed rate of solids. The cross sectional area A_s of the solids bed is given by

$$A_s = R^2(\Gamma - \sin\Gamma\cos\Gamma) \tag{4.11}$$

From the above equations velocity of the solids bed V_s is calculated as

$$V_s = \frac{A_s}{MRT \times dx} \tag{4.12}$$

The species considered in the solid bed are Ilmenite and coal.

For the case of Ilmenite, there is no generation and only consumption is the carbothermal reduction reaction. For the case of coal, again there is no generation and the consumption rate should include coal consumption for Boudourad reaction, loss of moisture and volatiles from coal.

(b) On the Free Board

The mass conversion equation for the gas species *j* in the freeboard is given as

$$\frac{dG_{gj}}{dx} - \sum r_{gj} + \sum r_{cj} = 0 \qquad (4.13)$$

Note that there is a sign change in the rates, since gases flows in a counter current way to the solids bed. The gas species considered for the present simulation includes CO, CO_2, CH_4, H_2, H_2O, N_2, O_2 and tar. The term G_{gj} represents the mass flux of gases

Nitrogen mass balance:

Rate of consumption of N_2 =0

Rate of generation of N_2= N_2 generated from volatiles in coal + N_2 generated from input air +N_2 generated from input air from pneumatic coal injection unit +N_2 generated from volatiles in coal from pneumatic coal injection unit

Oxygen mass balance:

Rate of consumption O_2= Rate of consumption of O_2 for burning of combustibles = O_2 used for combusting CO to CO_2 + O_2 used for combusting H_2 to H_2O +O_2 used for combusting CH_4 to CO_2 and H_2O+ O_2 used for combusting tar to CO2

Rate of generation of O_2 = O_2 generated from input air from shell fans and pneumatic coal injection unit

Carbon dioxide Balance:

Rate of consumption of CO_2 = 0

Rate of generation of CO_2 = rate of generation of CO_2 from combustible gases + rate of generation of CO_2 from volatiles from coal from solid bed and from pneumatic coal injection unit

Carbon monoxide balance:

Rate of consumption of CO = Rate of CO consumed for combustion reaction

Rate of generation of CO = rate of generation of CO from Boudourad reaction + rate of generation of CO from volatiles from coal from solid bed and from pneumatic coal injection unit

Methane Balance:

Rate of consumption of CH_4= Rate of CH_4 consumed for combustion reaction

Rate of generation of CH_4 = rate of generation of CH_4 from volatiles from coal from solid bed and from pneumatic coal injection unit

Water Vapor Balance:

Rate of consumption of H_2O= 0

Rate of generation of H_2O = rate of generation of H_2O from drying of coal from solid bed + rate of generation of H_2O from combustion products

Hydrogen Balance:

Rate of consumption of H_2= Rate of H_2 consumed for combustion reaction

Rate of generation of H_2 = rate of generation of H_2 from volatiles from coal from solid bed and from pneumatic coal injection unit

4.6.2 Heat Balances

Various models of the rotary kiln (Barr *et al.* (1989), Sass, (1967), Tscheng and Watkinson (1979)) have the capability of predicting the average conditions within both the bed and freeboard as functions of axial position. Under steady state conditions energy conservation for any slice requires that

$$\dot{Q}_{NET} = \sum(\dot{n}H)_{out} - \sum(\dot{n}H)_{in} \tag{4.14}$$

Since the conditions in the free board and solid bed are each assumed to be uniform in the transverse direction, we obtain the following equations in each control volume for both gas and solids phase.

$$\left(\sum n_i c_{pgi}\right)\frac{dT_g}{dx} = Q_{g\to ew} + Q_{g\to eb} + \sum \gamma_i A_g \tag{4.15}$$

$$\left(\sum n_j c_{psj}\right)\frac{dT_s}{dx} = Q_{g\to eb} + Q_{ew\to eb} + Q_{cw\to cb} + \sum \gamma_j A_s \tag{4.16}$$

where T_g, T_s are average axial gas and solid temperatures, and γ are the production rates for various species involved in either chemical reactions. One additional condition that must be met is that no net energy accumulation can occur within the wall. This yields an auxiliary condition

$$Q_{g\to ew} + Q_{eb\to ew} + Q_{cb\to cw} = Q_{shell} \tag{4.17}$$

The heat received by the solid bed from the free board gas and from the kiln wall is calculated by considering different modes of heat transfer in the kiln as shown in Figure 4.2. The contribution from each mode is as follows:

i. $Q_{cw\rightarrow cb}$ - Heat transfer between the covered wall and covered bed. Contribution is by the conduction of heat between the covered wall and the solid particles.

ii. $Q_{g\rightarrow ew}$ - Heat transfer between the exposed wall and free-board gas both by convection and radiation

iii. $Q_{g\rightarrow eb}$ - Heat transfer between the exposed upper bed and free-board gas both by convection and radiation

iv. $Q_{ew\rightarrow eb}$ - Heat transfer between the exposed bed and exposed wall. Contribution is only by radiation.

v. Q_{shell} - Heat loss from the outer shell of kiln to surroundings. It includes both convection and radiation.

The heat transfer by conduction between the covered bed and the kiln internal wall is given by

$$Q_{cw-cb} = h_{cw-cb} A_{cw} (T_w - T_s) \tag{4.18}$$

Here A_{cw} is the area of contact between the covered bed and the covered wall, T_w and T_s are the temperature of the wall and the solid bed respectively. $h_{cw\rightarrow cb}$ is the heat transfer coefficient which is evaluated using empirical correlation by Tscheng and Watkinsion (1979) as

$$h_{cw-cb} = 11.6 \frac{k_b}{A_{cw}} \left(\frac{\omega R^2 \Gamma}{\alpha_b} \right) \tag{4.19}$$

In the above expression k_b, Γ, ω and α_b are the thermal conductivity of bed, the angle of fill of the kiln, the rotational speed (rad/s) and the bed thermal diffusivity respectively.

Heat transfer by radiation between gas phase and bed and gas phase and the kiln internal walls is evaluated by the equations developed by Hottel and Sarofim (1967), valid for emissivity greater than or equal to 0.8, as given by the following equations:

$$Q^r_{g-eb} = \sigma A_{g-eb}\left(\frac{\varepsilon_b T_g^4 - \alpha_g T_s^4}{2}\right) \tag{4.20}$$

$$Q^r_{g-ew} = \sigma A_{g-ew}\left(\frac{\varepsilon_w T_g^4 - \alpha_g T_w^4}{2}\right) \tag{4.21}$$

Here A_{g-eb} and A_{g-ew} are the heat transfer area of the exposed bed and the exposed wall respectively, σ is the Stephan Boltzmann constant and ε_b, ε_w are the emissivity of the solid bed and the kiln wall respectively. ε_g and α_g are the gas emissivity and thermal diffusivity respectively. T_g is the free board gas temperature.

Convective heat transfer between gas phase and bed and gas phase and the kiln internal walls is evaluated by the following equations

$$Q^c_{g-eb} = h_{g-eb} A_{g-eb}\left(T_g - T_s\right) \tag{4.22}$$

$$Q^c_{g-ew} = h_{g-ew} A_{g-ew}\left(T_g - T_w\right) \tag{4.23}$$

The convective heat transfer coefficients are calculated as (Tscheng and Watkinson, (1979)):

$$h_{g-eb} = 0.46 \frac{k_g}{D_e} \mathrm{Re}_D^{0.535}\, \mathrm{Re}_\omega^{0.104}\, \eta^{-0.341} \tag{4.24}$$

$$h_{g-ew} = 1.54 \frac{k_g}{D_e} \mathrm{Re}_D^{0.575}\, \mathrm{Re}_\omega^{-0.292} \tag{4.25}$$

where k_g, D_e, Re_D and Re_ω are the gas thermal conductivity, the hydraulic diameter of the kiln, the axial and angular Reynolds numbers and they are given by the following expressions.

$$\mathrm{Re}_D = \frac{\rho_g u_g D_e}{\mu_g}\,;\ \mathrm{Re}_\omega = \frac{\rho_g \omega D_e^2}{\mu_g} \tag{4.26}$$

$$D_e = \frac{0.5D(2\pi - \Gamma + \sin\Gamma)}{(\pi - (\Gamma/2) + \sin(\Gamma/2))} \tag{4.27}$$

$$\eta = \frac{\Gamma - \sin(\Gamma)}{2\pi} \tag{4.28}$$

The radiative heat transfer between kiln internal walls and bed is given by

$$Q^r_{ew-eb} = \sigma A_{ew-eb} \varepsilon_b \varepsilon_w \Omega \left(T_w^4 - T_s^4 \right) \tag{4.29}$$

Ω is the form factor for radiation which is calculated as

$$\Omega = \frac{L_s}{2(\pi - \beta)R} \tag{4.30}$$

4.6.3 Rate Equations

(a) Rate of drying of coal:

Since the quantity of moisture in Ilmenite is very less, only drying rate of coal is considered for the present analysis. This data is taken from the work of Venkateswaran and Brimacombe (1977).

(b) Rate of release of volatiles from coal:

The coal particles in the solid bed first get heated by absorbing energy from the gas. The energy is received by convection and radiation. Because of heatup, the coal particle starts devolatilization. As the temperature in the solid bed reaches around 350^0C, volatile release from the coal particles starts and volatiles get transferred to the gas phase.

In the present model, the model developed by Solomon and Colket (1979) is applied to derive the rate equations for the volatile components. The volatile components released from coal are taken to be carbon dioxide, tightly bound carbon monoxide, loosely bound carbon monoxide, water vapor, methane, tar and hydrogen. The rate equation for evolution of volatile components is represented by the following equation in Arrhenius form (Donskoi *et al.* (2003), Kang Sun and Lu (2009)). For gas component Y, the equation is given by

$$R_Y = Y_i k_Y e^{-E_Y / RT_s} \tag{4.31}$$

where R_Y is the rate of evolution of component Y, k_Y is the pre-exponential factor and E_Y is the activation energy of the component. The values used in the model are listed in Table 4.1 and these values were reported originally by Solomon and Colket (1979).

Table 4.1 Values Used for Kinetics of Devolatilisation

Component	CO_2	CO (tb)	CO(lb)	H_2O	Methane	Tar	Hydrogen
Y_i	0.027	0.041	0.033	0.049	0.031	0.108	0.036
k_Y (s^{-1})	0.5	74.17	583.33	1.50	383.33	125.00	450.00
E_Y (J/mol)	33472	100416	86190	41421	81170	66944	106274

Once the volatiles are released to the freeboard, they get combusted depending upon the availability of oxygen in the control volume. The heat generated by combustion is treated as volumetric heat source.

(c) Rate of carbothermic reduction of Ilmenite:

The kinetics of the carbothermal reduction reaction of Ilmenite taking place in a rotary kiln reactor differ considerably from the kinetics elucidated using common lab scale experiments. Hence it is not suitable to include rate equations based on existing kinetic models in the overall model of the kiln. In the present work different possibilities have been explored for arriving at a tailor-made model which can replicate the scenario in rotary kiln reduction. A detailed report of the same has been depicted in Chapter 2 of this thesis. The kinetics of reduction depends strongly on factors such as the reducibility of Ilmenite and the reactivity of coal. The raw material characteristics control the overall kinetics to a great extent. For a given Ilmenite/coal combination, the reaction temperature and Ilmenite/coal ratio plays the crucial role where as minor effects are due to size distribution, mixing and segregation as well as reactor design and operating characteristics. In order to incorporate all these factors to the simulation of the reduction process, a semi empirical model is developed which takes care of the relative rates of the reduction and Boudouard reactions taking place in the rotary kiln reactor. The overall rate constant which is based on the various controlling factors was proposed and it enables the use of a first order rate equation of the form equation (2.29) for incorporating Ilmenite reduction kinetics in the one-dimensional model of the kiln.

4.7 Solution Methodology

Since the solids and gases flow in the counter-current fashion, the solution of the differential equations (4.6), (4.13), (4.15-4.17) poses some difficulties. The solid boundary conditions are known at the feed end and the gas boundary conditions are known at the discharge end. However in order to start the solution we need initial conditions for both solids and gases at either ends. This leads to two routes in solving this type of mixed boundary problems. The solution uses the fourth order Runge–Kutta method for the solution of the differential equations. We adapted the following iterative method to solve this problem. In this method, a temperature profile for the gas phase is assumed along with an arbitrary flue gas composition in the feed end. Using these values the solutions of differential equations for heat and mass balance of solids are carried out from feed end to discharge end. Then using these values, the gas phase heat and mass balance equations are solved taking into account the source terms from the solids phase from discharge end to feed end. This procedure is carried out iteratively until the gas and solid bed temperatures reach a converged value. The convergence criteria adapted in this work is as follows. The iteration is continued until the variation between the current iteration and the previous iteration values for both solid and gas temperature is within 1%. The flow chart for the propose algorithm is shown in Figure 4.6.

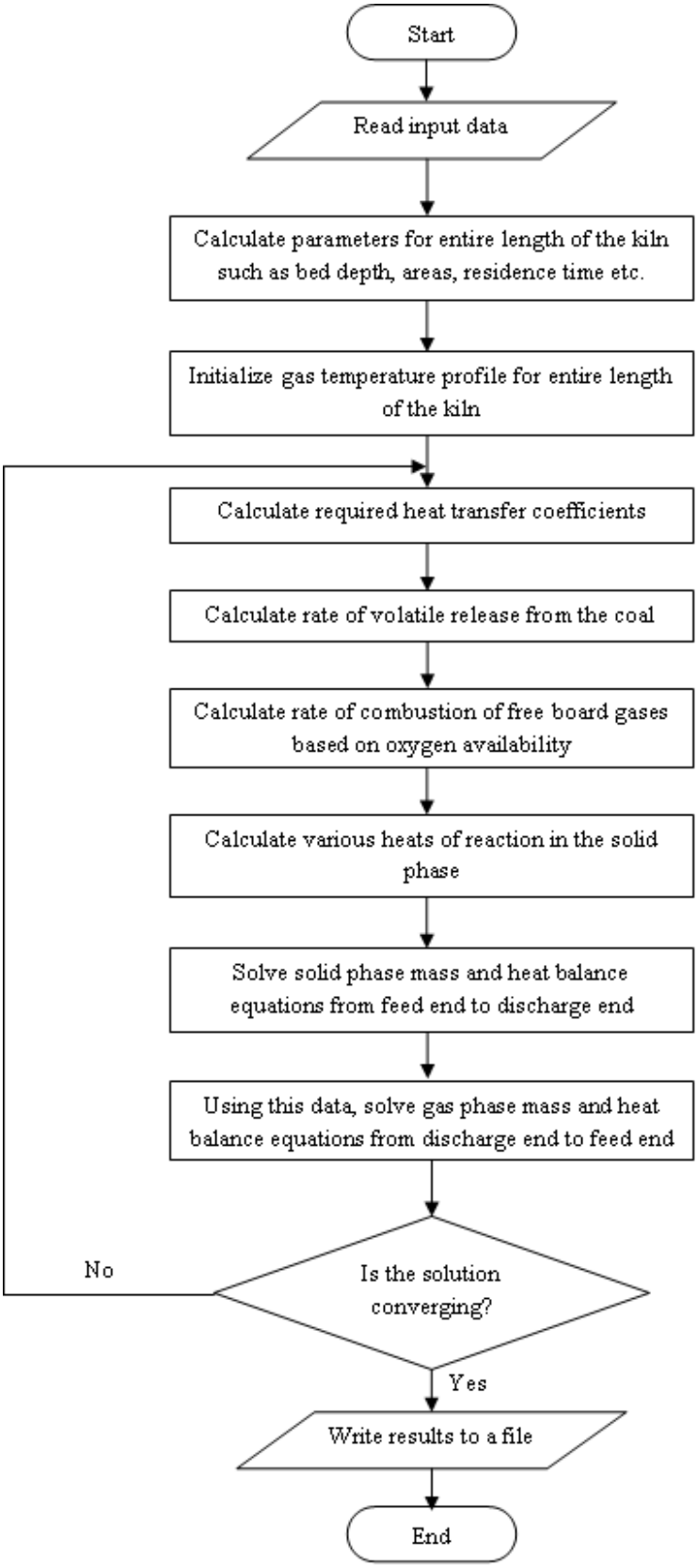

Figure 4.6 Flow Chart of the Algorithm

4.8 Results and Discussion

4.8.1 Validation for Ilmenite Reduction (Ramakrishnan and Sai (1999)

The only reported data available for validation of the present work is that of Ramakrishnan and Sai (1999) for Ilmenite beneficiation in a direct reduction rotary kiln. Hence simulations were carried out with operating conditions and input data used by Ramakrishnan and Sai (1999) as depicted in Table 4.2. For validation purposes pneumatic coal injection simulation is not included.

Table 4.2 Input Parameters (Ramakrishnan and Sai (1999)

Kiln characteristics				
Length of the kiln, m	45			
Degree of fill, pct	18			
Outer shell diameter, m	3.5			
Inner shell diameter, m	3.4			
Inner diameter of outer refractory, m	3.16			
Inner diameter of inner refractory, m	2.59			
Input characteristics				
Ilmenite feed rate, tons/annum	53,225			
Coal feed rate, tons/annum	19,054			
Pneumatic coal injection rate, tons/annum	1710			
Initial particle velocity, m/s	63.2			
Solid to air ratio	3.25			
Composition of charge, pct	Ilmenite		Coal	
	TiO2	53.5	Fixed carbon	42.1
	FeO	0.6	Moisture	25.0
	Fe2O3	44.7	Volatiles	27.4
	MnO	1.3	Ash	4.8
			Sulfur	0.7

The air distribution used for the present simulation is shown in Figure 4.7.

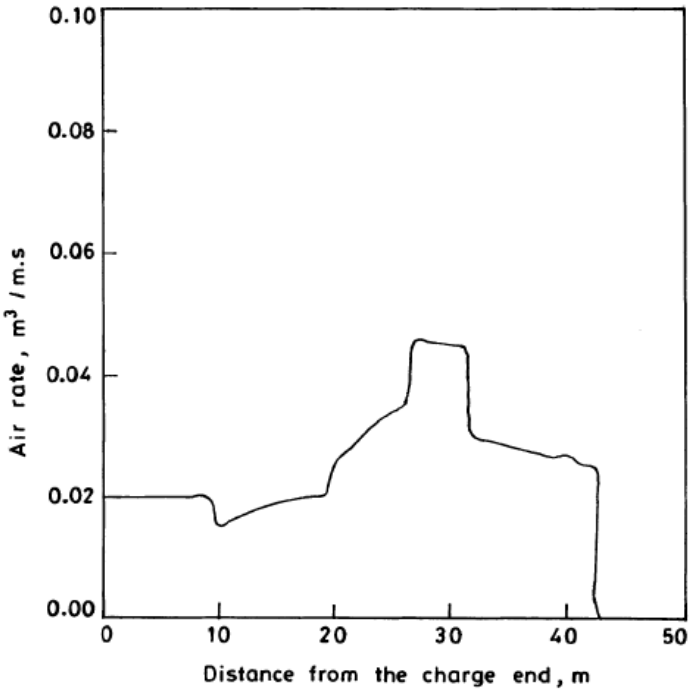

Figure 4.7 Air Profile used for Ilmenite Reduction (Ramakrishnan and Sai (1999))

The variations of the gas, solid and wall temperatures are shown in Figure 4.8 along with the reported results of (Ramakrishnan and Sai (1999)).

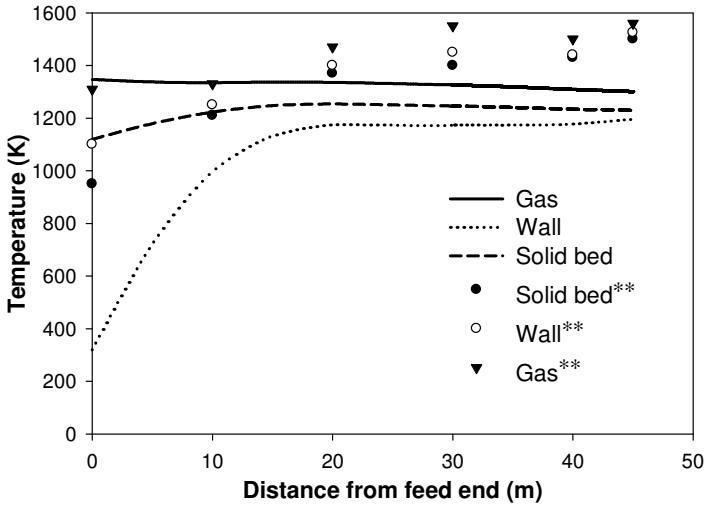

Figure 4.8 Temperature Distribution for Ilmenite Reduction (Ramakrishnan and Sai (1999))

It can be observed that the values predicted by the present simulation are less compared to the results of (Ramakrishnan and Sai (1999)) even though the qualitative trends are same. The reasons can be due to the way the solutions are obtained. Generally in literature heat transfer values are adjusted till the values matches with the experimental observations, whereas in the present simulation the values calculated by different empirical relations are used as such without any modification. Further in the present mathematical model, detailed kinetic modeling for coal devolatilisation is incorporated.

The variation of the reduction profile is shown in Figure 4.9 along with the results of (Ramakrishnan and Sai (1999)) and the agreement is quite satisfactory. It has to be noted here that, in the present work novel reduction mechanism is used whereas in their work, they have extended the reduction approach used for iron ore reduction.

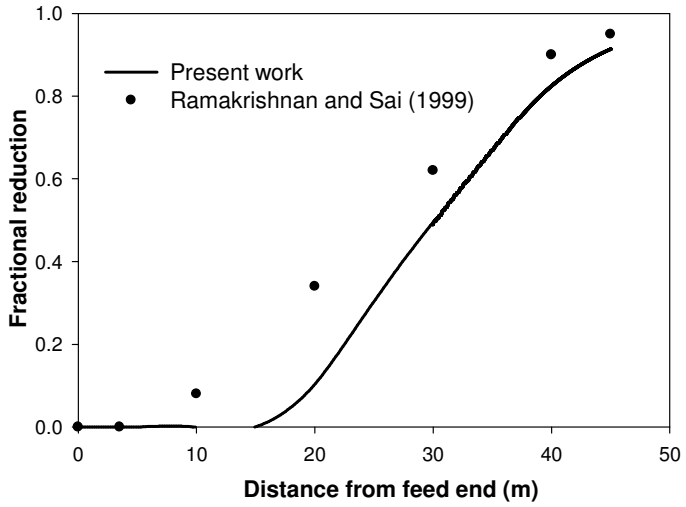

Figure 4.9 Variation of Fractional Reduction along the Axial Length (Ramakrishnan and Sai (1999))

Variation of partial pressures of different gas components obtained by the present simulation is shown in Figure 4.10 along with the results of (Ramakrishnan and Sai (1999)) in Figure 4.11. The agreement between the simulations is quite satisfactory.

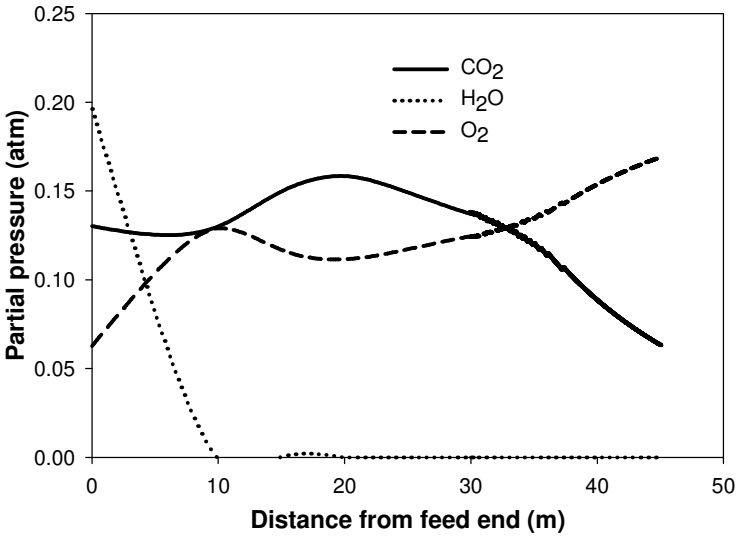

Figure 4.10 Partial Pressure Profile for Various Gas Components (Present Simulation)

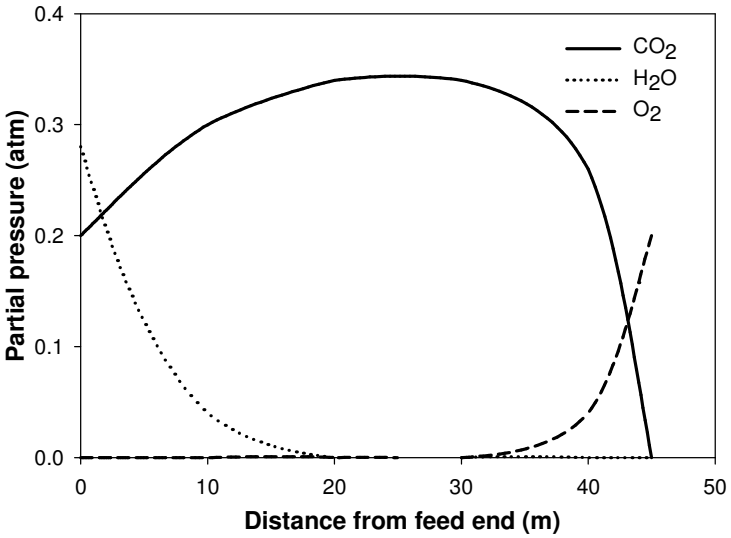

Figure 4.11 Partial Pressure Profile for Various Gas Components (Ramakrishnan and Sai (1999))

Figure 4.12 depicts the comparison of partial pressure profiles of water vapor between the present simulation and the simulation results of (Ramakrishnan and Sai (1999)) and the agreement is quite good.

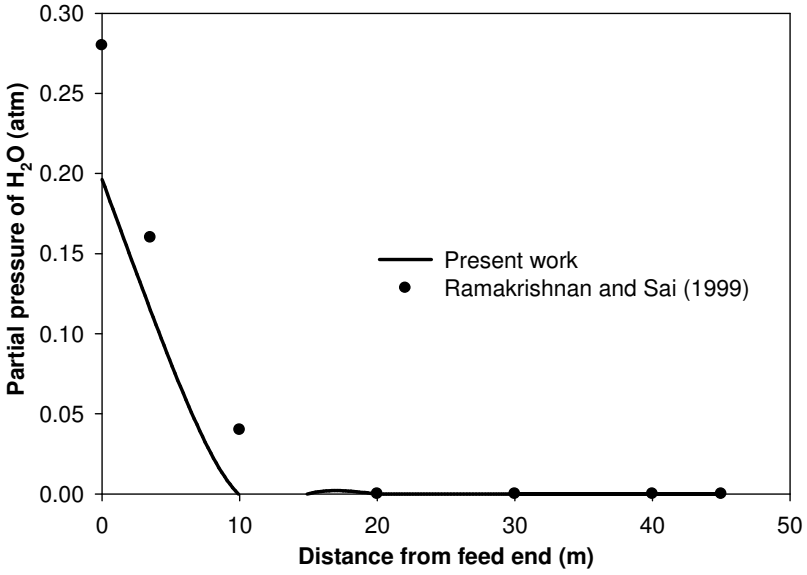

Figure 4.12 Comparison of Partial Pressure Profile for H_2O

4.8.2 Effect of Pneumatic Coal Injection

The effect of pneumatic coal injection on the reduction of Ilmenite using the present model is investigated. As stated in the earlier chapters, pneumatic coal injection not only supplies the heat required for reduction but also provide carbon load to the bed. In the present work, the results obtained by the 3-D CFD pneumatic coal injection simulation (Chapter 3) are averaged both in azimuthal and radial direction to get an axial profile of heat load and concentration profile of various gas components. These results are then coupled with the one dimensional steady heat and mass balance equations proposed in this chapter. Figure 4.13 to 4.15 shows the gas temperature solid temperature and fractional reduction profile.

It can be clearly seen that both gas and solid temperature are higher when pneumatic coal injection is incorporated and hence reduction is faster. The effect of pneumatic coal injection changes the profiles near the discharge end and the change is felt atleast up to 10 m form the discharge end.

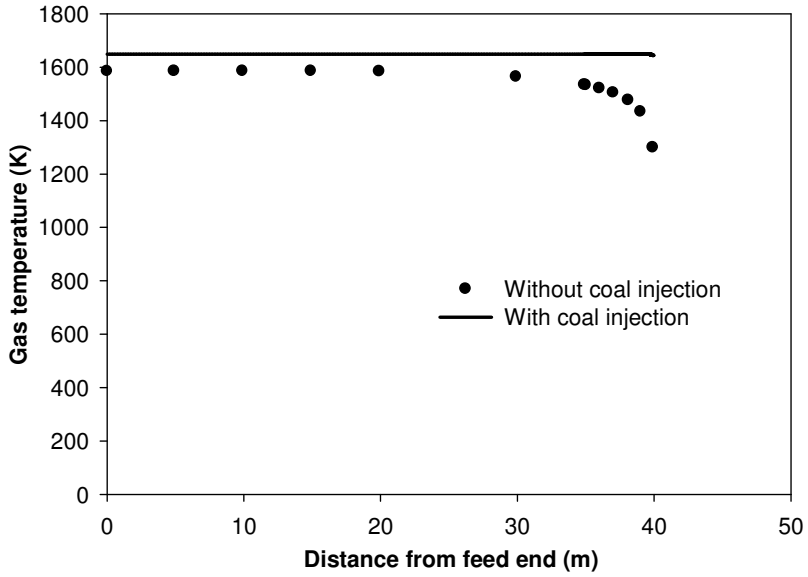

Figure 4.13 Variation of Gas Temperature along the Axial Length of the Kiln

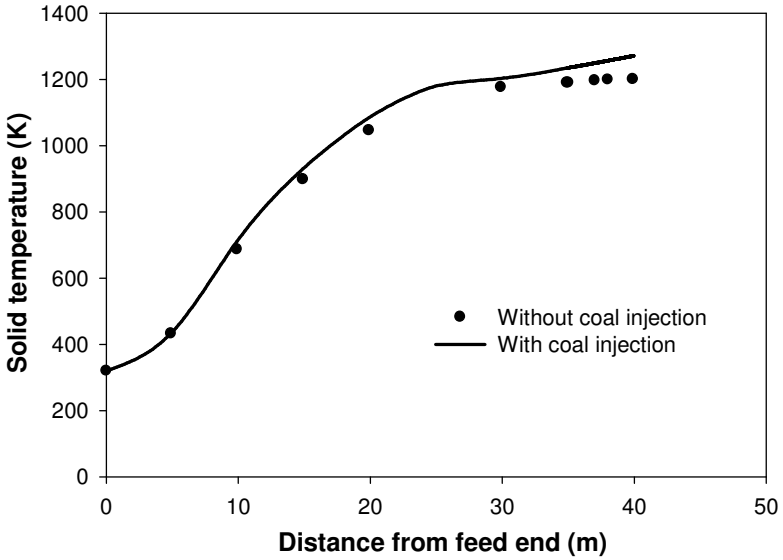

Figure 4.14 Variation of Solid Temperature along the Axial Length of the Kiln

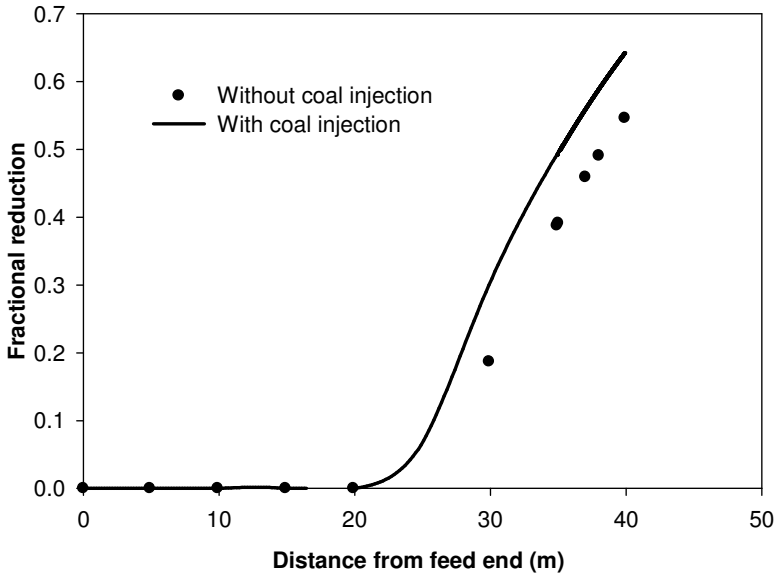

Figure 4.15 Variation of Fractional Reduction along the Axial Length of the Kiln

These results clearly indicate the effect of pneumatic coal injection in maintaining the reducing atmosphere and temperature in the kiln.

4.8.3 Effect of Air Distribution

For carbothermal reduction of Ilmenite, the air profile along the axial length of the kiln is a very crucial design parameter. Hence we have used the present mathematical model to simulate some results for various theoretical air distribution profiles. The air profiles chosen for the present simulation are presented in Table 4.3

Table 4.3 Different Air Distribution Profiles

	Air Rate (m^3/m. sec)				
	Distance from feed end (m)				
	0-10	10-20	20-26	26-32	32-42
Profile 1	0.02	0.019	0.0214	0.046	0.028
Profile 2	0	0	0	0	0.03
Profile 5	0	0.2	0.34	0	0
Profile 4	0.2	0	0	0.3	0
Profile 3	0	0	0.05	0.45	0.03
Profile 6	0.16	0		0	0.25

Though the values used are purely intuitive, the suggested range turned out to be suitable for the process being studied. It was also observed that the gas temperature and bed temperature are not much affected by the variation within this range.

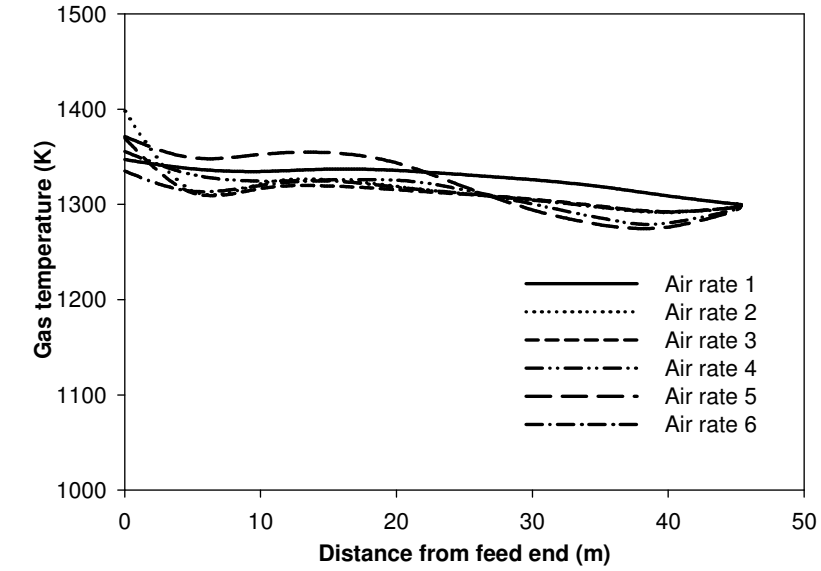

Figure 4.16 Effect of Air Distribution on Gas Temperature

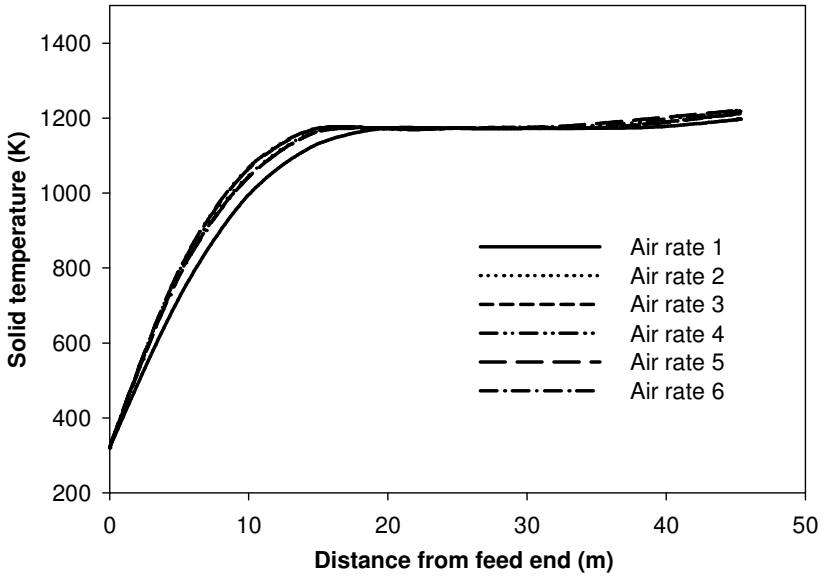

Figure 4.17 Effect of Air Distribution on Solid Temperature

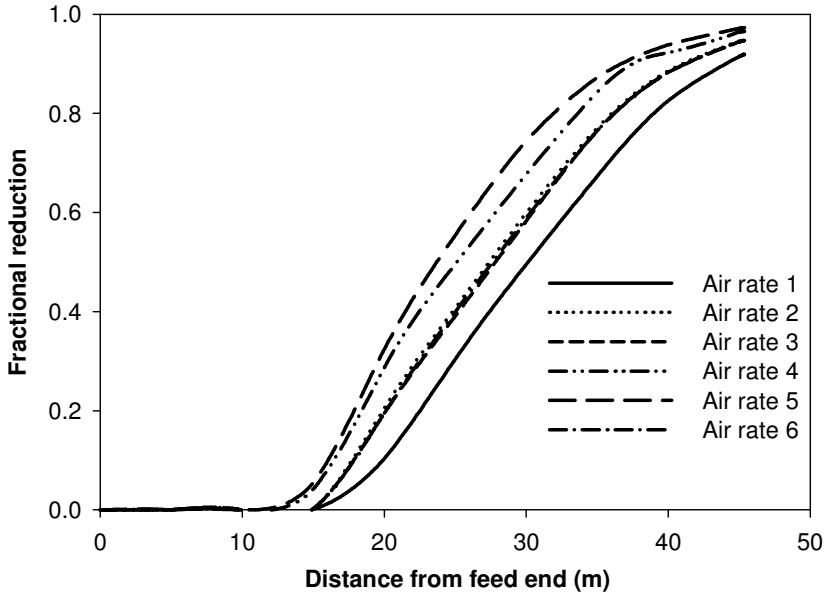

Figure 4.18 Effect of Air Distribution on Fractional Reduction

There is a variation in fractional reduction for different air profiles as shown in Figure 4.18. Figure 4.19 and 4.20 shows the variation of partial pressures of CO_2 and O_2 along the kiln length for different air profiles. It can be clearly noted that the partial pressure of oxygen in the free board has a controlling effect on the various reactions taking place in the kiln and also on the temperature of the phases. The presence of excess oxygen in the free board however shows an adverse effect on the temperature and hence on the degree of reduction. From these results it can be concluded that air profile is an import design parameter and it has to be properly chosen to achieve a desired degree of reduction and to maintain equilibrium partial pressures in the bed.

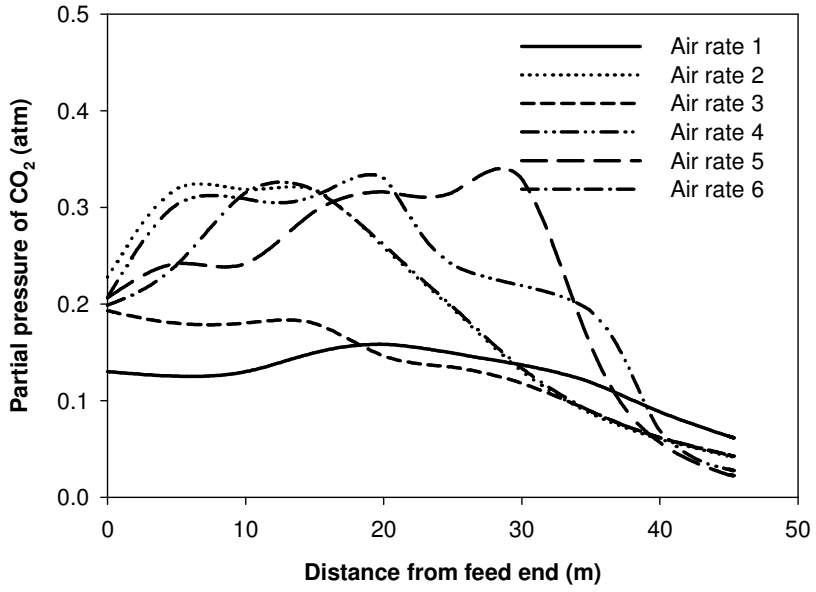

Figure 4.19 Effect of Air Distribution on Partial Pressure of CO_2

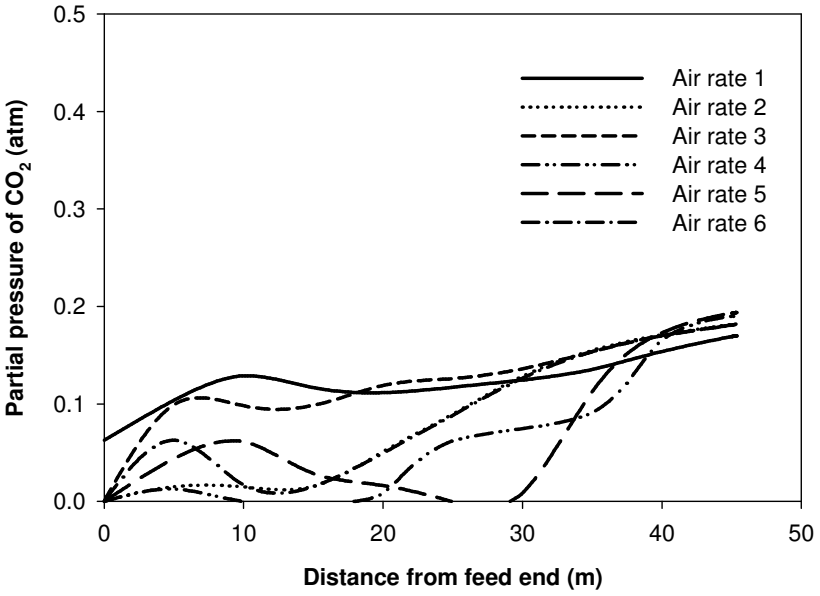

Figure 4.20 Effect of Air Distribution on Partial Pressure of O_2

4.9 Conclusions

In this chapter a comprehensive one dimensional mathematical model of the Ilmenite reduction rotary kiln reactor is developed and reduction process is simulated using various input parameters. The model developed in this chapter includes the kinetic model developed in Chapter 2 and the results of the three dimensional CFD model of the pneumatic coal injection process from the discharge end of the kiln (Chapter 3). The model is validated by comparing with the only reported result of this sort by Ramakrishnan and Sai (1999).

The following are the major conclusions from the simulation studies:

1. Heat transfer plays a major role in the overall rate of the carbothermal reduction process taking place in the rotary kiln reactor.
2. Careful designing of the pneumatic coal injection process with appropriate particle size distribution and initial velocity is extremely useful for optimizing the degree of reduction in the kiln.
3. The air distribution in the kiln has a crucial role in determining the rate of various processes taking place in the free board as well as the solid bed.

Chapter 5

CONCLUSIONS AND FUTURE SCOPE

5.1 Conclusions

A virtual simulator was developed for the carbothermal reduction of ilmenite in a rotary kiln reactor. The virtual simulator takes into account three important sub processes viz., (a) Kinetics of carbothermal reduction of Ilmenite (b) Pneumatic coal injection from the discharge end (c) Axial heat and mass balance. The simulator predicts the gas and solid flows, concentration profiles and thermal profiles along the axial length of the rotary kiln during the carbothermal reduction of Ilmenite under steady state conditions for a wide range of process conditions and reductant characteristics. The following are the sub modules developed and integrated into the virtual simulator:

1. A kinetic model for the carbothermal reduction of ilmenite at conditions prevailing in a commercial rotary kiln reactor which provides appropriate rate equations for the reduction reaction

2. A mathematical model of the pneumatic coal injection from the discharge end of the kiln to arrive at the carbon load in the solid bed and thermal load in the free board of the rotary kiln

3. A comprehensive 1-D model for predicting the heat and mass flows along the axial length of the kiln by incorporating modules 1 & 2.

The simulated reduction using the kinetic data show very good agreement with the experimental results and also with the results reported by Nicholson (1995) for static atmosphere test. Hence the model supports the suggested mechanism and successfully represents the reduction of Ilmenite in CO/CO_2 atmosphere.

The pneumatic coal injection and combustion process in a commercial rotary kiln is modeled using a three dimensional steady state multiphase Eulerian-Lagrangian CFD approach where the gas phase is treated as a continuous phase and the pulverized coal particles are tracked in the flow field in a Lagrangian way. The effect of initial particle velocity, particle size and kiln wall temperature on the particle dynamics and char burnout are investigated. The results indicated that the injection velocity and particle size has profound influence on determining the efficiency of the pneumatic injection in supplementing the reduction process. The effect of particle size distribution on the thermal and carbon load added to the bed was also studied.

The present model is thus useful in predicting the optimum particle size distribution and injection velocity for any given operating and physical conditions of the kiln. The particle size distribution show profound influence on the coal devolatilization and combustion reaction as the particle temperature is controlled by the particle size. Particles of size more than 5 mm just get heated up and they reach the solid bed almost unburnt, thus providing the carbon load for the reduction process. Smaller particles burn off completely in the free board and they contribute only to the thermal load which supplements the heat availability in the free board region. By simulating combustion and devolatilization reactions of different types of coals, the present model helps in selecting the suitable type of reductant for improved efficiency of the industrial reduction processes.

5.2 Scope for Future Work

The rotary kiln reactor involves many complex processes both in the solid bed as well as the gas phase. Though the one dimensional model provides a simple and reliable base for studying the overall processes taking place in the kiln, it often fails in representing the complex processes taking place in the kiln, especially in the free board region. A comprehensive three dimensional model of the kiln will be highly desirable and adequate for the realistic representation of the actual processes.

As there is considerable difference between the particle sizes of Ilmenite and Coal which together forms the solid bed of the kiln, the segregation of solid bed poses a serious problem in the design of ilmenite reduction kiln. This can be solved by incorporating appropriate solid bed segregation model in the rotary kiln model. Hence a comprehensive three dimensional mathematical model which incorporates both axial and radial movement of solids, gases will be developed in future.

REFERENCES

Abril E.R., Kinetics of iron oxide direct reduction by coal, *Latin American Applied Research*, **32** (2) (2002) 145-149

Anthony D. B., Howard J. B., Coal devolatilization and hydrogasification, *AIChE Journal*, **22** (1976) 625–656

Badzioch S., Hawksley P.G.W., Kinetics of thermal decomposition of pulverized coal particles, *Industrial and Engineering Chemistry*, **9** (1970) 521-530

Barr P.V., Brimacombe J.K., Watkinson A.P., A heat transfer model for the rotary kiln: Part I. *Pilot Kiln Trials, Metallurgical Transactions, B*, **20B** (1989a) 391-402

Barr P.V., Brimacombe J.K., Watkinson A.P., A heat-transfer model for the rotary kiln: Part II. *Development of the cross-section model, B*, **20B** (1989b) 403-419

Becher R.G., Improved process for the beneficiation of ores containing iron, *Australian Patent 247110,* (1963)

Biswas D.K., Asthana S.R., Rau V.G., Some studies on energy savings in sponge iron plants, *Journal of Energy Resources Technology (Transactions of the ASME)*, **125** (3) (2003) 228-237

Biswas D.K., Some design aspects of pneumatic coal injector for coal based direct reduction process in rotary kiln, *Powder Handling and Processing*, **5** (2) (1993) 145-52

Boateng A.A., Barr P.V., A thermal-model for the rotary kiln including heat-transfer within the bed, *International Journal of Heat and Mass Transfer*, **39** (10) (1996) 2137-2147

Briggs R.A., Sacco A., Hydrogen reduction mechanisms of ilmenite between 823 and 1353 K, *Journal of Materials Research*, **6** (3) (1991) 574-584

Brimacombe J.K., Watkinson A.P., Heat transfer in a direct fired rotary kiln: I. *Pilot Plant and Experimentation, Metallurgical and Materials Transactions B*, **9B** (1978a) 201-208

Brimacombe J.K., Watkinson A.P., Heat transfer in a direct fired rotary kiln: II *Heat Flow Results and their Interpretation, Metallurgical and Materials Transactions B*, **9B** (1978b) 209-218

Chaterjee A., Mukhopadhyay P.K., Srivastava M.P, Sathe A.V., Flow of materials in rotary kilns used for sponge iron manufacture, Part 1: *Effect of Some Operational Variables*.,**14B** (1983) 375

Coetsee T., Pistorius P.C., de Villiers E.E., Rate-determining steps for reduction in magnetite-coal pellets, *Minerals Engineering*, **15** (2002) 919–929

Dewan M., Zhang G., Ostrovski O., Carbothermal reduction of a primary ilmenite concentrate in different gas atmospheres, *Metallurgical and Materials Transactions B*, **41B** (2010) 182–192

Doan P.H, Sustainability development in the TiO2 industry, *TiO2 2003 Conference Intertech, Miami Florida* (Feb 2003)

Donnelly R.P., Brennan L.J., McMullan W. and Rouillard A., Reduction of iron oxide in ilmenite beach sands, *Australian Mining*, **3** (1970) 58-66

Donskoi E., McElwain D.L.S., Wibberley L.J., Estimation and modeling of parameters for direct reduction in iron ore/coal composites: Part II. *Kinetic parameters, Metallurgical and Material Transactions B*, **34B** (2003) 255-266

El_Tawil S.Z., Morsi I.M. , Francis A.A., Kinetics of solid state reduction of ilmenite ore, *Canadian Metallurgical Quarterly*, **32** (4) (1993) 281-288

El-Guindy M.I., Davenport W.G., Kinetics and mechanism of ilmenite reduction with carbon, *Metallurgical Transactions*, **1** (1970) 1729-1734

Eungyeul P., Oleg O., Reduction of titania-ferrous ore by carbon monoxide, *ISIJ International*, **43** (9) (2003) 1316-1325

Ferron J.R., Singh D.K. Rotary kiln transport processes, *AIChE Journal*, **37** (1991) 747-758

Fortini O.M., Fruehan R.J., Rate of reduction of ore-carbon composites: Part I. Determination of intrinsic rate constants*, Metallurgical and Materials Transactions B*, **36B** (2005) 865–872

Fruehan R.J, The rate of reduction of iron oxides by carbon, *Metallurgical Transactions B*, **8B** (1977) 279-286

Gibb J., *Lecture at course of pulverized coal combustion*, Imperial College, London (1985)

Gorog J.P., Adams T.N. and Brimacombe J.K., Heat transfer from flames in a rotary kiln, *Metallurgical and Materials Transactions B*, **14B** (1983) 411-424

Gorog J.P., Adams T.N. and Brimacombe J.K., Regenerative heat transfer in a rotary kiln, *Metallurgical Transactions B*, **13B** (1982) 153-163

Gorog, J.P., Adams, T.N., Brimacombe, J.K., Radiative heat transfer in rotary kilns, *Metallurgical Transactions B*, **12B** (1981) 55-64

Guo B. Y., Zulli P., Roger H., Mathieson J. G., Yu A. B., Three-dimensional simulation of flow and combustion for pulverised coal injection, *ISIJ International*, **45** (2005) 1272-1281

Gupta D. S., Bhatia S.K., Khakhar D.V., Axial transport of granular solids in horizontal rotating cylinders, Part 1: *Theory, Powder Technology*, **67** (1991) 145

Gupta S.K., Rajkumar V., Grieveson P., Kinetics of reduction of ilmenite with graphite at 1000 to 1100 0c, *Metallurgical Transactions B*, **18** (1987) 713-718

Gupta S.K., Rajkumar V., Grieveson P., The influence of weathering on the reduction of ilmenite with carbon, *Metallurgical Transactions B*, **20** (1989) 735-745

Gupta S.K., Rajkumar V., Grieveson P., The role of preheating on the kinetics of reduction of ilmenite with carbon, *Canadian Metallurgical Quarterly*, **29** (1) (1990) 43-49

Gupta S.K., Rajkumar V., Grieveson P., Phase transformations during heating of ilmenite concentrates, *Canadian Metallurgical Quarterly*, **22** (1991) 711-716

Hammond P.A., Taylor L.A., The ilmenite/titano-magnetite assemblage: kinetics of re-equilibration, *Earth and Planetary Science Letters*, **61** (1) (1982) 143-150

Henein H., Brimacombe J.K. and Watkinson A.P., Experimental study of transverse bed motion in rotary kilns, *Metallurgical and Material Transactions B*, **14B** (1983) 191-205

Hockin H.W., *US Patent No. 3890138*, 1975.

Hogg R., Austin L.G., Shoji, K., Axial transport of dry powders in horizontal rotating cylinders, *Powder Technology*, **9** (1974) 99

Hottel H.C., Sarofim A.F., Radiative transfer, *McGraw-Hill, Inc.,* 1967

http://ibm.nic.in/ilmeniteandrutile.pdf

Hussein m. K., Kammel R. , Winterhager H., A study on the reduction mechanism of ilmenite ores, *Indian Journal of Technology*, **5** (12) (1967) 369-377

Hussein M.K., EI-Tawil S.Z., Solid state reduction of egyptian black sand ilmenite by hydrogen, *Indian Journal of Technology*, **5** (1967) 97-100

Imber M., Paschkis V., Mathematical analysis of the rotary kiln heat exchanger Part 1. *The Well-Mixed Condition, Radex-Rundschau*, **4** (1960) 183-197

Iyer S.R., Murthy J. S. N., Pakala V. S., Gaseous reduction of iron ore in a rotary kiln, *Transactions of the Indian Institute of Metals* , **36** (6) (1983) 443-451

Jones D. G., Kinetics of gaseous reduction of ilmenite, *Journal of Applied Chemistry and Biotechnology*, **25** (8) (1975) 561–582

Jones D.J., Reaction sequences in the reduction of Ilmenite: 2 – Gaseous reduction by carbon monoxide, *Transactions of the Institution of Mining and Metallurgy (Section C: Mineral Processing and Extractive metallurgy*, **82** (1973) 186-192

Karki K.C., Patankar S.V., Grant J., Simulation of fluid flow, combustion and heat transfer in a coal-fired cement kiln, Combustion, *Fire and Computational Modeling of Industrial Combustion Systems (ASME)*, FACT **23**/HTD **367**, (2000)

Kramers H., Croockewit P., The passage of granular solids through inclined rotary kilns, *Chemical Engineering Science*, **1** (1952) 259–265

Kroll W. J., Method for the manufacturing of titanium and alloys thereof, *US Patent 2,205,854,* (1940a)

Kroll W. J., *Trans. Electrochem. Soc.* **112** (1940b) 35-47

Kucukkaragoz C.S., Eric R.H., Solid state reduction of a natural ilmenite, *Minerals Engineering*, **19** (2006) 334-337

Launder B. E., Spalding D. B., The numerical computation of turbulent flows, *Computer Methods in Applied Mechanics and Engineering*, **3** (2) (1974) 269-289

Lebas E.F., Hanrot F., Ablitzer D., Houzelot, J.L., Experimental study of residence time, particle movement and bed depth profile in rotary kilns, *Canadian Journal of Chemical Engineering* , **73** (1995) 173-179

Levenspiel O., Chemical reaction engineering, *John Wiley & Sons, New York* (1999)

Liu X.Y., Specht E., Mellmann J. Slumping–rolling transition of granular solids in rotary kilns, *Chemical Engineering Science*, **60** (2005) 3629– 3636

Liu X. Y., Spechta E., Gonzalezb O. G., Walzelb P., Analytical solution for the rolling-mode granular motion in rotary kilns, *Chemical Engineering and Processing*, **45** (6) (2006) 515-521

Liu X.Y., Specht E., Mean residence time and hold-up of solids in rotary kilns, *Chemical Engineering Science*, **61** (15) (2006) 5176-5181

Magnussen B.F., Hjertager B.H., On mathematical modeling of turbulent combustion with special emphasis on soot formation and combustion, *16th Symposium (International) on Combustion, Combustion Institute, Pittsburg, Pennsylvania*, (1976) 719-729

Mastorakos E., Massias A., Tsakiroglou C.D., Goussis D.A., Burganos, V.N., CFD predictions for cement kiln including flame modeling, *Heat Transfer And Clinker Chemistry, Applied Mathematical Modelling*, **23** (1999) 55–76

McKewan, W.M. , Kinetics of iron oxide reduction, *Transaction of the American Institute of Mining and Metallurgical Engineers*, **218** (1960) 2-6

Mellman J., The transverse motion of solids in rotating cylinders-forms of motion and transitional behaviour, *Powder Technology*, **118** (2001) 251–270

Merk R., Pickles C.A., Reduction of ilmenite by carbon monoxide, *Canadian Metallurgical Quarterly*, **27** (3) (1988) 179-185

Mukhopadhyay P.K., Sathe A.V. and Chatterjee A.A., A mathematical model of direct reduction of iron oxides in rotary kiln using TDR process, *Trans. IIM*, **37** (1984) 721-728

Nicholson T.A. , Mathematical modeling of the ilmenite reduction process in rotary kilns, *PhD Thesis, University of Queensland, Australia*, 1995

Olsson R. G. and McKewan W. M., Diffusion of H2-H2O through porous iron formed by the reduction of iron oxides, *Metallurgical Transactions*, **1** (1970) 1507-1512

Pesl J., Eric R.H., High temperature carbothermic reduction of Fe2O3–TiO2–MxOy oxide mixtures. *Minerals Engineering*, **15** (2002) 971–984

Poggi D., Charette G. G., Rigaud M., Reduction of ilmenite and ilmenite ores, *Titanium Science and Technology*, **1** (1973) 247-259

Ramakrishnan V., Mathematical modeling and optimization of direct reduction process in a rotary kiln, *M.S. Thesis, IIT Madras* (1996)

Ramakrishnan V., Sai P.S.T., Mathematical modeling of pneumatic char injection in a direct reduction rotary kiln, *Metallurgical and Materials Transactions B*, **30B** (1999) 969-977

Ranade V.V., Mujumdar K.S., CFD simulations of solid motion in the transverse plane of rotating kilns, *Third International Conference on CFD in the Minerals and Process Industries, CSIRO, Melbourne, Australia* (2003)

Saeman W.C., Passage of solids through rotary kilns - factors affecting time of passage, *Chemical Engineering Progress*, **47** (1951) 508-514

Saensunona B., Stewarta G.A. , Pax R., A combined 57 FE–Mössbauer and x-ray diffraction study of the ilmenite reduction process in a commercial rotary kiln , *International Journal of Mineral Processing*, **86** (1-4) (2008) 26-32

Sai P.S.T., Evaluation of mathematical models for the reduction of ilmenite with char in a rotary reactor, *Indian Chemical Engineering*, **50** (4) (2008) 312-322

Sai P.S.T., Damodaran A.D., Surender G.D., Prediction of axial velocity profiles and solids hold-up in a rotary kiln, *Canadian Journal of Chemical Engineering*, **70** (1992) 438

Sass A., Simulation of the heat transfer phenomena in a rotary kiln, *I & EC Process Design and Development*, **6** (4) (1967) 532-535

Satoshi I., Atsushi K., Reduction kinetics of natural ilmenite ore with carbon monoxide, *Materials Transaction*, **42** (7) (2001) 1364-1372

Shen Y., Guo B., Yu A., Maldonado D., Austin P., Zulli P., Three-dimensional modelling of coal combustion in blast furnace, ISIJ International*,* **48** (6) (2008) 777-786

Sohn, H. Y. and J. Szekely, The effect of reaction order in non-catalytic gas-solid reactions, *Canadian Journal of Chemical Engineering*, **50** (5) (1972a) 674-676

Sohn, H. Y., Szekely J., A structural model for gas-solid reactions with moving boundary. III. General dimensionless representation of irreversible reaction between a porous solid and a reactant gas, *Chemical Engineering Science*, **27** (1972b) 763-778

Solomon P. R., Colket M. B., Coal devolatilization , *17th Symposium (International) on Combustion, The Combustion Institute, Pittsburgh*, **17** (1) (1979) 131-143

Spurling R.J., Granular flow in an inclined rotating cylinder: steady state and transient, *Ph.D. Thesis, University of Cambridge*, 2000

Spurling R.J., Davidson J.F., Scott D.M., The transient response of granular flows in an inclined rotating cylinder, *Transactions of IChemE*, **79** (2001) 51–61

Sucre G.A., Ablitzer D., Brimacombe J. K., Kinetics of reduction of titaniferrous ores with lignite coal, *Proceedings of the International Symposium on the Physical Chemistry of Iron and Steel making, Toronto* (1982) 16-25

Sucre-Garcia, Kinetics of reduction of titaniferrous ores with lignite coal, *M.Sc. Thesis, The University of British Columbia, Canada* (1979)

Sullivan J.D., Maier C.G., Ralston O.C., Passage of solid particles through rotary cylindrical kilns, *US Bureau of Mines, Technical Papers* **384** (1927) 1-42

Sun K., Lu W.-K., Mathematical modeling of the kinetics of carbothermic reduction of iron oxides in ore-coal composite pellets, (2004) *B*, **40B** (2009) 91-103

Szekely J., Evans J.W., Sohn H.Y., Gas-Solid Reactions, Academic Press, New York (1976)

Teller R.G., Antonio M.R., Grau A.E., Gueguin M., Kostiner E., The chemistry of the thermal decomposition of pseudobrookite ferrous titanium oxides , *Journal of Solid State Chemistry*, **88** (1990) 351–67

Themelis N. J., Gauvin W. H., A generalized rate equation for reduction of iron oxides, *Transactions of Metallurgical Society AIME* **227** (1963) 290-300

Tscheng S.H., Watkinson A.P., Convective heat transfer on rotary kilns, *Canadian Journal of Chemical Engineering*, **57** (1979) 433–443

Ubhayakar S.K., Stickler D.B., von Rosenberg C.W., Gannon R.E., Rapid devolatilization of pulverised coal in hot combustion gases, *16th Symposium (International) on Combustion* (1977) 427–436

Venkateswaran V. and Brimacombe J.K., Mathematical model of the SL/RN direct reduction process, *Metallurgical Transactions B*, **8B** (1977) 389-398

Von Bogdandy L. and Engell H.J., The reduction of iron ores, *Springer verlog, Berlin*, (1971) 286-310

Walole E. A., P.N. Mohan Das, S. Suresh Kumar, In proceedings of the international symposium on metal and materials from titanium minerals (2004) 31-44

Wang Y., Yuan Z., Reductive kinetics of the reaction between a natural ilmenite and carbon, *International Journal of Mineral Processing*, **81** (2006) 133-140

Watkinson A.P., Brimacombe J.K., Limestone calcination in rotary kiln, *Metallurgical and Material Transactions B*, **13B** (1982) 369-378

Welham N.J., Williams J.S., Carbothermic reduction of ilmenite (FeTiO3) and rutile (TiO2), *Metallurgical and Materials Transactions B*, **30B** (1999) 1075–1081

Wingfield S.L., Prothero A., Auld J. B., Mathematical model of a rotary kiln for the partial reduction of iron ore, *Journal of the Institute of Fuel*, **47** (1974) 64-72A

Wouterlood H.J., The reduction of ilmenite with carbon, *Journal of Chemical Technology and Biotechnology*, **29** (1979) 603-618

Yamamoto K., Taniguchi M., Kobayashi H., Sakata T. and Kudo K., Validation of coal combustion model by using experimental data of utility boilers, *JSME International Journal Series B*, **48** (3) (2005) 571-578

Zhang G., Ostrovski O., Effect of preoxidation and sintering on properties of ilmenite concentrates, *International Journal of Mineral Processing*, **64** (2002) 201-218

Zhao Y., Shadman F., Kinetics and mechanism of ilmenite reduction with carbon monoxide, *AIChE Journal*, **36** (9) (1990) 1433–1438

LIST OF PUBLICATIONS

Conference Papers

1. **Manju M.S**., Premalatha M., Savithri S., Surender G.D., CFD Simulation of Pneumatic Coal Injection in a Direct Reduction Rotary Kiln, Ansys India Conference 2007 , Bangalore
2. **Manju M.S**., Savithri S., Mathematical Modeling of Carbothermal Reduction of Ilmenite, Proceedings, CHEMCON 2008, Chandigarh
3. **Manju M.S**., Savithri S. Finite Element Modeling of Carbothermal Reduction of Ilmenite, Proceedings, International Symposium For Research Scholars on Metallurgy, Materials Science & Engineering 2008, Indian Institute of Technology Madras
4. **Manju M.S**., Savithri S., Kinetics of the Carbothermal Reduction of Ilmenite: Grain Pellet Model, COMSOL Conference 2009, Bangalore (http://cds.comsol.com/access/dl/papers/7356/Savithri.pdf)
5. **Manju M.S**., Savithri S., Modeling of Pneumatic Coal Injection in a Rotary Kiln Reactor, Kerala Science Congress 2010, Peechi

Journal Articles Communicated

1. **Manju M. S**., Savithri S., Three Dimensional CFD Simulation of Pneumatic Coal Injection in a Direct Reduction Rotary Kiln, Fuel, (Communicated)
2. **Manju M. S.**, Savithri S., Kinetics of the Carbothermal Reduction of Ilmenite: Combined-reaction Model, Minerals Engineering (Communicated)